This is a repository copy of *A review of non-fullerene polymer solar cells: from device physics to morphology control*.

White Rose Research Online URL for this paper:
http://eprints.whiterose.ac.uk/143987/

Version: Accepted Version

A Review of Non-fullerene Polymer Solar Cells: From Device Physics to Morphology Control

Robert Gurney[1], David Lidzey[2] and Tao Wang[1*]

[1]School of Materials Science and Engineering, Wuhan University of Technology, Wuhan 430070, China

[2]Department of Physics and Astronomy, University of Sheffield, Sheffield S3 7RH, UK

E-mail: twang@whut.edu.cn

Abstract

The rise in power conversion efficiency of organic photovoltaic (OPV) devices over the last few years has been driven by the emergence of new organic semiconductors and the growing understanding of morphological control at both the molecular and aggregation scales. Non-fullerene OPVs adopting p-type conjugated polymers as the donor and n-type small molecules as the acceptor have exhibited steady progress, outperforming PCBM-based solar cells and reaching efficiencies of over 14 % in 2018. This review starts with a refreshed discussion of charge separation, recombination, and V_{OC} loss in non-fullerene OPVs, followed by a review of work undertaken to develop favorable molecular configurations required for high device performance. We summarize several key approaches that have been employed to tune the nanoscale morphology in non-fullerene photovoltaic blends, comparing them (where appropriate) to their PCBM-based counterparts. In particular, we discuss issues ranging from materials chemistry to solution processing and post-treatments, showing how this can lead to enhanced photovoltaic properties. Particular attention is given to the control of molecular configuration through solution processing, which can have a pronounced impact on the structure of the solid-state photoactive layer. Key challenges, including green solvent processing, stability and lifetime, burn-in, and thickness-dependence in non-fullerene OPVs are briefly discussed.

Keywords: polymer solar cells; organic photovolotaics; non-fullerene; morphology; efficiency

1. Introduction

Photovoltaic solar cells convert the energy of sunlight into electricity using the photovoltaic effect. In the last decades, organic photovoltaic devices (OPVs) have emerged as promising systems in the field of solar cell technology. OPVs usually comprise at least two types of semiconducting component in their photoactive layer, electron donors (D) where excitons are created upon photoexcitation, and electron acceptors (A) to which the electrons are transferred and transported to an electrode to generate current flow. The D-A strategy for OPVs quickly gained in popularity since they are solution processable, cost effective and potentially scalable for industrial manufacture [1]. The fact that organic materials have tunable bandgaps and energy levels in both donor and acceptor materials offers significant research opportunities in this area.

The architecture of OPVs has evolved from low efficiency bilayer D-A heterojunctions, to mixed D-A phase bulk heterojunction (BHJ) structures. Amongst BHJ solar cells, a notable highlight is the use of fullerene derivatives as the acceptor material, in particular [6,6]-phenyl-C61-butyric acid methyl ester ($PC_{61}BM$ or simply PCBM). From its rise in popularity in the 2000s, blends of a donor polymer with a fullerene acceptor rapidly progressed, with devices having power conversion efficiencies (PCE) in single junction cells of around 11 % [2]. Polymer-fullerene systems are undoubtedly a highly successful route to achieve a high PCE in OPVs, and in the last decade fullerenes have been the acceptor molecule of choice over their polymer and small molecule counterparts. This is likely due to the relative ease of processing and rapid improvement of the PCE of fullerene-based BHJ OPVs. Although some efforts have been made to tune the energy levels of fullerene acceptors [3,4], the most common (non-tuned) fullerene derivatives, $PC_{61}BM$ and $PC_{71}BM$, remain the dominant fullerene acceptors. However, progress has slowed in the last couple of years for several reasons; fullerene derivatives are expensive to synthesize at high purity [5], have poor light harvesting ability [6], small bandgaps [5] and show limited electronic tunability. Fullerene nanoparticles also tend to migrate and aggregate in the solid photoactive layer, thereby reducing device efficiency and lifetime [7,8]. This has meant that despite research into novel polymeric donors, progress is restricted by the limits of these fixed fullerene derivatives, to which no significant advancements are now likely to be made. Given the growth of research into BHJ D-A OPVs, research now increasingly addresses the development of new non-fullerene acceptor materials. Indeed, starting from Zhan's perylene diimide (PDI) acceptor in 2007 [9], a wide range of n-type small molecule acceptors (SMAs) have emerged as a viable route to non-fullerene solar cells, which increasingly appear to overcome the deficiencies of their fullerene counterparts. Here, the last few years have seen SMAs successfully employed in non-fullerene OPVs accompanied by a rapid increase in device efficiency. Many researchers have demonstrated devices having PCEs of over 10 % with significant advances in the understanding of donor-acceptor compatibility, energy level tunability, molecular design and processing techniques used to enhance device performance. At the time of writing (September 2018), several groups have reported champion PCEs over 13 % [10–13] and 14 % [14,15] in single junction non-fullerene devices, over 14 % in ternary OPVs [16,17], and over 17 % in tandem OPVs [18].

This review highlights ways in which researchers have used morphology control in non-fullerene-based OPVs to obtain high device performance. We start by refreshing the discussion of charge generation process in OPVs. A general requirement for efficient harvesting of solar energy is that the energy level offset between the highest occupied molecule orbital (HOMO) level of donor and the lowest unoccupied molecular orbital (LUMO) level of acceptor must be sufficient to overcome the exciton binding energy and facilitate efficient charge generation. Here, the offset ΔE_{DA} provides the energy required for charge separation [19]. This energy offset has been found to be significantly smaller in non-fullerene OPVs compared with their fullerene counterparts, and allows an exploration of the fundamental aspects of the charge generation process in OPVs. We then describe favorable morphological features of non-fullerene BHJ, including molecular

configurations and distributions that lead to high device efficiency. This is followed by a summary of how material chemistry, ternary-strategy, solution-processing and post-treatments influence molecular ordering and phase separation in solution-cast BHJ photoactive layers. We finish by presenting challenges and perspectives for the future of non-fullerene OPVs.

2. Discussion of charge separation, recombination, and V_{OC} loss

The relationship between the PCE of a device and its key parameters; open circuit voltage V_{OC}, short circuit current J_{SC} and Fill Factor FF is given by the following equation (where P_{in} is the incident solar power) [20]. The so-called Shockley and Queisser limit defines the maximum possible efficiency for a single-junction PV device, that in OPVs has been estimated to be around 35 % [21,22]. However, this applies to ideal systems subject to only intrinsic losses, when in reality there are multiple sources of loss that will have an adverse effect on individual parameters and the PCE. In many cases the complicated interdependence of these parameters, in particular the trade-off between photocurrent and photovoltage, is seen as one of the biggest challenges for improvement in OPVs [23]. Energy loss in OPVs can be split into two types: (1) radiative loss incurred due to charge generation, which is often thermodynamically unavoidable, and (2) non-radiative losses incurred during charge separation and transport; a process termed recombination.

Charge generation in OPVs occurs when photons from an incident ray of light are absorbed by the active layer components, with an electron immediately promoted to the LUMO of the donor (as shown in the diagram of figure 1a) via quasi-adiabatic charge transfer, leaving a hole in the HOMO. In organic semiconductor systems, this electron-hole pair, known as an exciton, exists in an intermediate bound state with a columbic binding energy of around 0.5 eV due to the low permittivity of organic materials [24]. This bound pair of charge-carriers remains electrostatically attracted for a certain time until they disassociate or recombine. In order to generate a photocurrent, the exciton must diffuse to a donor-acceptor heterojunction and disassociate into free charge carriers in a process known as charge separation (see figure 1b). If the charge carriers can be fully separated, this leads to the generation of a photocurrent (see figure 1c). This charge generation process occurs via an interfacial charge transfer (CT) state, and leads to the first part of energy loss ΔE_{CS}, with $\Delta E_{CS} = E_g - E_{CT}$ [25]. Here, E_{CT} is the energy of the CT state, and E_g is the smallest optical energy-gap of the two constituent materials. The second part of energy loss due to recombination to the ground state or other recombination processes (as shown in figure 1d) can be defined as $E_{CT} - qV_{OC}$ [26]. The total energy loss $E_{loss} = (E_g - E_{CT}) + (E_{CT} - qV_{OC}) = E_g - qV_{OC}$, with the elementary charge [27]. Typical values of in fullerene-based BHJ OPVs range from 0.6 to 1.0 eV.

It is noteworthy that the nature of the technique used to determine E_g is critical, with this having an impact on the measured voltage loss. For example, E_g can be determined from the onset of the absorbance or EQE spectra, or from the crossing point of the absorption and emission spectra. In a recent review, Wang et al. highlighted problems with these methods, and showed that E_g values determined using optical methods were reduced as a result of shifts in the absorption spectra caused as a result of blending different materials together [28]. Instead, two useful methods were highlighted that relied only on EQE measurements; namely extracting E_g from the edge of the EQE spectra, E_g^{edge}, or as a derivative of the EQE curve E_g^{PV}. Such measurements were shown to produce more consistent results without the necessity of using optical data, and using such methods an upper limit of PCE of around 18 % was predicted.

The relatively large binding energy of the CT state in OPVs indicates the need for a "driving force" to ensure charge separation. A way to achieve this is by having an offset between the LUMO states of the donor and acceptor respectively ($\Delta E_{DA} = D_{LUMO} - A_{LUMO}$) [29]. Many polymer-fullerene systems were engineered with

such a driving force of around 0.3 eV, such that $E_{CT} < E_g$ in order to drive charge generation. Without this offset, D-A pairs with bandgaps close to E_{CT} have been seen to suffer from losses due to recombination of electron-hole pairs or exciton decay directly to the ground state [5,30]. Many D-A pairs were engineered to utilize large energy offsets in order to successfully generate charges and enable charge separation rather than recombination. However, this comes at the cost of a reduction in internal quantum efficiency, and - since the donor must have a high LUMO to achieve this offset - restricts the tunability of the donor bandgap. While increasing ΔE_{DA} can help overcome the Coulomb barrier, promote charge separation and reduce losses through recombination, this offset is detrimental to other device parameters, in particular V_{OC}. For example, Vohra et al. explored PNTz4T:PC$_{71}$BM inverted cell solar cells that relied on an offset of ~0.5 eV to achieve a PCE of almost 10%, at the expense of V_{OC} (of around 0.7 V) with a total E_{loss} of 1.0 eV [31]. In fullerene systems, there are a few examples breaking this E_{loss} limit, but advances in non-fullerene SMAs has led to more and more systems that combat this problem. Various attempts to reduce this offset by lowering the LUMO level of the acceptor material have resulted in a voltage loss and a drop in V_{OC}, PCE and external quantum efficiency (EQE) [1,32,33]. Other groups have demonstrated an improved V_{OC} in polymer-fullerene systems, with values exceeding 1 V, but always at the cost of J_{SC} [34,35] or optical losses [6].
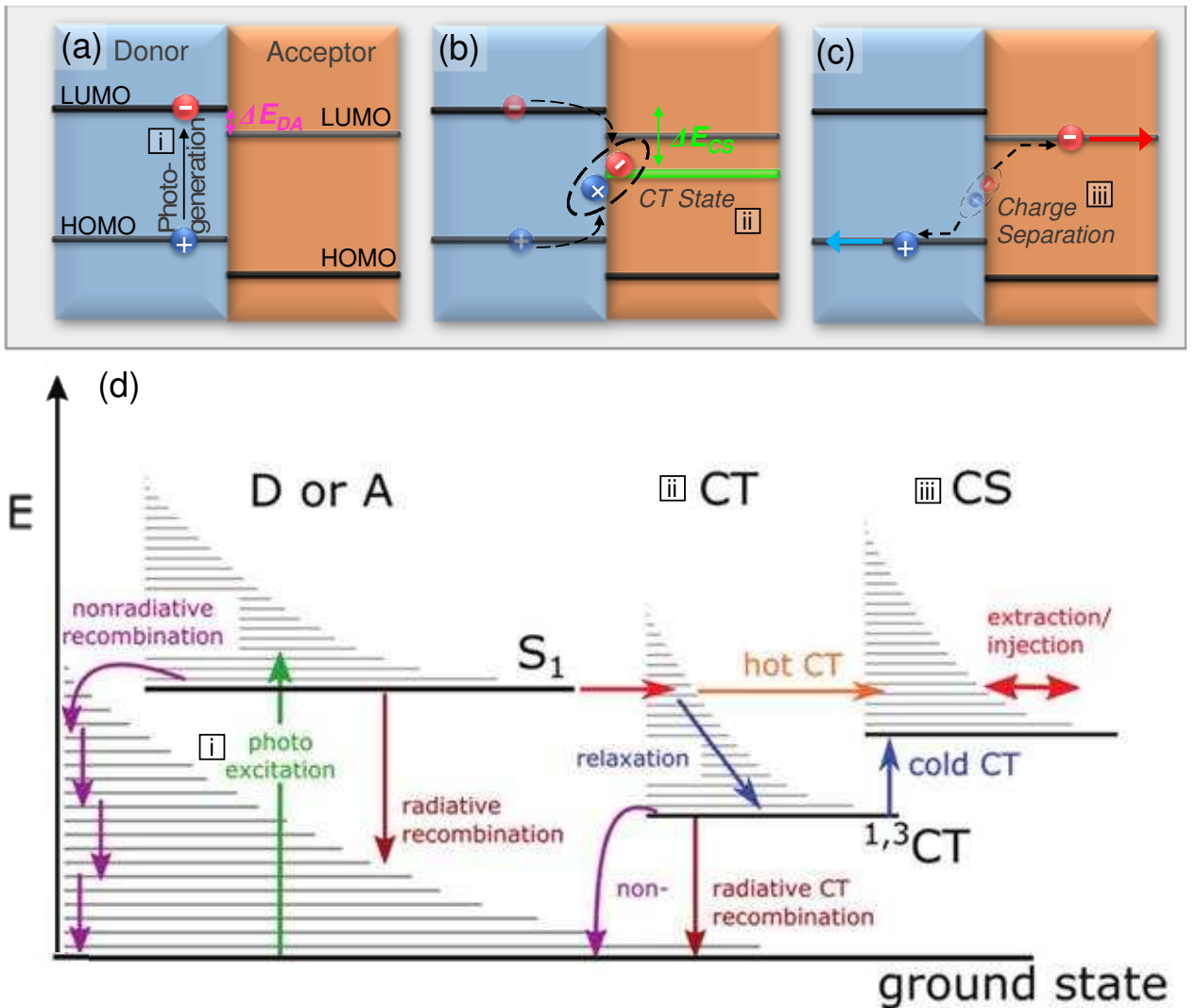

Figure 1. (a-c) Schematic showing photogeneration, charge transfer state and charge separation process across the D:A heterojunction in organic solar cells. (d) Qualitative scheme of the energy landscape of an organic donor–acceptor solar cell. At the interface of donor (D) and acceptor (A) phases, the charge transfer

(CT) state is formed, causing the singlet exciton S1 at either the donor or the acceptor state to undergo charge transfer. From the weakly bound CT state, dissociation into separated charge carriers (CS) can take place by either using excess energy from the singlet state (hot CT) or by thermal excitation from the relaxed CT state (cold CT). Besides dissociation, CT excitons may also recombine radiatively or non-radiatively to the ground state. If the solar cell is driven by an external chemical potential, free charge carriers are injected and recombine from the lowest available energy level, the CT state, leading to electroluminescence emission. figure 1d and caption reproduced with permission from reference [36].

As discussed above, fullerene acceptors are limited by a high binding energy of the charge transfer state, and it has often been seen that an excess of driving force can assist charge separation thus enhancing efficiency. However, this driving force results in energy loss due to the difference in energy of the polymer singlet excited state and the charge transfer state, which can vary between 0.1 and 0.3 eV [5,23]. This is a problem unique to organic photovoltaics, since non-organic and perovskite PV devices have sharp absorption edges, no CT states, and thus do not require a driving force nor suffer from this type of loss [37]. It is often assumed that small molecule acceptors share similar charge separation characteristics with fullerenes, and thus have similar CT state binding energies of around 0.3 eV. However, the evolution of OPV materials and particularly non-fullerene acceptors has challenged the notion of the role of the driving force, as there are growing examples of systems that function well without a ΔE_{DA} of 0.3 eV. The implication is that the binding energy can be lower than 0.3 eV, and that charge separation can occur more rapidly than was initially thought. An explanation comes in the form of delocalized charge transfer states: It is known that the delocalization of electrons and holes occurs in OPV materials, and charge separation is facilitated by the overlap of delocalized charges at the D-A blend interface. When excitons are generated near an interface, rapid charge separation occurs due to the delocalization of charges, with binding energies below E_{CT} (below k_BT), facilitating the separation of the electron-hole pair [38,39]. Menke et al. provided an explanation in terms of the relationship between the lowest singlet excitation energy (determined by E_g) and the coulomb potential as shown in figure 2 [27]. In order to overcome the Coulomb barrier and disassociate at distances beyond the Langevin recombination radius (ca. 5 nm), the energy of the charge transfer state must be greater than the long-range coulomb potential (as in the case of $S1_A$). In the case of systems with high charge mobility and small charge separation distance, delocalized CT states can be created at energies lower than the long range coulomb potential and still disassociate ($S1_B$). Hence, delocalized states are generated at interfaces within picoseconds (ps) of excitation at energies lower than the traditional E_{CT}, with these states possibly being responsible for improved charge separation. Gélinas et al. used ultrafast transient adsorption spectroscopy to reveal the behavior of excitons in the first femtoseconds (fs) after excitation, recording electrostatic peaks 40 fs after charge generation, corresponding to a charge separation distance of 4 nm; a distance at which the exciton binding energy is much smaller. These results indicate that large LUMO level offsets are in fact not vital for charge separation, since delocalized sub-E_{CT} states can separate if located within several nanometers of the D-A interface. These states are of considerably lower binding energy than E_{CT} and, as such, a much smaller or negligible ΔE_{DA} is sufficient for charge transfer in these cases. Bearing this in mind, it is not surprising to see more and more examples of polymer:non-fullerene OPVs which have little to no ΔE_{DA} but high V_{OC} together with reduced recombination and improved efficiency. Various examples of energy loss in fullerene and non-fullerene systems are plotted against their V_{OC}, PCE and EQE in figure 3.
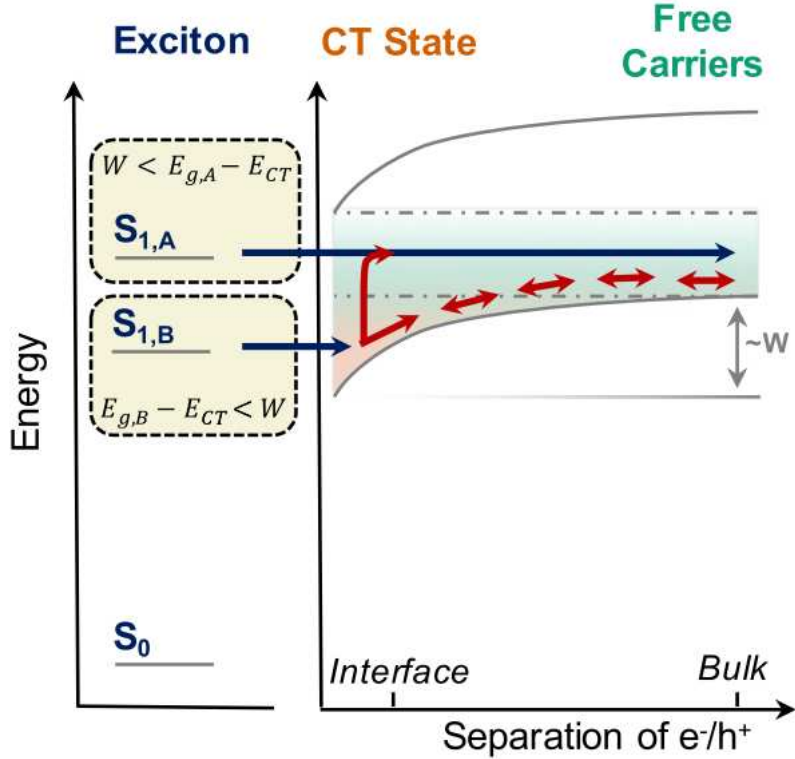
Figure 2. Schematic for charge generation in systems with a large offset energy such that the difference between the lowest singlet exciton energy (S1 or equivalently E_g) and the charge transfer state (E_{CT}) is greater (case A) or less (case B) than the long-range Coulomb potential (W), which needs to be overcome in order to separate charge and create free carriers beyond their Langevin recombination radius. For low E_{loss} systems, case B will dominate. Free carriers can be generated from localized CT states either by thermal promotion to delocalized states or by successive hopping. Figure and caption reproduced with permission from reference [27].
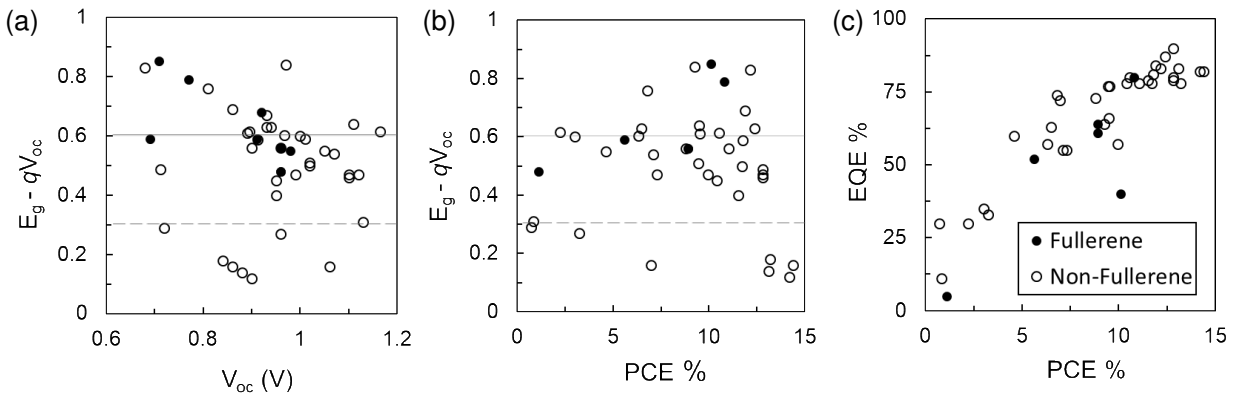

Figure 3. Comparison of the relationship between energy loss and (a) V_{OC} (b) PCE, and (c) PCE vs. EQE for OPVs employing fullerene and non-fullerene acceptors. Energy loss is calculated from $E_{loss}=E_g-qV_{OC}$. The grey solid and dashed horizontal lines offer a guide to the eye to show which systems achieve an E_{loss} of below 0.6 eV and 0.3 eV respectively.

The fact that high efficiency can be achieved in non-fullerene OPVs in which there is little or no energy offset between donors and acceptors motivates a rethink of the charge separation process and mechanisms. Hou et al. have provided new insight as to why charge separation is more efficient in non-fullerene OPVs compared to their fullerene counterparts by studying their electrostatic potential (ESP) [40]. They found that positive and negative charges were concentrated on the surface of the donor and acceptor respectively, which can be represented through models of the molecules as shown in figure 4. This indicates that for the small molecule acceptor, large parts of the surface have a positive ESP, while the donor has a net negative ESP, with all conjugated regions excluding the backbone having negative ESP. This results in the creation of a strong intermolecular field, favoring exciton disassociation and electron transfer from donor to acceptor. This can be compared to the ESP of C_{60}, in which case a homogeneous delocalization of charges over the surface is observed. While this distribution allows weak π-π interactions necessary for charge separation, the ESP is much weaker (0.11 eV) compared to a maximum of 0.98 eV for the SMA. It should be noted that non-symmetrical fullerene derivatives such as $PC_{61}BM$ and $PC_{71}BM$ were created with this in mind, incorporating side-chain blocks adjacent to the C_{60}/C_{70} sphere to generate a less even charge distribution and favor fast charge transfer. However, it is apparent that non-fullerene acceptors have significantly better charge transfer properties, in part due to their uneven and strongly negative surface ESP, which enables fast charge transfer at a D-A interface.
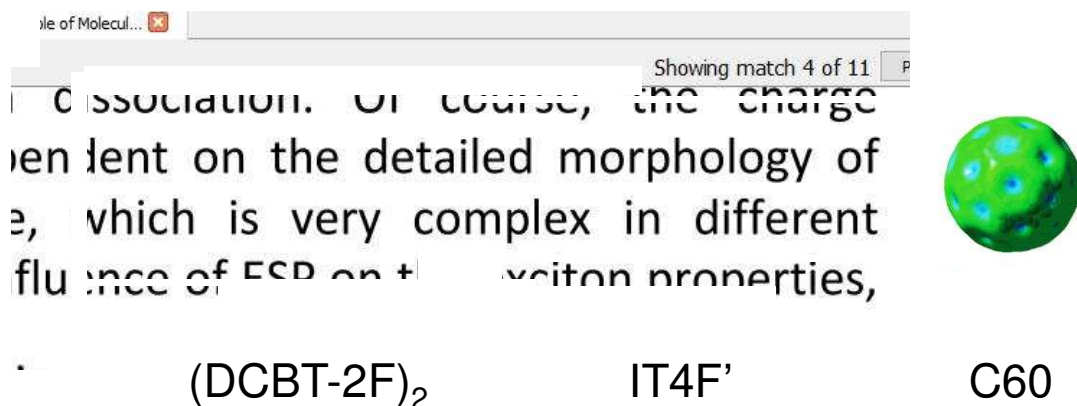

$(DCBT-2F)_2$ IT4F'   C60

Figure 4. ESP distributions on the polymer donor $(DCBT-2F)_2$, the non-fullerene acceptor IT-4F', C60 and $PC_{61}BM$. Blue represents a strong positive electrostatic potential (ESP), while red represents a strong negative ESP, and green a neutral ESP. Reproduced (adapted) with permission from reference [40]. Copyright 2018 American Chemical Society.

In polymer-fullerene systems, charge recombination is seen as a major source loss [5,41,42]. This phenomenon can occur thorough both geminate and non-geminate recombination, with the former referring to the recombination of a hole-electron pair soon after (<100 ms) charge separation (i.e. still in a bound state), and the latter referring to the recombination some time (and distance) after charges have been separated. Organic semiconducting materials usually have low charge mobility, meaning that there is a greater chance of geminate recombination for those materials with low charge separation energy ΔE_{CS} [43]. Non-geminate recombination can occur especially in BHJ devices since there is more chance of charges re-meeting during their transport process within the interdispersed D-A phases, leading to bimolecular recombination [44,45]. Another type of non-geminate recombination is trap-assisted recombination, where holes or electrons are firstly trapped within the band gap and then recombine with an oppositely charged carrier. Reducing the trap density in the BHJ layer can reduce trap-assisted recombination and hence increase the FF of OPVs, e.g. trap-filling of the polymer donors with the additive F4-TCNQ has been demonstrated [46]. The primary

source of such non-radiative (recombination) losses in OPVs remains under discussion, but it is generally accepted that non-geminate recombination is the dominant method in BHJ devices as a result of increased electron and hole recombination in the interdispersed bulk phase [45,47–50]. Recombination in OPVs was initially described by Langevin dynamics [51], but theoretical studies [42,52–54] and experimental measurements (including transient photovoltage and differential charging experiments [41,55], transient absorption spectroscopy (TAS) [56], time-of-flight transient spectroscopy [57], and linearly increasing voltage (such as photo-CELIV) [48,50,58]) have since shown that the recombination rate is in fact several orders of magnitude lower than predicted, leading to reduced or suppressed Langevin recombination [42,47,50,54,59]. This can be quantified as a total recombination rate k_R, which can be expressed simply as the Langevin recombination rate k_L modified by a dimensionless prefactor γ_{pre}, which is a function of current density or charge mobility [47].

$$k_R = \gamma_{pre} k_L = \frac{q}{\varepsilon}(\mu_p + \mu_n) \qquad \text{Eq. 1}$$

Here ε is the combined D-A permittivity, q the elementary charge, and μ_p and μ_n are the electron and hole mobility respectively. Wetzealer et al. extended this to derive the prefactor in terms of carrier current, and found that the values of γ_{pre} were typically on the order of 10^{-3} and 10^{-1} for fullerene and non-fullerene systems respectively, with differences occurring due to different electron mobility and recombination rates, with the coefficient determined by the slowest carrier mobility. Credgington & Durrant derived the relationship between recombination and the open circuit voltage for polymer fullerene systems, and showed that non-geminate recombination limits V_{OC} [49].

Tuning the donor-acceptor energy offset to achieve charge separation whilst minimizing voltage loss from factors such as recombination to achieve a high V_{OC} is an issue that researchers have started to address in non-fullerene donor-acceptor systems. There is mounting experimental evidence showing that efficient charge separation can occur without a driving force, i.e. where D-A HOMO/LUMO levels are in near-equilibrium [60–63]. For example, fast charge transfer can occur by improving the mobility of active layer materials, thus enabling donor-acceptor pairings with smaller energy gaps to have reduced V_{OC} losses [23,27,63,64]. Furthermore, the small offset due to low-lying HOMO levels reduces radiative losses from absorption above the charge transfer energy but below the bandgap [65,66]. Early examples were seen with polymer-fullerene systems using low bandgap polymer donors [23,67,68]. with work by Kawashima and coworkers achieving a V_{OC} of 0.96 V and an efficiency of 8.9 % due to fast charge transport of a narrow bandgap polymer donor PNOz4T with PCBM [69]. In fullerene devices, it was found that high internal quantum efficiency (IQE) values could be obtained with no dependence on the charge transfer states [61]. High values of IQE indicate that very few generated charges are lost to recombination, i.e. most generated charges are separated and make it to the electrodes.

The link between energy loss and quantum efficiency has since been explored in non-fullerene OPV devices, with Li and coworkers finding that PTB7-Th:IDTIDT-IC devices have very high internal and external quantum efficiency (EQE) values and $E_{loss} < 0.6$ eV. It was suggested that this was due to planar π-π stacking of the IDTIDT-IC acceptor enhancing charge mobility, or decreasing the exciton binding energy of the CT state [70]. Thus the measured losses are attributed to radiative losses only (i.e. losses due to recombination are negligible). The following equation was used to quantify non-radiative V_{OC} loss as a function of EQE (where EQE_{EL} is radiative quantum efficiency) [70]:

$$\Delta V_{OC}^{non-rad} = -\frac{kT}{q} \ln EQE_{EL} \qquad \text{Eq. 2}$$

Qian and coworkers demonstrated experimentally that such a relationship between V_{OC} and EQE_{EL} holds true, with systems such as PDCBT-2F:IT-M and PTB7-Th:IEICO that have high EQE_{EL} values also have high V_{OC} values and low voltage losses due to reduced recombination rates. Furthermore, they proposed that systems that otherwise demonstrate high efficiencies but with low values of EQE_{EL} may show capacity for improvement if non-radiative recombination rates can be reduced [71]. As figure 3c demonstrates, there is a strong correlation between EQE and device performance, stemming from the link between EQE and non-radiative recombination. Indeed, improvements in thin film morphology that result in efficient charge dissociation are likely to result in improved short circuit current and correspondingly higher EQE values. Liu and coworkers [64] achieved an internal quantum efficiency of 87 % with an impressively high V_{OC} of 1.11 V resulting in a PCE of 9.5 % in a P3TEA:SF-PDI2 non-fullerene system. A low voltage loss of 0.61 V was reported as a result of high mobility and efficient charge separation with negligible driving forces, and furthermore it was found that by comparing systems with different driving forces, the low driving force did not have a negative impact on device performance. This voltage loss was reduced to 0.54 V in subsequent follow-up work, where the positions of the alkyl side chains and carboxylate substituents were switched to create the polymer P3TAE [72]. This led to a downshift of energy levels, which reduced the driving force and resulted in a high V_{OC} of 1.2 V. Here, the more twisted polymer backbone inhibited molecular aggregation, although both J_{SC} and EQE were reduced. Nevertheless, this potentially offers a route to tuning crystallinity and photovoltaic properties in donor polymers. In a further example, Chen and coworkers found that a high PCE of 10.4 % could be achieved using a PffBT2T-TT:O-IDTBR system in which the energy levels of the donor and acceptor were aligned. The high V_{OC} of 1.08 and low V_{loss} of 0.55 V observed were thought to result from reduced non-radiative recombination rates which were correlated with a high EQE_{EL} of ~1 x10^{-4} [73].

Xie [62] and Zhang [74] reported similar results with PBDB-T:IT-M and PBDB-T:ITIC OPVs respectively, citing the out-of-plane π-π stacking of the donor as a source of high mobility. The acceptor ITIC has been shown to have a broad absorption spectrum, and its high mobility and lower LUMO levels allowed good compatibility with low bandgap donors such as PTB7-Th and PBDB-T [75–77]. Xu and coworkers achieved a PCE of 12.8 % with PBDTS-TDZ as donor and ITIC as acceptor, with a V_{OC} of 1.1 V and E_{loss} of 0.48 eV [12]. Li achieved an impressive PCE of 12 % from IT-M coupled with PBDB-T. This occurred as a result of favorable phase separation, despite resulting in a slightly lower EQE [78]. In an early work, Chen showed that interchain aggregation of a conjugated polymer could be beneficial for high mobility, allowing a low-bandgap donor to achieve high efficiency over a range of active layer thicknesses [30]. Zhang also achieved a high PCE of 11.3 % using π-π conjugated polymers (based on PffBT) as donors with ITIC as the acceptor, with an offset of only 0.04 eV [79]. Shi et al. amongst others highlighted the importance of device morphology, stating that optimal device structure mitigates recombination losses due to slow charge transfer [60,61,80]. Figure 3c highlights the importance of achieving a high EQE in high efficiency systems.

There are several other photovoltaic analysis techniques that can be used in order to quantify charge-carrier mobility, and thus shed light on recombination processes in OPVs. Two such experimental tests are measurements of (i) photocurrent density (J_{ph}) as a function of effective voltage (V_{eff}), and (ii) V_{OC} or J_{sc} versus light intensity (P_{in}). The saturation point (J_{sat}) of the photocurrent density can be correlated with the disassociation of charge carriers, and a high J_{sat} is indicative of low recombination. High values of J_{sat} also correlate with a broader EQE spectrum [81]. By characterizing devices at a range of light intensities and determining the gradient of the subsequent V_{OC} vs. $\ln(P_{in})$ and $\log(J_{SC})$ vs. $\log(P_{in})$ curves, information can be obtained regarding the degree of monomolecular, bimolecular or trap-assisted recombination [82].

In general, by controlling the conjugation lengths and stacking properties of photovoltaic materials, losses due to recombination can be minimized, meaning less dependence on driving force was required to ensure charge separation. This has reduced the dependence on energy offset between donor and acceptor, and hence allows lower bandgap materials to be used. There are a growing number of examples of non-fullerene OPVs which do not suffer losses and have high values of V_{OC}, outperforming other OPVs in this respect as seen in figure 3a. This is through careful design advances such as improving charge transfer efficiency and increasing charge mobility to reduce recombination loss and increase EQE. Improved charge transfer efficiency has also been achieved through favorable mixing of D/A phases, resulting in shorter distances between donor and acceptor phases; an effect that also reduces recombination losses caused by poor charge mobility. These factors have significantly reduced non-radiative recombination losses and raised the V_{OC}, which in turn means that a significant energy level offset (previously required for driving charge separation) is not necessary, thus materials can be utilized with smaller bandgaps and closer-spaced HOMO/LUMO levels.

It is well accepted in the OPV community that film morphology and aggregation at molecular length-scales play critical roles in controlling the optoelectronic properties, via its effects on light absorption, exciton dissociation, charge generation and recombination. For this reason, a growing understanding of the use of processes to control and tune morphology through chemical or processing methods is allowing rapid progress to be made in the development of efficient OPVs. In the following sections, we will highlight how molecular morphology can be tuned through chemical design and processing control, leading to improved photovoltaic properties.

3. "Favorable" morphology leading towards improved performance

In the present generation of OPVs, active layer morphology is one of the main factors that influence charge separation and transport properties. In contrast to bilayers, a mixed donor-acceptor phase in which D-A junctions are distributed throughout the bulk has been widely reported to be the most effective morphology for good OPV device performance [5]. In a heterojunction device, miscible D/A polymers form multiple phases that result in interconnected domains. Optimal devices combine a high degree of D:A interfacial contact, while maintaining pure D/A domains to achieve high mobility and to avoid recombination. To this end, various processing techniques (such as solvent additives [83], solvent vapor annealing [84] and thermal annealing [85]) have been employed to modify the morphology of the active layer. Both molecular parameters and processing techniques play a significant role in determining these morphological properties, which then determine the device performance. This relationship is shown schematically in figure 5.
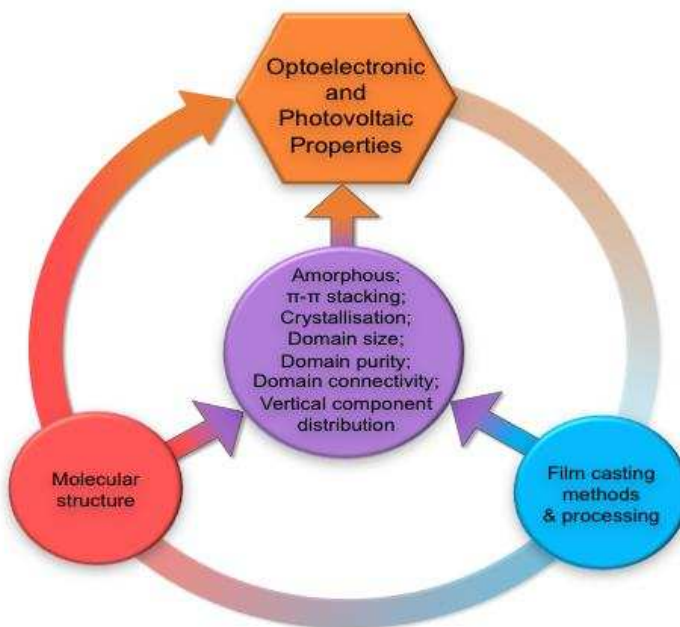
Figure 5. Relationship between chemical structure, film processing and properties of photovoltaic devices.

In polymer:fullerene and polymer:non-fullerene systems alike, the influence of morphology and particularly molecular ordering within domains, domain size, domain purity and domain connectivity play a key role in determining device efficiency. A requirement for good device efficiency is the proximity of excitations to domain boundaries, with domain size being correlated with exciton diffusion length to minimize exciton decay. In polymer:fullerene systems, this parameter has been determined using photoluminescence measurements as a function of layer thickness, with values of 5-20 nm being reported. In non-fullerene blends this diffusion length has been reported to be 10-20 nm [86–90]. For this reason, domain sizes on the order of ~20 nm are necessary when using organic materials with short exciton diffusion lengths [91–93]. Pure crystalline phases, however promote increased mobility and thus reduce bimolecular recombination, thus a morphological trade-off exists for domain size [83,92,94]. It has been shown that poor domain purity, i.e. poor control of aggregation and over-mixing results in a drop in performance in both fullerene and non-fullerene systems [79,95–97]. It is therefore important that the phases are not over-mixed (i.e. forming small or impure domains). Higher domain purity helps improve charge generation [98], as shown by Liu and coworkers who found that by using thermal annealing to control the domain purity of an ITIC derivative (IT-M) it was possible to improve electron mobility and reduce the active layer thickness dependence on OPV performance [99].

There are several techniques that are commonly employed to investigate the morphological properties of semiconducting and conjugated materials at the molecular level. Grazing-Incidence Wide-Angle X-ray Scattering (GIWAXS) can provide valuable insight into the morphology of crystalline regions in conjugated materials, with this technique being used extensively to characterize molecular ordering and orientation [11,32,94,96,99–105]. Grazing-Incidence Small-Angle X-ray Scattering (GISAXS) and Resonant Soft X-ray Scattering (R-SoXS) can be used to determine the average domain size of different phases, with the later able to provide information on domain purity [100,106–108]. Neutron Scattering (NS) [109,110], Near Edge X-ray Absorption Fine Structure (NEXAFS), Secondary-Ion Mass Spectrometry (SIMS) [111–113] and X-ray Photoelectron Spectroscopy (XPS) with ion-etching ability can also be used to characterize the distribution of components in the photoactive layer in a vertical direction [81,114–116]. Scanning

electron/probe microscopy techniques have been widely used to identify phase separation and surface roughness of photovoltaic films [82,117]. Figure 6 lists these techniques and their advantages and limitations in the study of morphology of photovoltaic blends.
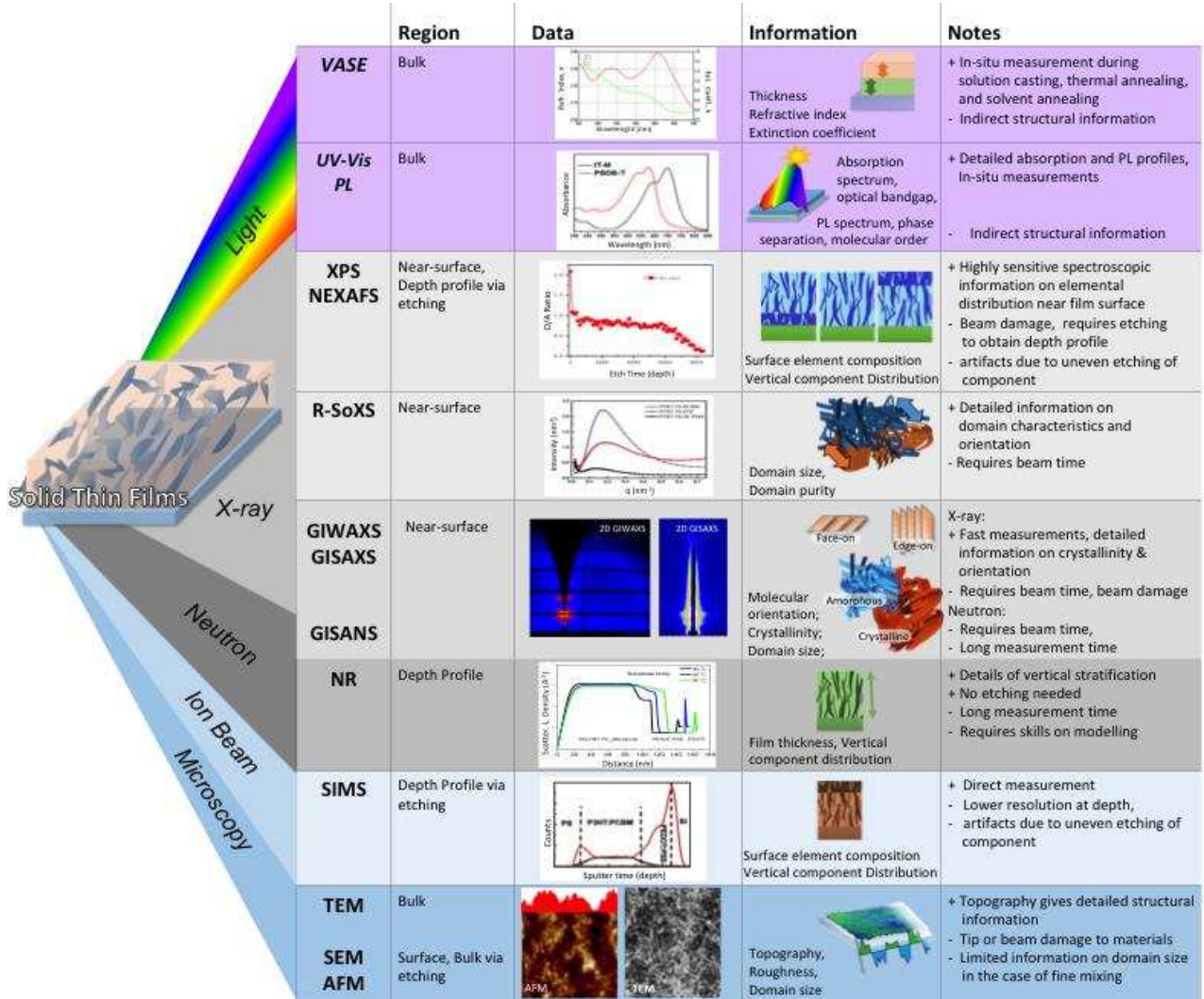
Figure 6. Comparison of different solid-state characterization techniques for photovoltaic thin films. Images in the "data" column are adapted with permission from the following references: UV-Vis [81], XPS [81], R-SoXs [118], GIWAXS & GISAXS [119], NR [120], SIMS [113], AFM & SEM [117].

3.1. Molecular Configuration

Molecular configuration is an important factor in controlling the optoelectronic properties of OPVs, e.g. light absorption, exciton diffusion, charge separation and transport, as well as controlling the physical morphology of the system [64,87,121–124]. Interactions between conjugated materials can influence solubility and miscibility [125] of photovoltaic blends in a liquid state, but also affect π-π stacking and crystallization in solid-state films. Indeed, charge mobility correlates with π-π stacking intensity and the degree of planar alignment and is often used as an indicator of good photovoltaic performance [126–131]. In OPVs, the preferential orientation of conjugated materials in photovoltaic blends corresponds to face-on orientation, that is, with the conjugated backbone of the molecule laying parallel to the substrate, as opposed to edge-on (in which case it is oriented perpendicular to the substrate). Face-on orientation is preferential

because as it can result in improved orbital overlap between donor and acceptor and also improve charge transport and exciton dissociation. An increased degree of face-on orientation has also been seen to benefit charge transport and reduce recombination [31,132], thereby leading to higher FF and J_{SC} [133].
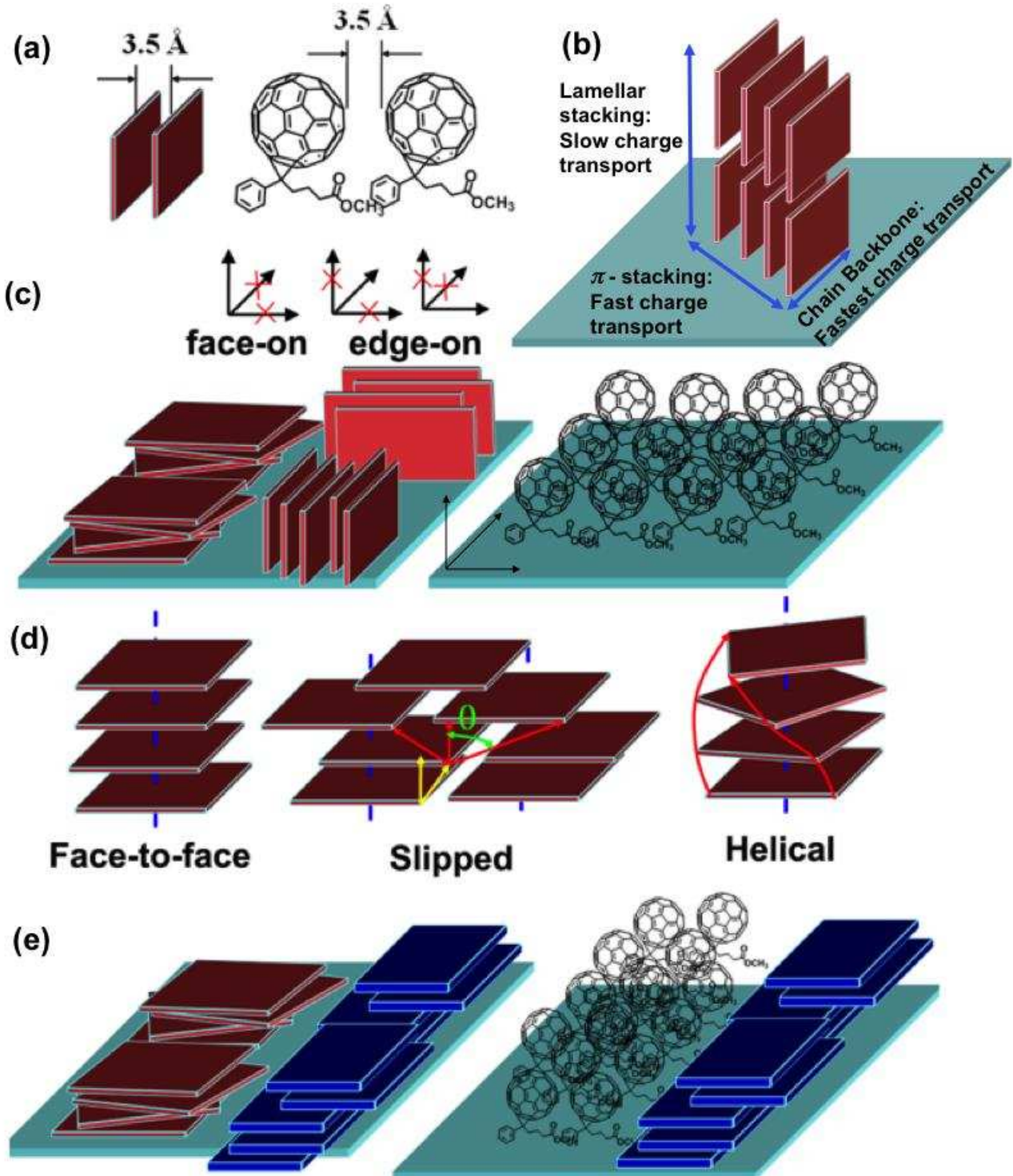
**Figure 7.** (a) $\pi-\pi$ stacking between conjugated molecules and between PCBM nanoparticles. (b) Stacking orientations and their charge transport efficiency (c) Face-on and edge-on orientation of molecules on a substrate. (d) Schematic models of H-aggregation (face-to-face), J-aggregation (slipped face-to-face), and helical aggregation between conjugated molecules. (e) Depictions of ideal $\pi-\pi$ stacking orientation between

13

donor and acceptor in both fullerene and non-fullerene OPVs. Modified and reproduced with permission from authors [125].

PCBM molecules undergo close packing, forming isotropic domains. This results in comparable charge transport mobility in all directions, which is one of the reasons that PCBM is an ideal electron acceptor when combined with various electron-donating materials. This isotropic nature however is not present in non-fullerene OPVs. As shown in figure 7, SMAs can undergo H-aggregation (face-to-face), J-aggregation (slipped face-to-face), or helical aggregation. This anisotropic $\pi-\pi$ stacking leads to anisotropic charge transport properties, with a higher mobility along the $\pi-\pi$ stacks. A preferential orientation of both donors and acceptors with a face-on configuration is expected to be ideal for high performing non-fullerene OPVs. A longstanding question in organic electronics concerns the effect of molecular orientation at donor/acceptor heterojunctions. By investigating a well-controlled donor/acceptor bilayer system, Nguyen et al. determined that devices containing donor molecules that are face-on to the acceptor interface have a higher charge transfer state energy and undergo less non-radiative recombination, resulting in a larger open-circuit voltage and higher radiative efficiency. In contrast, devices containing donor molecules that have edge-on orientation at the acceptor interface are more efficient at charge generation; a feature attributed to reduced electronic coupling between charge transfer states and the ground state, together with a lower activation energy for charge generation [134].

In non-fullerene OPVs, the molecular orientation at the D/A interface is extremely important for charge generation efficiency [135]. As for fullerene derivatives, it has been found that for systems in which there is isotropic non-planar π-stacking, devices have better efficiencies than comparable systems with planar stacking. There are a series of rylene diimide based functionalized polymer acceptors which have been successfully employed due to their favorable absorption and mobility properties, as well as tunability [136]. For example, Rajaram and coworkers show that the non-planar orientation of their perylene diimide (PDI)-based acceptors significantly improves photovoltaic properties [137], with non-planar orientated IDT-derived acceptors also showing improved performance [138]. By increasing the dimensionality of the acceptor (thus increasing the spatial dimensions of the D-A interface), charge separation efficiency can be improved [139]. This is because the Coulombic attraction energy is inversely proportional to the separation length; indeed it has been estimated that the Coulombic energy drops from ~0.4 to 0.1 eV at a distance of 4 nm [140]. Ye et al. show the influence of molecular orientation by changing the planarity of the polymer donor PBDTBDD using alkylthienyl side groups to create PBDTBDD-T. When blended with the acceptor PNDI, the modified donor had a much more anisotropic orientation [141]. Molecular orientation also affects molecular aggregation in solution, resulting in improved phase separation. Their devices incorporating non-planar-orientated PBDTBDD have superior current density, EQE, J_{SC} and V_{OC} than their planar counterparts, with PCE increasing from 2.4 to 5.8 %. Here, the non-planar orientation results in more favorable $\pi-\pi$ interactions between donor and acceptor, improving charge transport efficiency.

3.2. Vertical component distribution

It is known that efficient charge transport can be achieved through control of interfacial properties between transport layers and active materials. For example, by controlling interlayer morphology [142], roughness [143] or work function [144] it is possible to increase charge extraction efficiency. Similarly, the vertical component distribution of donor and acceptor materials towards their respective electrodes can result in improved charge extraction and collection processes. Stratification within active materials can result from methods employed to control thin-film vertical morphology, including thermal annealing [110], solvent annealing [145,146], washing [117], or novel preparation techniques such as off-center spin casting [147],

the use of chemical/solvent additives [106,148,149] or tuning component surface energies [115,150]. The degree of stratification is often investigated using optical techniques such as NS, NEXAFS, XPS and SIMS.[114]. The extent to which vertical stratification affects non-fullerene devices remains an open question, in part due to the difficulty of obtaining high-resolution depth profiles of the active layers. Despite this, there are growing examples of favorable donor enrichment at the substrate interface that benefit device performance when an enriched region is in contact with its corresponding electrode [151–153]. Here, figure 8 depicts a favorable component distribution in the vertical direction in the photoactive layer of a non-fullerene OPV.


Figure 8. Graphical representation of vertical component distributions within the photoactive layer of a non-fullerene OPV. Modified and reproduced with permission from reference [81].

In fullerene systems, the mechanisms controlling vertical stratification have been reviewed by Yan et al. who described the main contributing factors to be the thermodynamics in solution, solubility, and film drying kinetics, along with the surface free-energies of the different materials [93]. Here, as the solvent evaporates, interactions between active materials will increase, which promotes phase separation [154] and drives stratification of donor or acceptor materials. It is widely reported in fullerene systems that thermal annealing invokes vertical stratification via the diffusion of PCBM to the air interface, which can be beneficial for charge extraction in OPVs having a conventional device structure. For example, in P3HT:PCBM films fabricated in ambient conditions, Rujisamphan et al. saw an unfavorable P3HT-rich layer at the surface [155], while van Bavel et al. found that thermal annealing created a PCBM rich surface layer in the same blend [146]. In a non-fullerene system, Vaynzof and coworkers used XPS to identify stratified regions in non-fullerene solar cells, with an enriched P3HT layer found at the film-surface [151]. However, they found that they could not distinguish whether the annealing increased the donor/acceptor stratification. In a recent study from our laboratory, Li and coworkers used XPS depth profiling to identify stratification of the active layer components as shown in figure 10 [81]. It was found that both surface free energies and thermal annealing affected the vertical component distribution in a non-fullerene PBDB-T:IT-M system, noting that under ambient processing, a polymer-rich layer was located at the film surface, as has been observed in fullerene systems. Likewise, thermal annealing resulted in the depletion of this polymer-rich layer if the PBDB-T:IT-

M blend was positioned on a PEDOT:PSS substrate. This was found to be advantageous in a conventional device structure as the polymer acted as a blocking layer hindering electron transport.

Surface and interfacial energies also play an important role in the self-assembly of donor/acceptor materials in the active layer. By modifying the surface energy of the interfacial layer, or by adjusting processing techniques, a donor or acceptor material can be made to preferentially locate at either the substrate or the air interface. Yan et al. used a methanol rinsing technique to induce stratification of PCBM to the film surface, finding the PCBM-rich interface was beneficial to charge transport [117]. Huang et al. found that stratification occurred in both polymer:fullerene and polymer:non-fullerene blends, and showed that by reducing the surface energy of the ITO it was possible to encourage the polymer phase to preferentially locate at this interface, thereby leaving an acceptor rich layer towards the air interface. By applying suitable layers of small molecules to control the ITO surface energy, it was also possible to control the degree of vertical stratification which enhanced overall device performance [116]. Recently, Wang and coworkers used XPS to characterize the top and bottom regions of their PTB7-Th:ITIC active layer, finding that ITIC was located towards the substrate, as shown in figure 9. The reason for this, although not explored in the article, is presumably the preferential migration of ITIC to the substrate interface (away from the air interface) due to its higher surface energy. This stratification benefitted the inverted device structure (where the acceptor-rich region located near the cathode), which had a PCE of 7.89 % compared to 6.10 % for the conventional device, as well as significantly improving device stability [156]. As in polymer-fullerene systems, the acceptor-rich region positioned at the cathode reduces the probability of recombination and aids charge extraction, with the same being true for a donor rich region located at the anode.

These few studies demonstrate that vertical stratification in non-fullerene systems follows similar mechanisms to that observed in fullerene-containing devices. That is, both solution and film-drying dynamics together with surface energy play an important role in determining the vertical stratification of active layer materials, with polymer components often preferentially located at the top surface without thermal annealing. Control of active component distribution can result in enriched layers at the anode or cathode which facilitate hole or electron transport. Care must be taken to correlate the stratification with device architecture, since an enriched layer that facilitates electron transport in one configuration may act as an electron blocking layer in an inverted structure device.
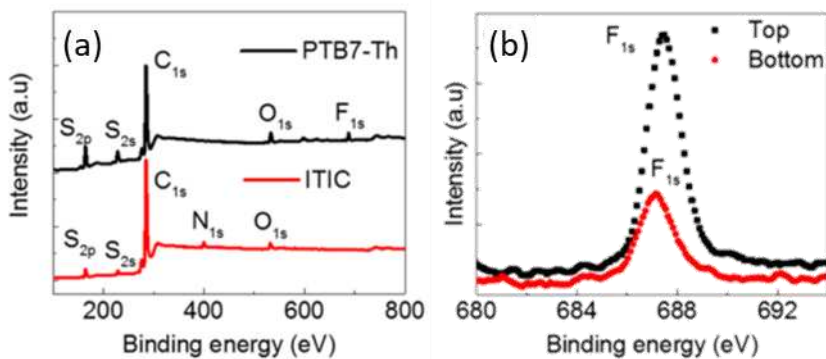

Figure 9. XPS spectra for (a) the individual PTB7-Th and ITIC films and (b) N1s (from ITIC) XPS spectra measured for the top and bottom surfaces of the PTB7-Th:ITIC blend film. Reproduced with permission from [156] . Copyright 2017 American Chemical Society**.**
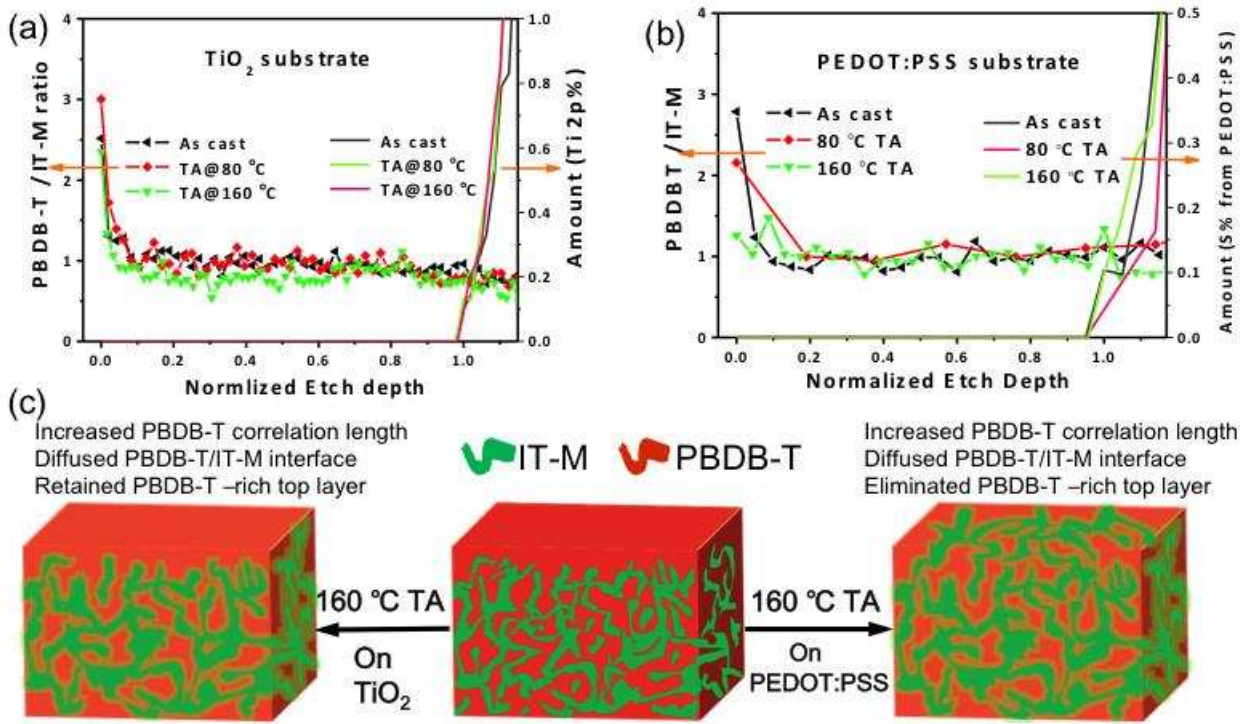
Figure 10. XPS depth profiles of PBDB-T:IT-M films cast on (a) TiO₂ and (b) PEODT:PSS substrates at different annealing temperatures. (c) Schematic of three-dimensional morphology evolution upon thermal annealing at 160 °C on TiO₂ and (b) PEODT:PSS substrates. Figure reproduced with permission from reference [81].

4. Approaches for morphological optimization

In many cases, molecular design using e.g. conjugated backbone moieties, side-chains, fluorine substitution [88,96,126,157,158], or promoting inter-chain π-π stacking [127,128,130], has a pronounced influence on the nanoscale morphology of photovoltaic blends. Early SMAs, particularly PDIs were incompatible with existing donors and suffered from strong self-aggregation due to their planar core [159]. Small molecule acceptors have differing miscibility compared to fullerenes, so when the same polymer-donors were used, the NFAs were seen to be poorly miscible as in the case of PBDTTT-C-T and PDI[153,160] (also, see reviews by Eftaiha or Lin, or Hou, Li or Yan for examples or early and new acceptors, respectively [40,66,77,161,162]). In another example, Zhou used a fluoranthene-fused imide acceptor with poly(3-hexylthiophene) P3HT, and compared its performance with PC₆₁BM [163]. While this work demonstrated the viability of non-fullerene acceptors, the poor miscibility and aggregation resulted in a poor comparative device-performance. Indeed, early SMAs did not have complementary adsorption spectra with polymer-donors such as P3HT resulting in poor light harvesting and low EQE values [164]. More recently, new acceptors have been synthesized that have suitable energy levels and complementary adsorption spectra for existing donors such as P3HT (a material that remains a popular donor material owing to its relatively simple synthesis [165] and potential for upscaling) [101,166–168]. However, the performance of OPV devices using P3HT are limited by their adsorption spectra and relatively high energy levels. Donors such as PBDB-T and PTB7-Th have better-aligned HOMO and LUMO levels to exploit the reduced need for an energetic driving force, and have better miscibility and orientational compatibility with NFAs, as will be explored in the following section [11,99,169,170]. Further advancements have been made

17

by modifying the chemical structure of donor/acceptor molecules to enhance their energy levels, compatibility and performance. The energy levels of P3HT, PBDB-T and PTB7-Th can be seen in comparison to other polymer donors in figure 13.

4.1. Acceptor design

Figure 11 shows the chemical structure and energy levels of NFAs discussed in this review. It is of note that many of the new generation of SMAs utilize electron withdrawing indanone-based end groups and an aromatic fused-ring core resulting in a ladder-like donor-acceptor-donor (A-D-A) backbone structure [171]. Such structures are beneficial since they result in strong intra-chain charge transfer between donor and acceptor moieties, creating materials that have high extinction coefficients and high absorbance (almost double that of PDI-based acceptors) while also having narrower bandgaps [172]. Furthermore, such a core structure allows four side chains to be attached to the aromatic core, a property that opens significant structural and electronic tunability, many examples of which will be outlined in this section. A notable example was reported by Zhan et al. in 2015, who showed that ITIC (3,9-bis(2-meth- ylene-(3-(1,1-dicyanomethylene)-indanone)-5,5,11,11-tetrakis(4-hexylphenyl)-dithieno[2,3-d:2′,3′-d′]-s-indaceno [1,2-b:5,6-b′]dithiophene), could surpass the PCE of fullerenes when coupled with PTB7-Th [75]. ITIC combines a broad absorption spectrum, high charge-carrier mobility and lower LUMO levels, allowing compatibility with low bandgap donors. ITIC has good electron-withdrawing properties due to its cyano- and carbonyl groups, with the rigid structure of the large alkyl-phenyl side chains facilitating π-π interchain overlap. Together with ITIC, there are many other examples of molecular engineering based on indaceno[2,1-b:6,5-b0]dithiophene (IDT) or indacenodithieno[3,2-b]thiophene (IDTT) backbones, many of which have been shown to be improvements on ITIC. Li and coworkers' IDT-IC and IDTIDT-IC are similar in nature to ITIC and are also based on fused ring molecules, with high V_{OC} achieved upon combination with PTB7-Th. This comes, in the case of IDTIDT-IC, as a result of higher LUMO levels and low recombination [70]. IDTIDT-IC has the larger conjugation length of the two, and a lower degree of rotational freedom, the first of which decreases the exciton binding energy of charges in the CT state, resulting in lower recombination and E_{LOSS}, with the latter extending PL lifetime. Several recent publications from Guo et al. reported an alternative synthetic route to control the conjugation length in n-type semiconducting molecules, with an imide-functionalized structure used to construct chains of up to 15 rings forming an electron-deficient ladder-type backbone [173–175]. The resulting A-A planar molecules have high solubility and crystallinity as well as tunable conjugation lengths, and show noteworthy electron mobility of $0.013 – 0.045$ cm^{2}V^{-1}s^{-1}. This approaches that of A-D-A molecules, demonstrating the viability of this alternative route to fabricate materials for OPVs. A more comprehensive presentation of these and other ladder-type electron acceptors can be found in a recent review by Jiang et al. [171].
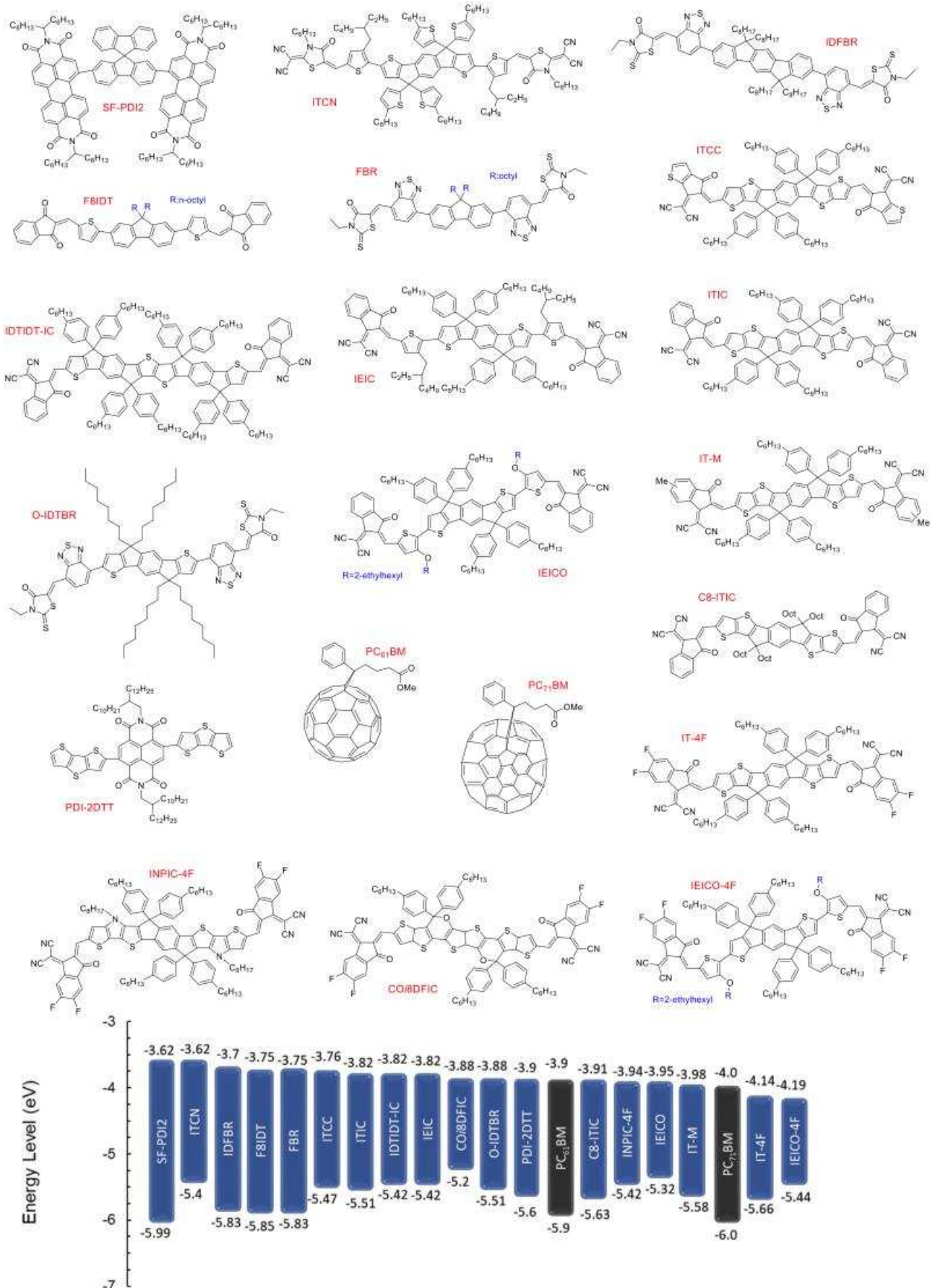
Figure 11. Molecular structures and HOMO/LUMO energy levels of fullerene and non-fullerene acceptors.

Other examples of IDT and IDTT modifications, including adding side chains to reduce the acceptor HOMO level, which, coupled with improvements in phase separation morphology and charge-carrier mobility, results in the creation of devices having high efficiency [166,176–181]. One promising direction of molecular engineering is the design of conjugated materials having different side-chains to impart improved structural properties. It has been seen that the addition of a rigid side-chains along a conjugated backbone can impart favorable phase separation and miscibility properties [60,182]. There are also many studies that support the notion that the addition of methylated, fluorinated or alkylated side chains to ITIC can improve its device-applicable characteristics [78,88,179,183–186]. Here, some of the highest PCEs to date have been achieved using fluorinated analogues of ITIC. The addition of side chains can be used to introduce advantageous mobility properties [187] or modify HOMO/LUMO levels [130]; an effect nicely demonstrated by Hsiao and coworkers, who modified a haptacyclic carbazole-based acceptor with rigid side-chains called DTCCIC-C17. It was found that the resulting acceptor had favorable miscibility resulting in low roughness and ideal domain size, together with a raised LUMO level which improved the V_{OC}.[130] Zhou et al. also showed that polystyrene-based side-chain engineering of an isoindigo-containing polymer donor can help achieve favorable phase separation with a polymeric non-fullerene acceptor P(TP), yielding high mobility, even with an energy offset of less than 0.1 eV [60]. In Hou's group, high PCEs of 13-14 % have been achieved using the fluorinated ITIC analog IT-4F [10,15]. This acceptor has down-shifted HOMO and LUMO levels, and a red-shifted absorption that complement the properties of the donor polymer PBDB-T and its analogues, as discussed in the following section.

Another method to tune non-fullerene acceptors is the use of a TBR moiety. Here, the McCulloch group have explored materials based on an IDT core with several modifications made to the chain backbone, notably using rhodanine terminations in the case of IDTBR and its derivatives [166,188]. This structure imparts good blend morphology that inhibits recombination, with the electron-withdrawing properties of rhodanine reducing the energy offset and improving the V_{OC} [179]. Of particular interest is the ability to further tune the IDTBR acceptor by choice of side chain. Holliday and coworkers compared linear (O-IDTBR) and branched (EH-UDTBR) chain modifications, realized by the addition of octyl- or alkyl moieties respectively [166]. Film morphology was studied using GIXRD, and it was found that both modifications improved crystallinity and compatibility with the donor polymer P3HT, but crucially the linear modified acceptor showed improved morphology after thermal annealing, as seen in the GIXRD data reproduced in figure 12. This resulted in a champion performance of 6.4%, as well as showing superior oxidative stability to other SMAs and fullerene derivative acceptors.
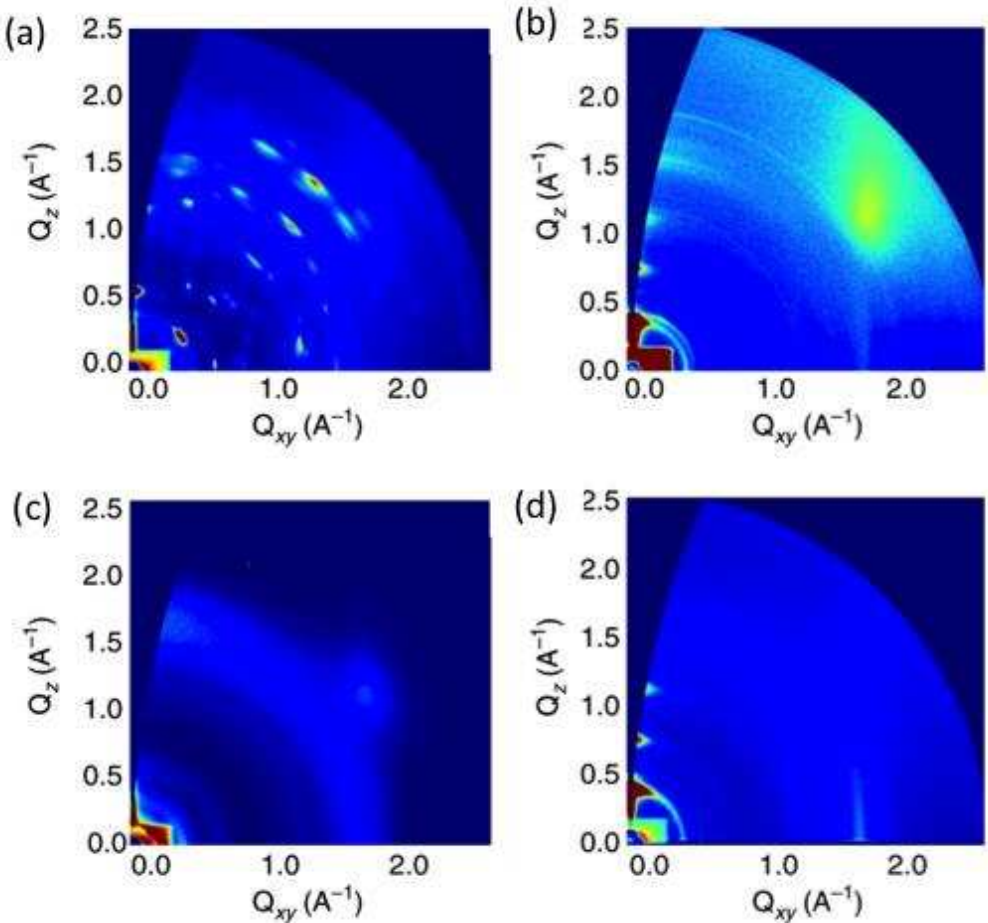
Figure 12. GIXRD of acceptors and IDTBR:P3HT blend films. (a) O-IDTBR; (b) O-IDTBR:P3HT (1:1); (c) EH-IDTBR; (d) EH-IDTBR:P3HT (1:1). Figure reproduced with permission from reference [166].

4.2. Donor design

As acceptor design moves towards highly crystalline, low-and-wide bandgap small molecules such as those detailed above, there has been a shift in donor polymer design to maximize compatibility. The most noticeable change is the downshift in HOMO and LUMO levels from traditional donors such as P3HT to maintain a small offset with ITIC-derived acceptors. To achieve this, donor polymers are of increasing molecular complexity, as can be seen by the molecular structures shown in figure 13. A key factor in improving performance is the ability to retain the correct level of crystallizability, phase separation and domain size in the blend. The crystallinity of IDT and IDTT derivatives can be suppressed by the polymer donor phase, so careful tuning of the donor (often aided by processing such as thermal or solvent vapor annealing) can improve the miscibility and morphology, improve charge transport and reduce recombination, and thereby improve device performance [183]. These factors allow for lower offsets, which are also facilitated by the electron withdrawing properties of the donor and acceptor modifications [179].
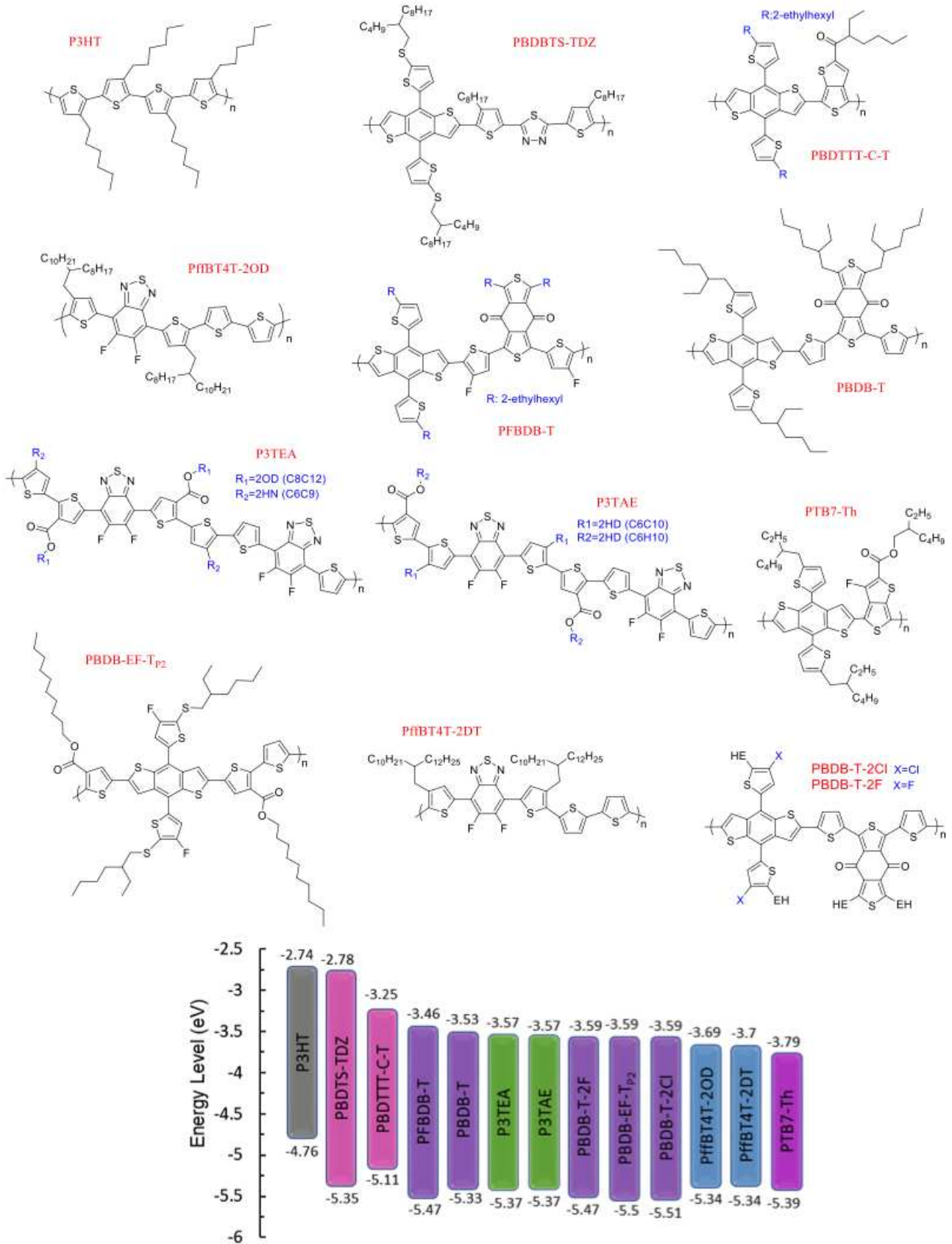
Figure 13. Molecular structures and HOMO/LUMO energy levels of polymer electron donors.

The PBDTTT-type conjugated polymer PTB7 was initially a popular alternative to P3HT and is often used in combination with PCBM, with this active layer combination showing appropriate phase separation, resulting in PCEs of around 7 % with the aid of DIO [189]. PTB7 was soon superseded by its analogue PTB7-Th, which combines a 2-ethylhexyl-thienyl group with a BDT unit. By retaining the fluorinated TT unit a lower bandgap can be achieved, which lies at -5.22 to -3.64 eV compared with -5.14 to -3.51 eV of PTB7. The molecular coplanarity also results in improved absorption, with PTB7-Th:PC$_{71}$BM devices achieving PCEs of around 9 % [190]. PTB7-Th blends form an appropriate morphology, however when used with fullerene derivative acceptors this combination has a large D$_{HOMO}$-A$_{HOMO}$ offset of around 0.6 eV. A breakthrough for polymer:non-fullerene solar cells occurred in 2015, when the non-fullerene IDT acceptor ITIC could compete with PCBM when coupled with PTB7-Th [75]. The mutual miscibility resulted in favorable phase separation forming domains that supported efficient charge transfer, with a device performance comparable with the fullerene derivatives achieved. Others researchers have shown the potential of PTB7-Th:non-fullerene systems: e.g. PTB7-Th:BTA7 blends have good charge transfer properties and achieve a low E$_{loss}$ of 0.55 eV, and a high V$_{OC}$ of 1.05 V [191], and PTB7-Th:ITIC can achieve a PCE of 10.42 % with the addition of the additive DIO to improve phase separation [192]. However, the efficiency of PTB7-Th devices is somewhat limited by its relatively narrow bandgap of 1.6 eV which limits V$_{OC}$ to below ~1 V, as well as the fact that its absorption spectra is weak over visible wavelength regions. Its absorption characteristics are similar to that of many early SMAs, and their overlapping spectra resulting in relatively low EQE values [193,194], which is a strong sign of non-optimal performance (see Figure 3c). This shortcoming has been successfully addressed by the use of low bandgap acceptors with strong adsorption in the near IR region, such as IEICO-4F [195]. The complementary absorption characteristics as shown in Figure 14a result in a broad maximum EQE of over 90 % and a PCE of up to 12.1%, despite devices having a low V$_{OC}$ of 0.71 V. In another example, IDT-derived PTB7-Th:COi8DFIC based system achieved a high EQE with a maximum of 83 % due to a wide (albeit blue-shifted) absorption spectrum, and achieved a PCE of 12.16 % with a remarkable J$_{SC}$ of 26 mAcm^{-2}. This was achieved with a V$_{OC}$ of just 0.68 V, highlighting the importance of a high EQE.[196] This system was also used as part of a ternary device (with PBDB-T) to achieve a PCE of 14 % [16].
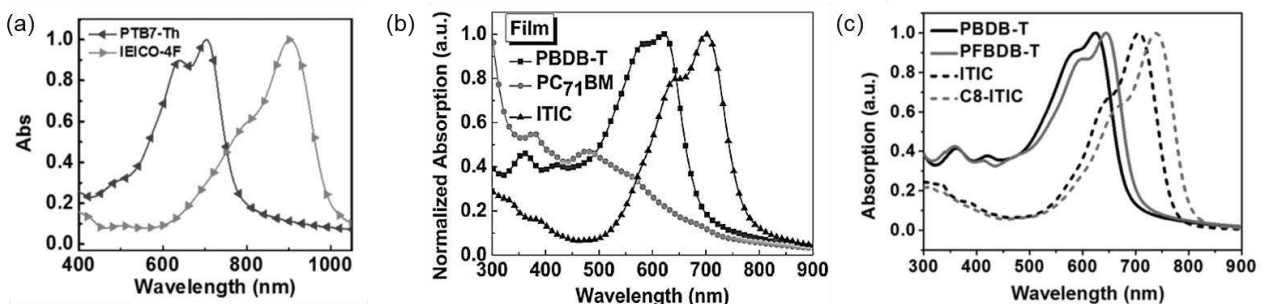
Figure 14. (a) Normalized thin film absorbance of PTB7-Th and IEICO-4F, (b) normalized absorption spectra of PBDB-T, PC$_{71}$BM and ITIC films and (c) thin film UV–Vis absorption spectrum of PBDB-T, PFBDB-T, ITIC and C8-ITIC in drop-cast films. Figures a, b and c are reproduced with permission from references [195], [76], and [11] respectively.

The aforementioned conjugated polymer donor PBDB-T follows a series of conjugated donors based on 2D conjugated benzo[1,2-b:4,5-b']dithiophene (BDT) units, such as PBDT-TPD [197], PBDTBDD [198] and PBDTBDD- T [199]. These donors are designed to incorporate side chains in order to move from a 1D to a 2D conjugated structure with suitable light harvesting properties [199]. PBDB-T emerged as a promising

candidate due to its complementary absorption spectra and strong aggregation properties which promote favorable morphology [200], and achieved PCEs of around 9.5 % with $PC_{71}BM$. When paired with ITIC, the PCE rose to 11.2 % with a V_{OC} of 0.9 V [76]. The complementary absorption spectra (seen in figure 14b) resulted in a broader EQE spectrum with a maximum of 75%. The PCE was further raised to 12 % in PBDB-T:IT-M systems, with the authors citing the elevation of the ITIC-analog acceptor's LUMO level, due to the electron-withdrawing properties of the methyl group, resulting in low voltage losses and a high V_{OC} of 0.97 V [78].

One of the most successful non-fullerene OPVs to date, used to create devices having a PCE of over 13 %, comes as a result of side-chain modification of PBDB-T. Here, Fei and coworkers used a fluorinated PBDB-T (PFBDB-T) donor and a modified ITIC acceptor with linear alkyl side chains to form C8-ITIC [11]. In both donor and acceptor, the alkyl side chains reduce the optical bandgap, and notably increase the crystallizability of the blend, thus improving mobility and reducing recombination. This was demonstrated by GIWAXS measurements, which are shown in figure 15. While ITIC crystallization is suppressed in the polymer phase with no characteristic peak observed, C8-ITIC displays a well-defined peak around $q \approx 0.36$ A^{-1} (d ≈ 1.75 nm), which is further enhanced by thermal annealing. Overall, improved device parameters resulted from red- and blue- shifted absorption spectra of the alkylated acceptor and fluorinated donor respectively (figure 14c) which resulted in a superior EQE. The fluorinated donor had deeper HOMO and LUMO levels, which resulted in a lower energy offset and improved V_{OC}. Two other OPVs achieved PCEs over 13 % by employing similar strategies; using both a fluorinated PBDB-T (PFBDB-T-SF or PDTB-EF-T) donor and an IT-4F acceptor [10,15]. It was found that both hole and electron mobility in the donor and acceptor respectively were improved, with HOMO and LUMO levels slightly downshifted. It was also suggested that fluorine modifications impart good chemical stability and polarizability. Further improvements to this system were achieved by employing a chloride substituted PBDB-T (namely PBDB-T-2Cl) with IT-4F, resulting in a PCE of 14.4 % [14]. The chlorine, substituted for fluorine, simplified chemical synthesis and did not affect polymer confirmation, and could lower the energy levels of the donor further reducing the D-A offset, resulting in a higher V_{OC} of 0.86 V.
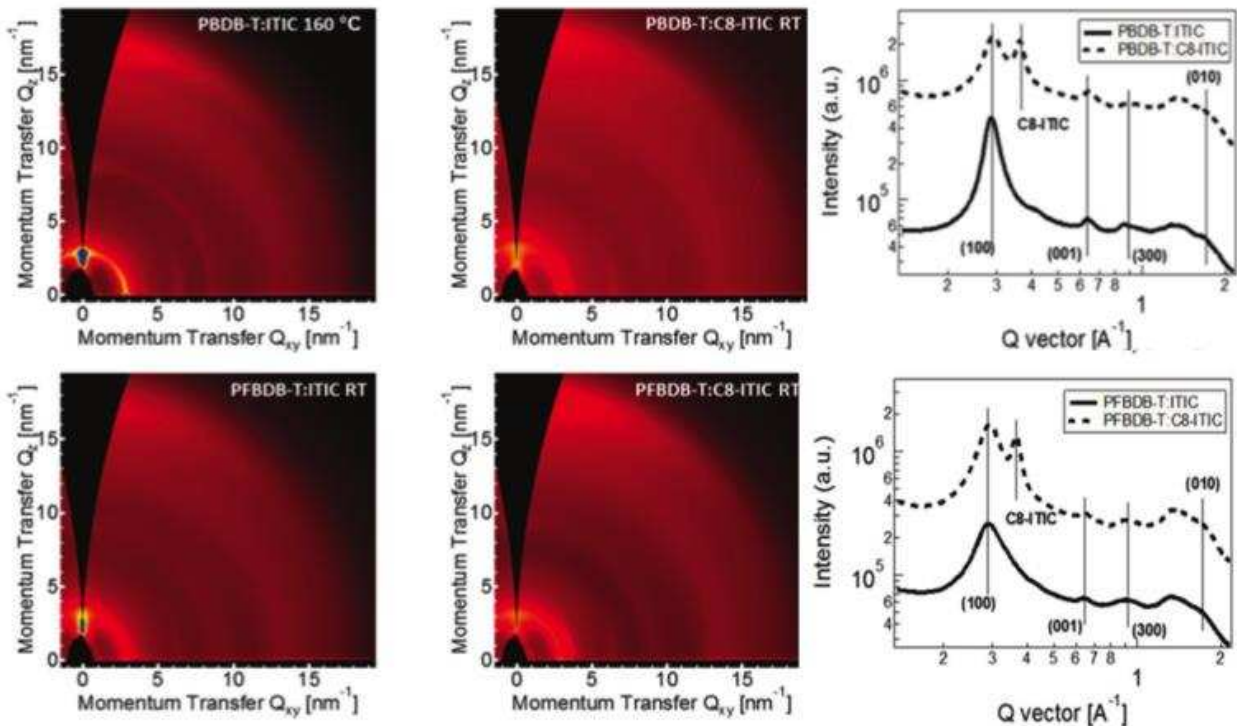
Figure 15. 2D GIWAXS patterns of blends of PBDB-T/ITIC, PBDB-T/C8-ITIC, PFBDB-T/ITIC, and PFBDB-T/C8-ITIC processed under optimized conditions for device performance. Figure reproduced with permission from reference [11].

It is clear that there are many promising candidates, especially ITIC and its derivatives, which provide a family of excellent non-fullerene electron acceptors. Some of the most beneficial factors these new SMAs bring to non-fullerene solar cells are the ability to fine-tune the HOMO and LUMO levels to match those of the donor, reducing the energy offset, and often red-shifting the absorption spectra, resulting better light harvesting, higher EQE, higher V_{OC} and overall improved PCE. Improvements in photovoltaic device performance would impossible without pairing these acceptors with suitable conjugated polymer donors; modifications of ITIC-derived acceptors, and tuning the donor polymer PBDB-T have both played a vital role in the continuing success of these new SMAs because of their tunability and morphological and spectroscopic compatibility. There are also promising signs in PTB7-Th based devices, such as the high J_{SC} from PTB7-Th:COi8DFIC, or the high EQE of PTB7-Th:IEICO-4F with relatively low V_{OC}, that indicate that there is still room for improvement in device efficiency.

4.3. Ternary strategy

Researchers have found that the introduction of a third component, as a second donor or acceptor, can offer a further opportunity to manipulate the morphology and phase separation compared to binary systems, in addition to extending photon absorption characteristics and enhancing charge carrier mobility [82,201–204]. In polymer:fullerene systems, strategies for realizing a ternary device generally rely on the use of a second donor polymer or small molecule in a blend with PCBM [82]. Successful ternary OPV devices with improved efficiency have also been achieved using non-fullerene SMAs as the third component, together with PCBM or another SMA electron acceptor [205]. As depicted in figure 16, the third component can be embedded in the primary donor or acceptor domain, or located at the interface of the primary donor/acceptor domains. Alternately, it can form continuous network and work with the primary donor or acceptor as a new

solar cell in parallel with the primary one, or form alloy with the primary donor or acceptor if miscibility requirements are met [206,207].
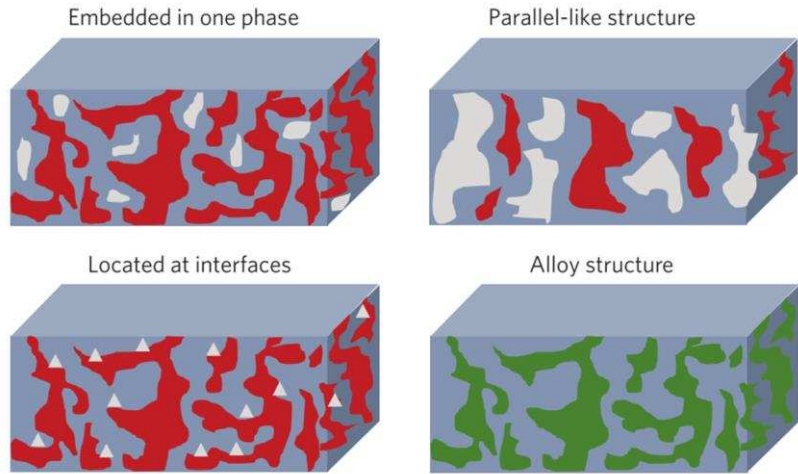
Figure 16. Schematic of the microstructure of ternary BHJ solar cells. Figure reproduced with permission from reference [206].

Several optoelectronic processes can occur, separately or in combination, creating multiple energy transfer pathways between the three components in a ternary OPV device as shown in figure 17b. Here, photons absorbed by the third component can generate excitons and therefore work as a separate cell in addition to the primary cell [207]. However, energy can also be transferred to the other donor material via Forster resonance energy transfer, where there is an overlap between the absorption band of the acceptor and the emission band of donor [208]. A charge transfer process can also occur in a ternary system, where holes or electrons can be transferred from one component to another component before being collected at their respective electrodes [209].
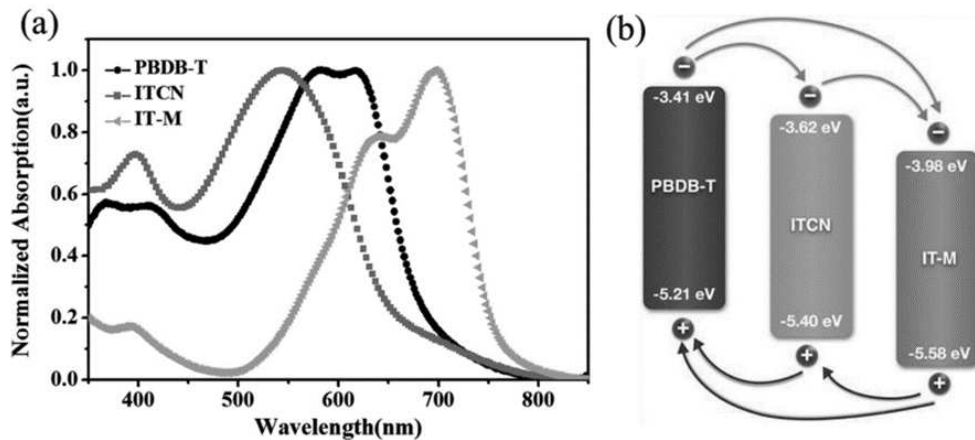
Figure 17. (a) Normalized UV–Vis absorption spectra of PBDB-T, ITCN, and IT-M films. (b) Schematic of energy and charge transfer in a PBDB-T:ITCN:IT-M ternary solar cell. Figure reproduced with permission from reference [210].

Ternary strategy has been successfully utilized to improve non-fullerene OPV performance. For example, Zhao et al. used PCBM as a third component in a PBDB-T:IT-M system, where its energy levels sit between donor and acceptor, allowing cascading energy transfer in both directions. The PCBM provides increased optical absorption and, at low concentrations, results in favorable phase separation leading to an improved PCE over that of the binary device [211]. In a PTB7-Th:BTR:PC$_{71}$BM ternary system studied by Zhang et al [169], broadening of absorption occurred over the visible range (the absorption spectrum of BTR in the short wavelengths complements that of PTB7-Th). BTR was also found to have a favorable influence on blend morphology and reduced the $\pi-\pi$ stacking distance and increased domain purity, leading to better charge transport and reduced recombination. As shown in figure 18, the addition of smaller amounts of BTR (25%) increased the efficiency of out-of-plane $\pi-\pi$ stacking, as seen in the (010) PTB7-Th peak which direction shifts to a higher q from 1.53 Å^{-1} to 1.67 Å^{-1}, resulting in optimal d-spacing of around 3.77 Å, and gave the highest domain purity.

Some of the most remarkable performances in single junction BHJ solar cells have been achieved using this two-acceptor ternary strategy by combining both fullerene and non-fullerene acceptors. For example, Li et al. achieved a champion PCE in excess of 14 % in PTB7-Th:COi8DFIC:PC$_{71}$BM OPV cells [16]. Here, the wider bandgap of the PC$_{71}$BM resulted in cascading energy transfer to both donor and primary acceptor, albeit at the expense of V$_{OC}$, whose low value of 0.727 indicated there was still further capacity for optimization. Zhao et al. achieve a V$_{OC}$ of around 0.95 and a PCE of 12.2 % using a ternary configuration of PBDB-T:PC$_{70}$BM:IT-M [211]. In this case, the PCBM acted as a third component and served to increase the charge-carrier mobility of the other components due to its location at the blend interface.

There are an increasing number of examples of non-fullerene ternary systems, which show great promise. In a recent review, Xu and Gao outlined the benefits of non-fullerene ternary systems [212], including better control of ternary component distribution as design rules for tuning polymer and small molecule morphologies are better understood. They highlighted the need for more suitable polymer donors to better match the energy levels of the wide range of non-fullerene acceptors. The use of complementary non-fullerene acceptors can also be used to increase the coverage of the OPV absorption spectrum, tune energy levels, and provide morphological optimization [213]. For example, Jiang et al. studied the inclusion of a second acceptor ITCN to PBDB-T:IT-M[210], with ITCN having comparable HOMO/LUMO energy levels to bis[70]PCBM (-3.62 and -5.4 eV compared to -3.83 and -5.60 eV respectively). As was observed in its fullerene counterpart, this strategy facilitated a cascading energy transfer route in both directions, as well as creating a complementary absorption spectra as shown in figure 17a. PBDB-T:ITCN:IT-M OPV cells had a champion PCE of 12.16 % compared to 12.2 % with bis[70]PCBM, indicating that small molecule acceptors are suitable fullerene replacement as electron-cascading ternary components in OPVs.
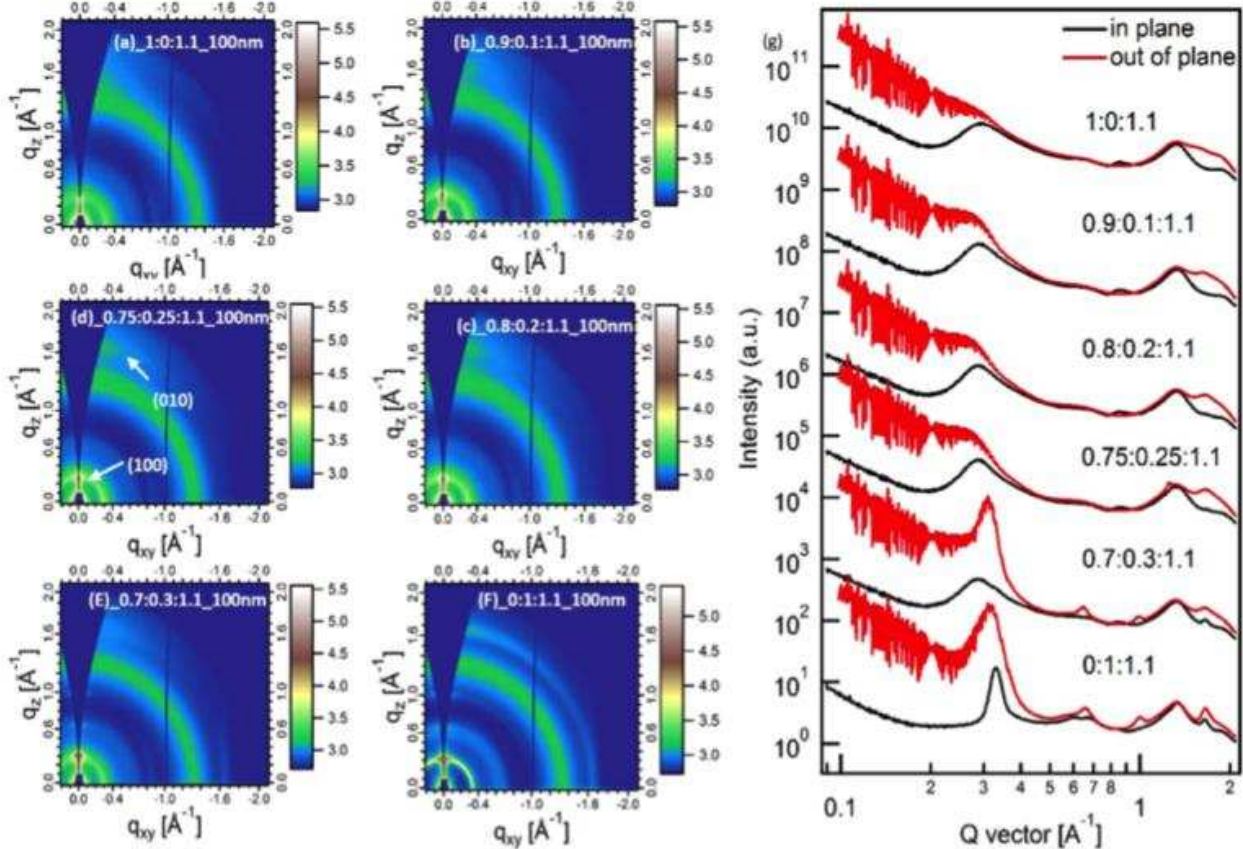
Figure 18. (a–f) GIWAXS 2D patterns for the ternary system PTB7-Th:BTR:PC$_{71}$BM blend films with various contents of BTR, (g) 1D profiles in in-plane and out-of-plane directions. Figure reproduced with permission from reference [169].

Another impressive non-fullerene ternary system (in this case employing a dual donor system), was demonstrated by Ma and coworkers using two well-known donors: PBDB-T and PTB7-Th. The donors had good miscibility and broadened the photon absorption range to 300-1000 nm using the wide gap IDT-derivative acceptor IEICO-4F. Their OPV cells had a high J$_{SC}$ of 24.14 mA cm and a PCE of 11.62 % [214]. Here, the PTB7-Th acted as an intermediary component for electron transfer, and was able to modify the molecular arrangement of PBDB-T, improving morphology with particular enhancement in the (100) peak evidenced by GIXD. This indicated a so-called 3-D molecular orientation (a favorable mixture of face-on and edge-on π-π stacking). Xu et al. also used PTB7-Th and PBDB-T in conjunction with the IDT-derived acceptor SFBRCN, citing the complementary adsorption spectra, small offset between the donors and acceptor, as well as hole-back transfer between the two donors as the reasons for improved efficiency[215][215][215][215][215][215]. The multiple FRET pathways between the three components served to reduce recombination and improve charge separation, resulting in a high V$_{OC}$ of 0.93 and PCE of 12.27 % [215].

4.4. Optimizing morphology via control of molecular aggregation in solution

The solution state of donor-acceptor mixtures is an important component in the creation of a favorable active layer morphology, and careful control of miscibility in the solution state has been seen to be as effective as post-deposition treatments in creating appropriate morphological conformation. Here, molecular

aggregation in the solution state is thought to be an important precursor to crystallinity and domain purity [198], however excessive aggregation results in the formation of rough films and oversized domains with poor D:A interfacial contact. Efficient solution processing must deliver an optimal aggregation-controlled domain purity while maintaining smoothness of the solid-state layer. The concentration, molecular weight, solvent, aging time and temperature of the solution are all key influencing factors, and studies have shown that aggregation and ordering characteristics in the solution state are highly correlated with those of the solid state [216]. Figure 19 lists techniques used to investigate the material characteristics in solution state.
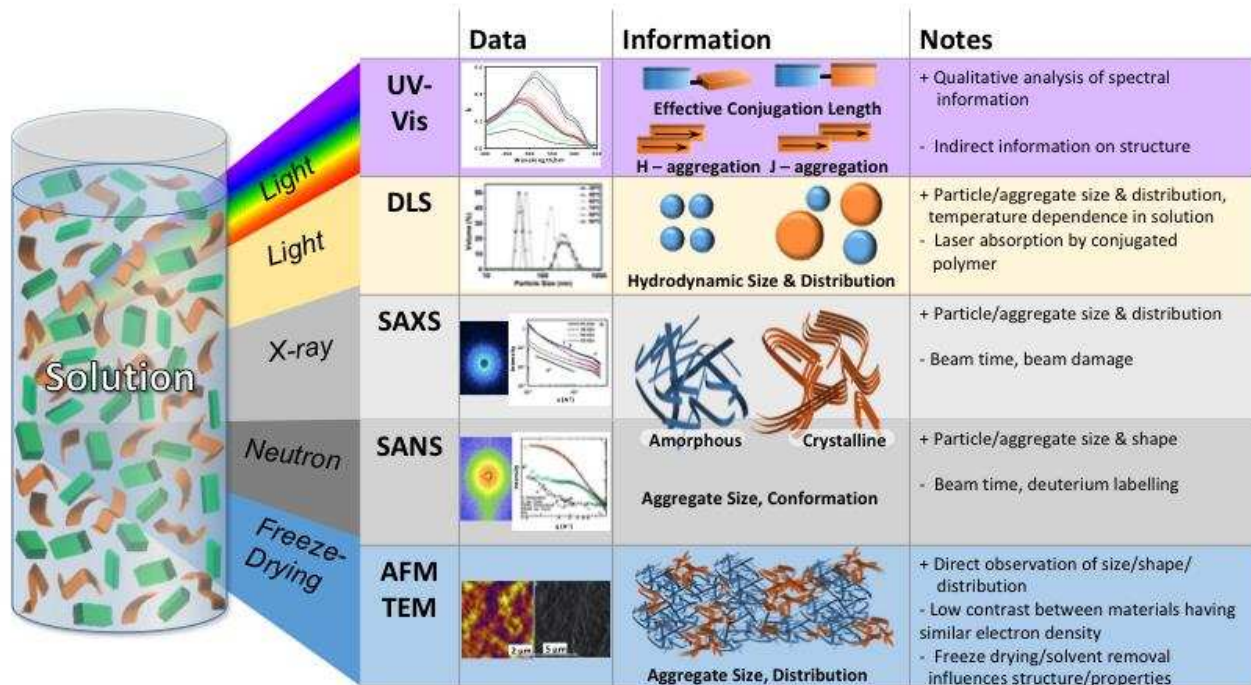
Figure 19. Characterization techniques of photovoltaic blends in solution state. Images in the "data" column are adapted with permission from the following references: UV-Vis [217], DLS [218], SAX[219], SANS[113], AFM & TEM [220].

There are many interesting reports on the control of aggregation in solution and its effect on the miscibility with a fullerene acceptor. However, there are obvious differences in the structural properties of conjugated polymers, fullerene derivatives and small semiconducting molecules. Semiconducting polymer donors consist of repeating units with varying molecular weights, with total lengths varying from tens to a few hundreds of nm (high-M_w P3HT molecules, for example, have a length of 80 nm [221]). Fullerene derivatives are mainly ellipsoidal with a diameter of around half a nanometer, with clusters commonly forming having a size of 30 - 100 nm. In contrast, small molecule acceptors are planar molecules with sizes of several nm (ITIC for example is platelet shaped with dimensions 2 x 3 nm), which also form aggregates but with very different surface energies, steric behaviors, and chemical properties. It follows that the mixing behavior of donor / non-fullerene systems are most unlikely to be analogous to those in polymer-fullerene systems, with the solution dynamics of these systems not yet being well explored. Nonetheless, there are lessons to be learned from the solution dynamics of other systems.

In polymer:fullerene systems, it is well documented that changes in miscibility and aggregation are related to the solution stirring / ageing time. In P3HT:PCBM, for example, the PCBM can diffuse into

aggregated polymer regions over time, forming unfavorable micro-domains (considered as domain impurities) [222]. However, this same trait can be beneficial, as demonstrated by Han et al. who found that the performance of PTB1:PCBM increased with up to 48 hours solution ageing, before undergoing over-mixing and diffusion of PCBM into polymer domains [223]. Twisted molecules can have a similar effect to bulky side groups, and Liu et al. reported a similar effect when using the small molecule acceptor TPE-PDI$_4$. While PDI is known to aggregate easily in solution, the highly twisted structure of TPE prevents aggregation; a feature that enabled them to achieve more favorable domain sizes in the final films [224].

It has been seen that polymer solutions at high concentrations can become highly entangled, leading to improved phase separation when blended with fullerenes, which is then reflected in enhanced domain purity and crystallinity of blended films [225]. The solution properties of the polymer, e.g. longer chains, that are more entangled and thus stiffer, can suppress the miscibility of PCBM resulting in purer domains and better stability [226]. Although there exists a limit over which longer molecular chains are no longer favorable [227]. In a polymer:non-fullerene solution, Eastham et al. saw that by increasing the molecular length (M_n) of the donor polymer, the aggregation and crystallization behavior in the solution could be tuned [228]. Ma and coworkers showed that low and high molecular weight (M_w) solutions of the polymer donor PffBT4T-2OD have different aggregation behavior, with a low M_w polymer forming significantly less aggregates, leading to mixed phases and poor domain purity [229]. In the solid state, both systems underwent lamellar stacking, however the higher M_w system had better molecular ordering with enhanced in- and out-of- plane π-π stacking. This was attributed to aggregation and correlated with improved charge mobility. As discussed earlier, side-chain modification can impart many properties including enhanced rigidity of molecular structure. This can be done in such a way to improve the solubility, as in the case of DTCCIC-C17 (an IDT-derived acceptor modified with bulky 4-octylphenyl side chains), which reduced intermolecular interactions (due to the positioning of the side chain at the nitrogen) and improved solubility [130].

By increasing the solution temperature of semicrystalline polymers above their melting temperature, and then controlling the film-forming temperature, molecular arrangement can be controlled. For example it has been shown that the orientation can be flipped from face-on to edge-on (and indeed vice versa [110,230]) by slowing the cooling rate [231], In many other works [2,42,48,94,126,232,233], the temperature dependence of the solution state can be used to tune aggregation in solution. For example, Qian et al. demonstrated the temperature dependence of PBDTBDD aggregation in solution [198]. It was shown that aggregation behavior is controlled by the interchain π- π interactions; at low temperature, there is high steric hindrance resulting in strong aggregation of these chains, whereas at high temperature, the steric hindrance effect is reduced and aggregates do not form. In UV-Vis spectroscopy, a red shift (indicating less aggregation) is seen from the well-mixed polymer-fullerene blend at high temperature compared to the aggregated mixture at room temperature (shown in figure 20), whereas the low temperature solution matches the spectra of the as-cast film. However, temperature did not seem to affect molecular orientation, as seen from GIWAXS data. It was noted that best device performance was seen from films that had moderate aggregation in solution, i.e. those were cast from low temperatures. Similar temperature-dependent aggregation has been seen using donor polymers PffBT4T-2OD and P3HT [234]: In PffBT4T-2OD, Liu and coworkers observed a similar temperature dependence, but found the crystallization process to be dependent on the drying process. A device PCE of 10.4 % was achieved by casting films from a warm solution, and then adjusting the spin speed to control the crystallization [94].
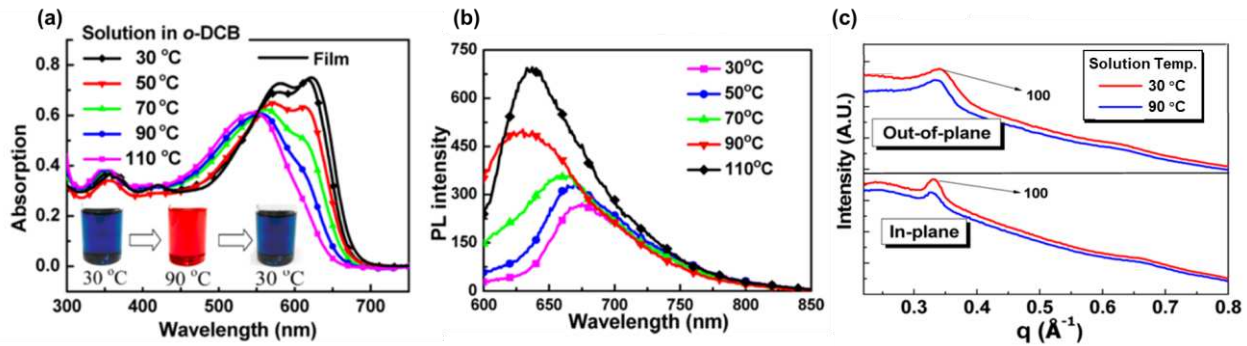
Figure 20. (a) Comparison of UV−Vis spectra for PBDTBDD in a film state, and in o-DCB solutions prepared at different temperatures (b) Temperature-dependent photoluminescence spectra of PBDTBDD in o-DCB. (c) GIXD curves for PBDTBDD. Figure reproduced with permission from reference [198].

A major difficulty in correlating solution properties with the solid-state film morphology lies in characterizing the solution state. In many cases, absorption profiles in solutions are indistinguishable [235], and most other techniques are unable to characterize liquid systems. Zheng et al. provided an interesting insight into the relationship between a conjugated polymer and its suspending solvent by comparing the effect of a good and bad solvent for a BDOPV-based polymer, with controlled addition of a bad solvent fraction being able to favorably tune aggregation [220]. In order to observe the effect of these solvents on the polymer in solution, they borrowed an innovative technique from bio-molecular studies in which a solution is freeze-dried in liquid nitrogen before an AFM cross section image is measured. This allowed them to observe the solution-state properties with solid-state techniques. It was found that the polymer formed 1-D rod-like structures in a good solvent (oDCB, figure 21 b-e$_1$), but formed a 2-D lamellar structure in a poor solvent (toluene, figure 21 b-e$_2$), which correlated with trends in higher crystallinity and electron mobility. From GIWAXS measurements, it was found that in the mixed solvent solution, some aggregates formed with an intermediate state between the 1-D and 2-D structures (figure 21 b-e$_3$)), without interrupting the favorable geometry achieved in the good solvent. By adjusting the concentration of toluene in solution, they were able to control the aggregation. It was found that the polymeric structures observed in solution could be passed on to the solid state films, with aggregation caused by the poor solvent resulting in favorable crystallinity and domain interconnectivity, and using 20 % toluene a peak value of electron mobility was obtained.
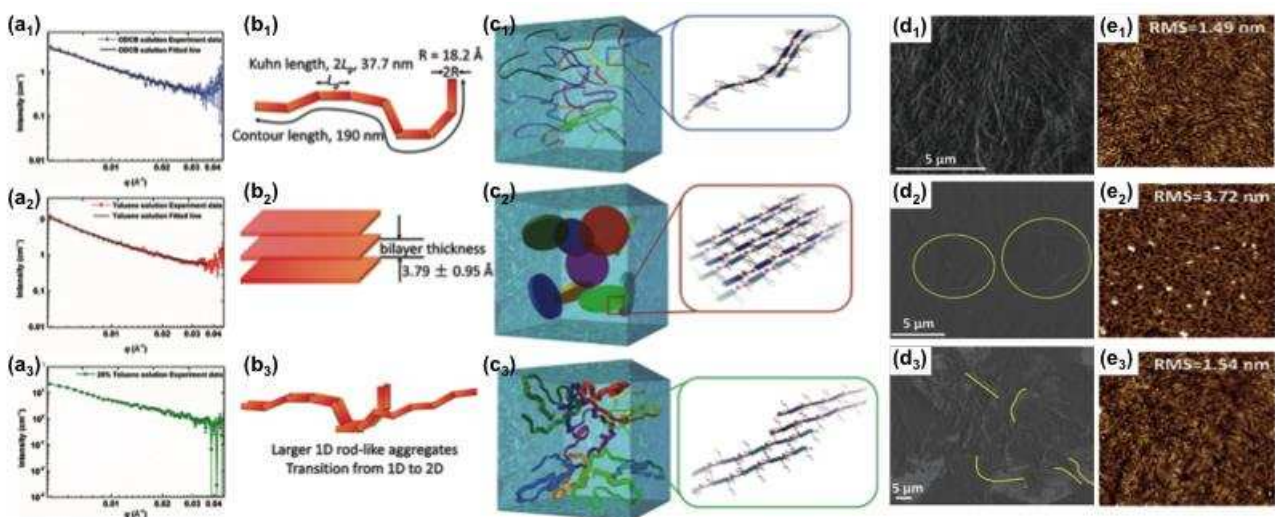
Figure 21. SANS intensity plots of BDOPV-2T solutions using (a$_1$) oDCB, (a$_2$) toluene, and (a$_3$) toluene:oDCB (2:8) as solvent. (b$_1$) diagram of 1D rod-like chain for polymers in oDCB obtained from

SANS analysis, and (c1) proposed rod-like polymer aggregates in oDCB. (b₂) diagram of 2D lamellar polymers in toluene, (c₂) proposed lamellar polymer aggregates. b₃) diagram of polymer aggregates transition from 1D rod-like structure to 2D lamellar structure, (c₃) proposed polymer aggregates in toluene:oDCB (2:8) mixed solvents. SEM image of freeze dried BDOPV-2T in (d₁) oDCB, (d₂) toluene solution, and d₃) toluene:oDCB (2:8) mixed solvents. AFM height images of solid-state BDOPV-2T films cast from (e₁) oDCB, (e₂) toluene solution, and (e₃) toluene:oDCB (2:8) mixed solvents. Figure reproduced with permission from reference [220].

Non-fullerene materials are often composed of a core molecule bolstered by side chains that can modify both semiconducting and structural properties. Planarization in these molecules occurs due to the covalent attachment of adjacent aromatic units, and this bestows beneficial coplanarity and good semiconducting properties. However, the effect of these structural designs on the attractive interactions between molecules is another important consideration when designing non-fullerene acceptors. In highly coplanar molecules, strong π-π interactions can result in insolubility [236]. Highly planar SMAs have shown a propensity to π-stack in solution leading to insolubility and self-aggregation, so it is necessary to balance the planarity with the tendency to aggregate in order to optimize the performance. As we have seen, molecular engineering of side chains to fused-ring SMAs is a pathway to modify the degree and orientation of π-π stacking, extend the conjugation length, enhance charge mobility and adjust the energy band-gap [237]. The design must also address molecular interactions in solution in order to facilitate good device morphology. For example, Zhang et al. used alkyl side chains to tune both solubility and π-π stacking in a series of IDT derived acceptors [236]. A fluorinated analogue of ITIC was used named FTIC (with a fluorenedicyclopentathiophene core and 2- methylene-(3-(1,1-dicyanomethylene)-indanone end caps) as the base acceptor due to its planar backbone and compatibility with side chain modifications [238]. The length of out-of-plane alkyl side chains was varied and a correlation was found between device performance and the length of the side chains, with longer n-hexyl and n-octyl groups performing better. It was found that all modifications promoted good solubility in various solvents, however devices using the acceptor substituted with two n-hexyl and four n-octyl side chains (FTIC-C6C8) had the best microphase separation and electron mobility. The longer side chains of the optimal acceptor induced a fibrous structure in the polymer donor PBDB-T which enabled good interfacial contact between the D:A phases.

4.5. Optimizing morphology during film casting

4.5.1. Solvent and additive processing

Solvents and solution additives provide a means to influence both the solution state behavior, and morphology and orientation after film formation. In polymer:fullerene systems, one of the most widely used additives is 1,8-diiodooctane (DIO) [239]. By adding a small amount of DIO, this additive can selectively dissolve PCBM, and has been seen to improve phase separation [240], aggregation [241], tune domain size and purity [95,104,242], and increase π-π stacking coherence length.[92] The high boiling-point of DIO (~332 °C) results in an extremely slow rate of evaporation, with reports of DIO remaining in the solid film many hours after casting [95,243]. This slow drying enables formation of well-orientated and purer crystalline domains.

However, similar strategies applied to polymer:non-fullerene solutions may not yield positive results. Song et al. reported a direct comparison of PTB7-Th with PC₇₁BM and ITIC acceptors, finding that while 3 wt.% DIO optimized domain sizes and purity in the fullerene system, the same treatment resulted in overly separated phases in the non-fullerene system [244,245]. The GIWAXS of pure PTB7-Th films cast with and without DIO have also been measured, indicating that the addition of DIO reduces the alkyl stacking distance

(peak at q= 0.26 Å⁻¹) from 24 to 23 Å. This demonstrates that DIO is a good solvent for IDT-derived acceptors as it affects their alkyl side chains, but it must be used selectively to achieve the desired effect. Indeed, the use of DIO as a solvent additive has been seen to have a beneficial effect in other non-fullerene systems. Zhao et al. found that PBDB-T:ITIC out-performed its fullerene counterpart thanks, in part, to the addition of 0.5 wt.% DIO which produced a favorable aggregation resulting in good charge transfer, low energy loss and high performance [76]. It is likely that DIO influences the orientation of the alkyl side chains present on the IDT backbone, reducing steric hindrance between molecules leading to better miscibility. This in turn promotes finer phase separation and creates purer crystalline phases [138]. This was nicely demonstrated by Ye *et al.'*s GIWAXS measurements on polymer:non-fullerene systems with and without DIO, which showed a strong increase in crystallinity after processing with DIO as seen in figure 22 [246]. Films cast with DIO showed a strong increase in the out-of-plane π-π stacking diffraction peak at around 1.7 - 1.8 Å⁻¹. The polymer donor's π-π coherence lengths doubled in PBDB-T:IT-DM and PBDT-T:IT-M systems, resulting in improved charge transport. Similarly, Hsiao et al. modified another IDT-derived acceptor by adding rigid side chains to modify the molecular structure and to adjust the LUMO level, and found that a PCE of 8.16 % observed in inverted devices was boosted to 9.48 % with the aid of DIO [130]. It is noteworthy that in both cases and others [247], the authors obtained optimal efficiencies using a combination of thermal annealing and addition of DIO, indicating that for these IDT derivatives, the additive benefits the solution properties of the co-solvent, but film drying properties must ultimately be adjusted by thermal annealing (to influence drying speed, or remove residual solvent).
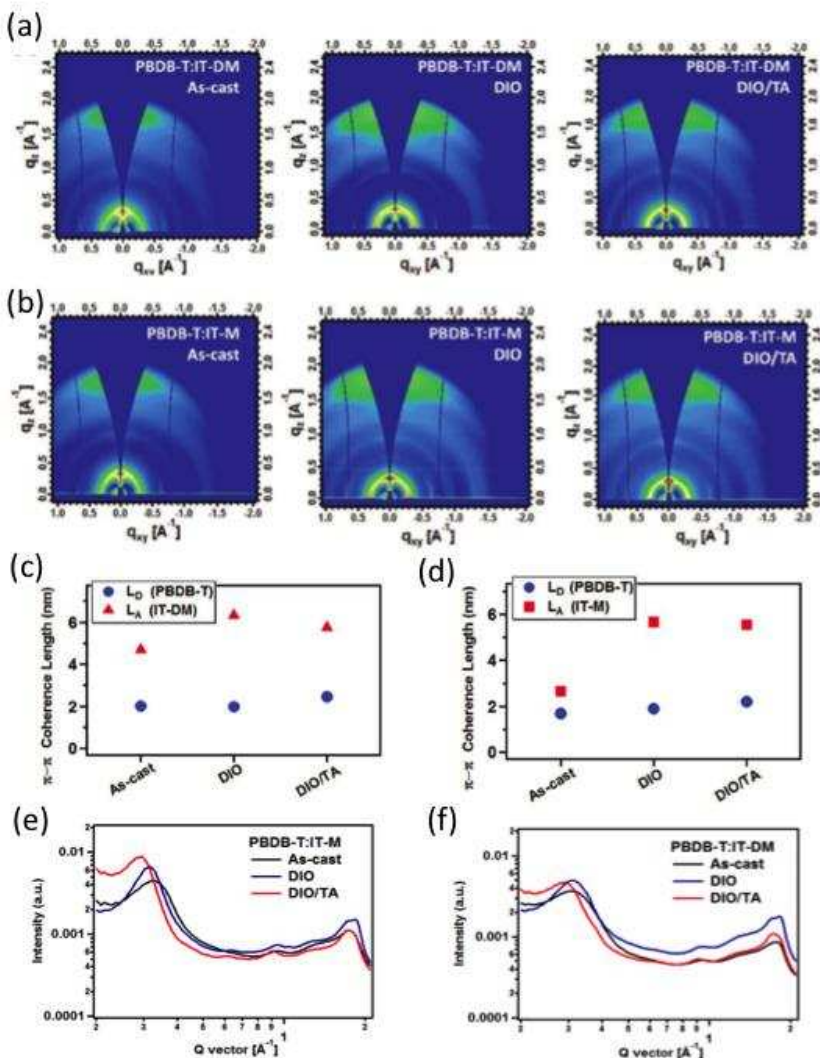
Figure 22. 2D GIWAXS patterns of (a) PBDB-T:IT-DM and (b) PBDT-T:IT-M blend films using different processing routes. OOP ($q_{xy} = 0$) π-π coherence lengths of the polymer and SMA in the (c) PBDB-T:IT-DM and (d) PBDB-T:IT-M blend films. OOP 1D profiles of (e) PBDBT:IT-M; (f) PBDB-T:IT-DM blend films processed via various conditions. Figure reproduced with permission from reference [246].

Another high boiling point solvent additive employed in a similar manner is 1-chloronaphthalene (CN) [248]. Song et al. explored the effects of various amounts of CN as a co-solvent on PTB7-Th:IEICO-4F films [195]. With increasing concentration of CN additive, the authors found increases in crystallization, with stronger π−π stacking peaks in the blend. The coherence length of the IDT-derived acceptor also increased from 2.8 to 4.0 nm in the optimized system comprising 4 % CN. Interestingly, a change in the ratio of edge-on to face-on molecular orientation was observed, with a maximal amount of favorable face-on orientation seen with at the optimal CN concentration. These effects were attributed to the high boiling-point of CN ($\sim$269 °C) which significantly slowed evaporation and film drying, allowing purer crystal domains to be formed and inducing the orientational switch, resulting in increased charge transport and reduced recombination. The PCE of devices increased from 9.41 to 12.8 % with a notable increase in FF. Above 4 % CN, device performance decreased, and it was postulated that this was due to coarsely separated phases.

It is also possible to choose a pair of additives to selectively influence the donor and acceptor. This strategy has been successfully employed in fullerene systems; for example the high boiling point solvents DIO and CN have been used to control PCBM crystallization and polymer solubility respectively [249,250]. The same binary additive combination has also proved to be effective in non-fullerene OPV systems, with reports of improved performance over neat or single additive systems [168,251]. One such example is work on PBDTBDD:SDIPBI devices, whose efficiency increased from 3.11 % to 3.91 % PCE with the addition DIO, and then further to 4.39 % with DIO and CN. XRD was used to observe the crystal diffraction peaks and it was found that the combined additive devices had stronger π-π stacking.[164] This is indicative that such additives promote aggregation in solution and, along with their slower evaporation time, lead to purer domains that are reflected in higher charge-carrier mobilities.

Despite the benefits of the use of high boiling-point additives, their slow evaporation brings some drawbacks such as slow fabrication time; devices are typically held under vacuum for 12 hours to remove any residual solvent. Given that there is a high likelihood of residual solvent remaining in the film, the propensity of these molecules to generate radicals under UV illumination [252] or create a pathway for oxygen to penetrate the film which in turn leads to film degradation and poor device stability. Holliday introduced an alternative pair of additives, namely the low boiling-point solvent o-xylene (o-XY, boiling point 144.4 °C) and small the conjugated molecule N-methylpyrrolidone (NMP, boiling point 202 °C), which were able to favorably influence the drying conditions despite their comparatively lower boiling-points and retain better device stability than devices made with high boiling-point additives [253].

4.5.2. Retarding crystallization

In many examples, synthesis routes or processing techniques have been used to increase molecular order or crystallinity, e.g. by increasing aggregation in solution [228,229] or through solvent vapor annealing (SVA) to enable greater molecular ordering [254]. However, some of the latest indanone-derived acceptors show an extreme tendency to crystallize (see figure 23a,b), which unfavorably increases phase separation between donor and acceptor, resulting in poor charge transport properties. In a very recent report, Li and coworkers demonstrated a novel way to controlling excessive crystallization in PTB7-Th:COi8DFIC and PBDB-T:INPIC-4F non-fullerene solar cells by casting films on hot substrates [13,255]. They demonstrated

the ability to increase or decrease molecular order via casting in the presence of solvent vapor or casting on a hot substrate respectively. By retarding the crystallization of INPIC-4F, it was inhibited in forming large spherulites and instead underwent fine phase separation with the donor PBDB-T. This lead to a material in which there was efficient exciton dissociation and balanced charge transport, leading to a maximum PCE of 13.1%. Notably, by hot-substrate casting the PTB7-Th:COi8DFIC system, the molecular order and orientation of COi8DFIC can be tuned from flat- and edge- on lamellar crystalline to H- and J- type $\pi-\pi$ stacking (figure 23a). This results in broadened photon absorption (see figure 23c) and fine phase separation with the electron donor PTB7-Th. This favorable morphology with face-on $\pi-\pi$ stacked electron donors and acceptors promotes efficient exciton dissociation at the donor/acceptor interface, together with enhanced and balanced carrier mobility. As shown in figure 23d, The enhanced short-circuit current density and fill factor lead to devices having a maximum PCE of 13.8 % in binary, single-junction PTB7-Th:COi8DFIC non-fullerene polymer solar cells, with such devices also exhibiting superior stability. This hot-substrate casting method could be adopted during large-scale roll-to-roll device fabrication process, and is therefore a promising approach for morphology control. We envisage that other approaches to control molecular configuration during solution casting, e.g. employing solvents with different evaporation rates, can also lead to enhanced control of molecular order and aggregation which will ideally be used to improve device performance.
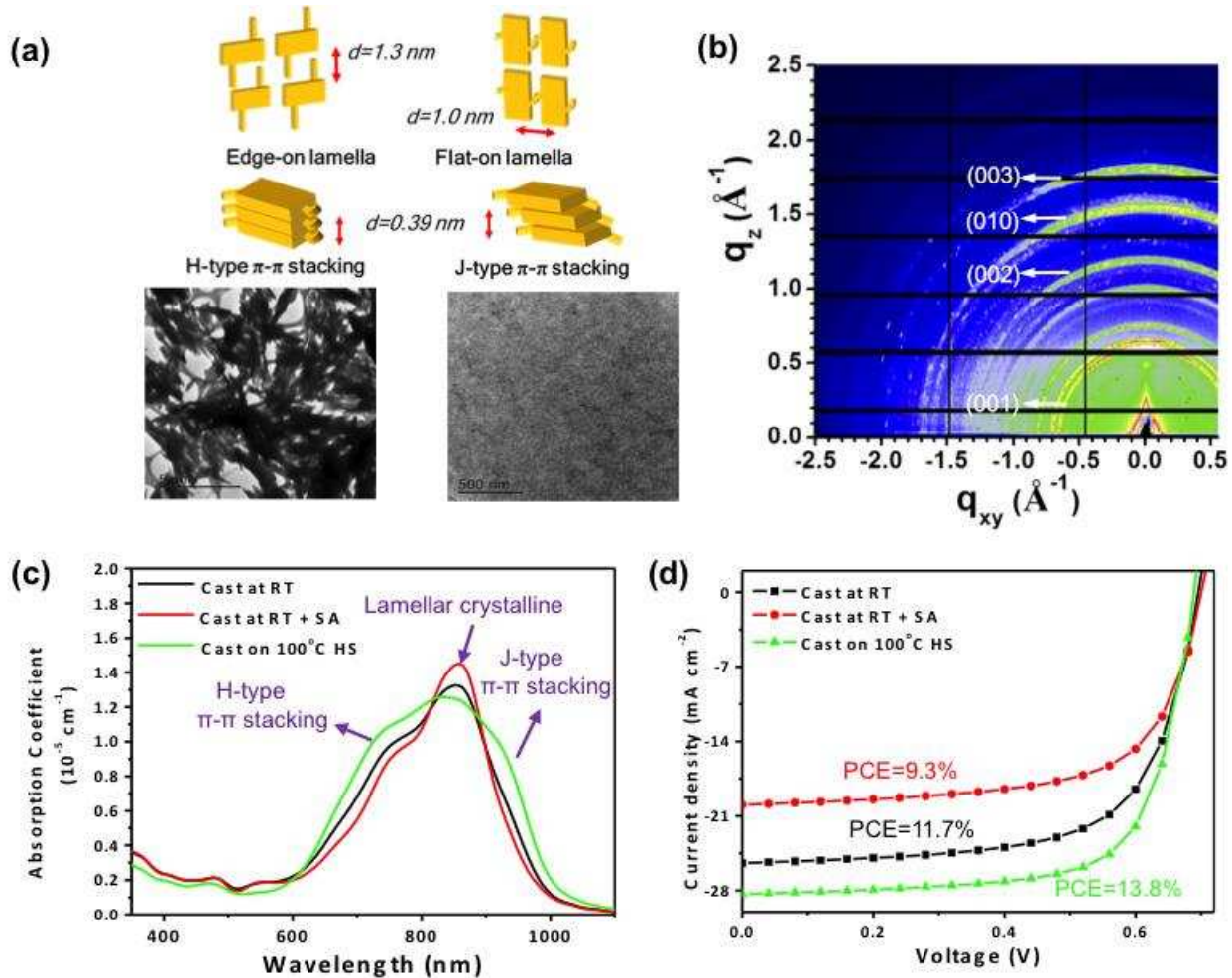

Figure 23. (a) Above: Schematic of flat-on and edge-on lamellar crystalline, H- and J- type $\pi-\pi$ stacking of COi8DFIC. Below: TEM images of COi8DFIC films (left) cast at RT and (right) cast on a hot substrate. (b) 2-D GIWAXS diffraction pattern of COi8DFIC. (c) Absorption spectra of COi8DFIC films and (d)

champion J-V curves PTB7-Th:COi8DFIC devices cast at RT, at RT in the presence of a solvent vapor or on a hot substrate. Figure modified and reproduced with permission from reference [13].

4.6. Optimizing morphology via the use of post-deposition treatments

Similar to their fullerene-based counterparts, non-fullerene photovoltaic blends exhibit temperature-dependent behavior that can be exploited to tune SMA materials as well as their D:A-blends. Researchers have shown that thermal annealing continues to be a valuable tool in controlling film morphology in non-fullerene solar cells, with many reporting beneficial effects on improving phase separation, i.e. domain purity [99,256] and domain size [85,257]. As we have seen above, thermal annealing can also be used to remove residual solvents such as DIO [246]. Thermal annealing is known to induce phase separation in photovoltaic blends heated above their glass transition temperature, but can also affect crystallization and conformation [258,259], which then strongly influence charge transfer dynamics and ultimately device performance parameters [260]. While strong molecular ordering and pure domains brought upon by good crystallization have been shown to be favorable, excessively strong crystallization results in overly large domains that inhibit interfacial contact between donor and acceptor phases. The degree to which crystallization is affected by thermal annealing is dependent on the steric and interaction forces of constituent materials.

4.6.1. Thermal Annealing

In polymer:fullerene systems, there are reports of thermal annealing causing a red-shift in the absorption spectrum as a result of improved crystallinity [19], and these phenomena have also been seen in polymer-non-fullerene systems. Liu et al. reported the use of thermal annealing as a means to control crystallinity in PBDB-T:IT-M films, and found that annealing increased the π-π coherence lengths of both donor and acceptor phases, with an increase in crystallinity in the out-of-phase direction after annealing (see figure 24b) [99]. The films also showed reduced surface roughness after annealing (figure 24a). A red shift in the absorption spectra was also observed (see figure 24c). It is of note that the peak around 700 nm attributed to IT-M is most affected by thermal annealing, indicating that it is the SMA crystallinity that affects the absorption spectra. These results directly correlate with electron mobility measurements of the pure acceptor, which is significantly higher after thermal annealing. Alongside the effects on crystallinity, thermal annealing is often associated with morphological reconfiguration, such as an increase in phase separation and therefore domain size and surface roughness [231,257,261,262], or arrangement into ordered phases [263]. This was the case in PDCBT:ITIC non-fullerene films after thermal annealing, where it was found that annealing induced a fibrous structure (as seen in TEM results shown in figure 25) where increased interfacial interactions between phases helped improve charge disassociation and transport [128]. Interestingly this did not occur in thermally-annealed P3HT:ITIC films, with the authors noting that the carbonyl functional groups of PDCBT are responsible for the thermally-induced nanostructural rearrangement.
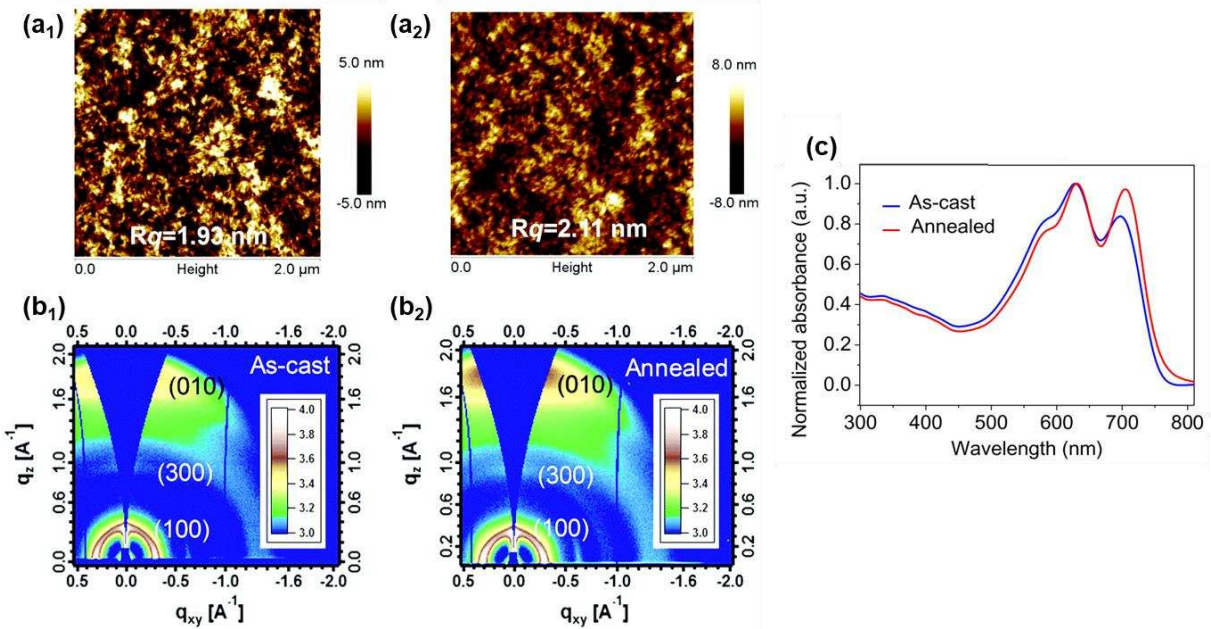
Figure 24. Tapping mode AFM topography of PBDB-T/IT-M based thick-film devices with (a_1) annealing treatment and (a_2) as-cast treatment; (b_1 and b_2) 2D GIWAXS patterns of as-cast and annealed PBDB-T:IT-M thick-films (∼250 nm). (c) UV-vis absorption spectra of as-cast and annealed PBDB-T:IT-M blend films with a thickness of ∼250 nm. Figures reproduced with permission from reference [99].
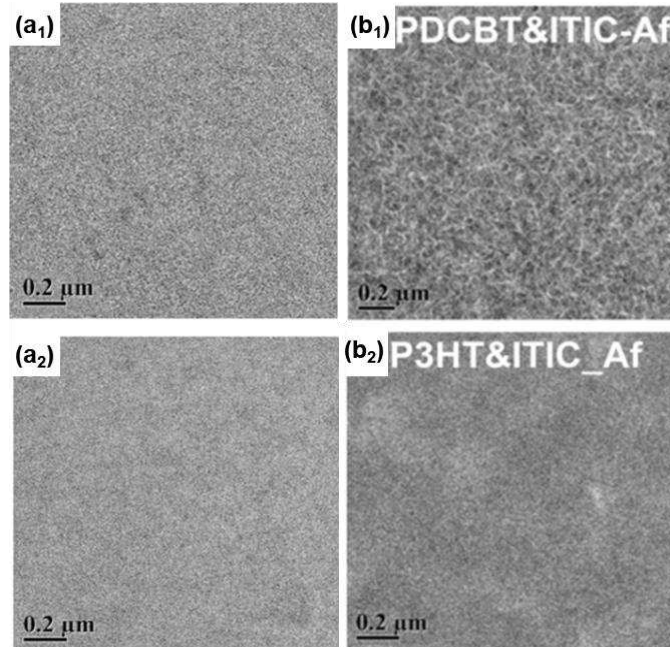
Figure 25. TEM images of (1) PDCBT&ITIC and (2) P3HT&ITIC (a) before and (b) after thermal annealing. Figures reproduced with permission from reference [128].

4.6.2. Solvent Vapor Annealing

The use of solvent vapor annealing (SVA), during- or post- casting the active layer has been shown to dramatically improve photovoltaic properties in non-fullerene photovoltaic blends. When a photovoltaic blend film is placed in a chamber with containing a solvent vapor, the effect of the vapor is similar to what is seen in thermal annealing, with the solvent vapor penetrating the film and influencing miscibility and molecular orientation. During solvent annealing, solvent is absorbed by the film, which lowers its glass transition temperature and facilitates translational movement of polymer chains and reconfiguration of the molecular orientation and conformation [264]. SVA offers the advantages of avoiding solvent additives, and allows films to be processed at room temperature, although a sealed chamber is required to contain the solvent vapor. SVA promotes thermodynamic rearrangement and, similar to thermal annealing, it can been seen that domain size and purity can increase with SVA time; indeed a peak annealing time can be observed after which domains become unfavorably large [265,266].

In polymer:fullerene systems, SVA with a CS_2/THF solvent blend was seen to control aggregation of PCBM [84,145,267] and induce ordering and crystallization in the polymer domains [266]. Acetone vapor induces P3HT crystallization in a P3HT:PCBM system despite not being a good solvent for the polymer due to high vapor pressure [268]. There are several recent examples of the effective application of SVA to non-fullerene systems where, as for their fullerene counterparts, a trend of using good, volatile solvents is seen to be effective to optimize domain size, phase separation and crystallinity; factors that result in improved charge transport [184,269,270]. For example, Zhang and coworkers showed the positive effects on PTB7-TH:ITIC following exposure to solvent vapors either during- or post-spin-casting [254]. In a blend film, a significant increase in the intensity was found for out-of-plane ITIC lamellar and π-π stacking peaks, as can be seen in figure 26. This correlates with reduced recombination, higher charge transfer efficiency and improved PCE from 6.25 to 7.21 %. Interestingly, the SVA did not affect the crystalline properties of a pure PTB7-Th film as can be seen from the unchanged spectra in the 1-D GIWAXS results. This indicated that the solvent vapor selectively drives conformational changes of the SMA, likely due to the high susceptibility of alkyl side chains to conformational rearrangement upon stimulus. It was also found that by employing SVA during the spin-casting step, the fast motion of the spinning substrate inhibited some of the solvent vapor from penetrating the film; an effect that restricted the effectiveness of SVA compared to post-casting SVA. This is reflected in domain size measurements where the ITIC domains increased from 41.1 to 56.7 or 149.5 nm for in situ-SVA and post-cast SVA respectively, with the latter being considered too large. A co-solvent system also gave similar results and was also considered too "strong", but significant differences between the different solvent vapors were not reported. Indeed, it was found that the solvent choice, being either CF, o-DCB or a mixture of the two, did not impact greatly on the intensity of the change caused by SVA. It is noteworthy that while both are good solvents for many SMAs, the two solvents have very different boiling points and vapor pressures.
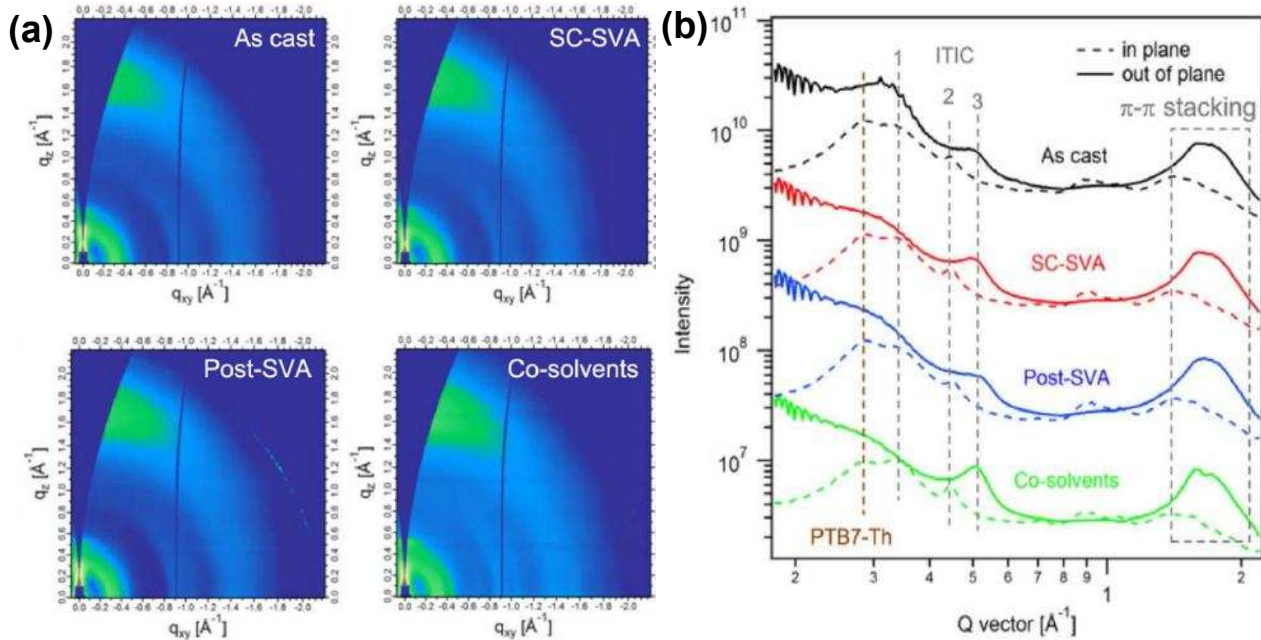
Figure 26. (a) GIWAXS 2D scattering patterns, and (b) line profiles of PTB7-Th:ITIC blend films with various solvent annealing processing conditions. Figures reproduced with permission from reference [254].

One complication in the understanding of SVA is that treatments often employ a home-made solvent chamber set up using varying solvent quantities and chamber sizes, with this combination not necessarily leading to solvent vapor saturation, thus vapor pressures are difficult to report. This means that annealing times vary largely from system to system. In many cases, highly volatile solvents such as CB, CF, THF and DCB (which are also good solvents for typical OPV materials) are seen to be effective, due to greater vapor pressure and increased probability of film penetration and interaction with the donor/acceptor molecules [268,271–273].

It should be noted that post-treatments, i.e. thermal or solvent vapor annealing, sometimes only produce a negative influence on the photovoltaic performance of non-fullerene OPVs [255]. This happens more often in photovoltaic systems where high crystallization and phase separation had occurred during the solution casting process, with further activation of the materials towards structure rearrangements goes beyond the optimal morphology to maximize charge generation and collection. In this case, adding additives to hinder, or a manipulation of the solution drying process to kinetically inhibit crystallization and phase separation processes should be approached, as our previous section has summarized.

5. Challenges and perspectives

5.1. Green solvent processing

In the search for alternative clean renewable energy sources, there are concerns about the impact of using toxic and environmentally harmful solvents in the processing of solar cells [274,275]. Chlorinated solvents, the traditional choice for the solution processing of organic photovoltaics, as well as additives such as DIO, are toxic to humans and harmful to the environment. As polymer solar cells move towards being a realistic source of alternative renewable energy, there is increased focus on environmental concerns and there is a desire to use "green" solvents and processing methods. However, OPVs have proved to be particularly sensitive to processing conditions and solvent choice, making a transition to greener solvents more challenging. Nevertheless, there are increasing reports of green solvent use, with the aim of eliminating some

of the more biologically hazardous traditional solvents whilst maintaining the morphological control afforded by solution processing.

Hydrocarbons have been proposed as one alternative to chlorinated and other halogenated solvents. In their polymer:fullerene system, Zhao et al. introduced the hydrocarbon solvent 1,2,4-trimethylbenzene (TMB), which is able to dissolve many polymer donors at elevated (80 °C) temperatures, along with the additive (2-phenylnaphthalene) [2]. TMB has quite a high boiling-point of 332 °C, as does the additive PN (325 °C), but when casting from a preheated solution (100 °C) the slower evaporation of these solvents helped improve morphology by promoting more favorable face-on orientation, as well as reducing domain size and increase domain purity. They also found that the alkyl side chains of the donor polymer were particular sensitive to these solvents, and by adjusting the length of these alkyl groups they could adjust domain spacing and purity, eventually finding the best TMB-PN system had a PC of 11.3 % compared to 10.0 % in CB-DIO. This solvent pair was tested for a polymer:non-fullerene system, but reduced the PCE likely due to the high solubility of the non-fullerene acceptor resulting in excessive phase separation [276].

In non-fullerene systems, mesitylene, o-Xylene and TMB have been proposed as non-halogenated solvent replacements. The former two have significantly lower boiling points (around 140 °C compared to TMB's 332 °C). Wadsworth and coworkers compared all three to a CB benchmark using a PffBT4T-2DT:EH-IDTBR system, and found in each case the PCE was higher than that processed with CB (10.2%), with mesitylene performing the best (11.1 %) [276]. Both CB- and mesitylene-processed films underwent similar crystallization despite the different processing techniques. It is of note that CB-based solutions were cast at higher temperatures due to temperature dependent aggregation, which was also seen to be beneficial to crystallization. The mesitylene-processed films had slightly weaker lamellar ordering, but stronger face-on π-π stacking, which evidently contributed to high efficiency. The mesitylene-processed devices also showed better reproducibility, with the authors attributing this to the low viscosity solution and lower casting temperature. They also reported good stability, retaining over 90% efficiency after 4000 hours, compared to 85 % for CB processed devices.

There are a range of low-toxicity non-halogenated biodegradable solvents that offer similar characteristics to halogenated solvents. Carbon disulfide (CS_2) is one such solvent that can easily dissolve many conjugated polymers and SMAs despite its lower boiling point (46 °C). This low boiling point results in its fast evaporation and drying, as well as limiting aggregation in solution. This appears favorable in certain systems, such as those based on larger small molecules with bulkier side chains which would normally be prone to strong aggregation [65]. THF is another low boiling point (66 °C) non-halogenated alternative considered to be more environmentally friendly. Zheng et al. found it can facilitate stronger inter-chain π-π interactions, resulting in favorable aggregation and good film morphology in their PBQ-4F:ITIC system [56]. Another halogen-free solvent, o-xylene, was used in PBDT-TDZ: and PBDTS-TDZ: ITIC devices. O-xylene has a higher boiling-point (144 °C) and similar properties to CB, and as such the authors were able to exploit temperature dependent aggregation in solution leading to better crystallization in the dry films [12]. Interestingly, they found that although the PN additive improved domain purity by increasing aggregation, it also resulted in the formation of rather coarse domains which were detrimental to charge transfer and device performance.

5.2. Stability and device lifetime

As PCEs head towards 15 %, OPVs increasingly look to be a realistic commercially attractive solar cell technology. For this reason, much attention is paid to OPV device stability and lifetime. Silicon solar cells often have warranties lasting 25 years that sets a high benchmark for future generations of commercial

photovoltaic devices. There are a number of factors that have been seen to reduce the stability and lifetime of OPVs. One of the major problems is exposure to oxygen or moisture, which results in increased recombination rates and a loss of device efficiency. Oxygen or water can penetrate into a film, reacting with the components to create meta-states that act as recombination sites [277]. Residual solvents such as DIO can provide a pathway through the bulk material for contaminants to reach the active layer, amplifying this problem [252], although low boiling-point additives [253] or vacuum treatment can minimize this effect. It has also been seen that defects act as pathways for contaminants [278]. These issues are usually addressed by encapsulation, where the device is coated with an epoxy resin and then covered with a glass side to prevent contaminants from reaching the active materials. Encapsulated devices show considerably higher lifetimes than uncoated devices. Several groups have reported that encapsulated OPVs can maintain 80 % of their PCE for several years [279,280]. Furthermore, accelerated aging studies have predicted that with care to avoid oxygen and water entry, polymer solar cells can have lifetimes exceeding 15 years in ambient conditions [281].

Both heat and light are known to destabilize solar cells. In fullerene devices, thermal degradation can cause rearrangement of the active layer with fullerene moving to the interface, blocking charge transfer.[282] There are also some reports of non-fullerene devices having good thermal stability benefitting from the thermal insensitivity of the active layer components; a promising indication for increased device stability [76,213]. Light degradation can occur in OPVs even when encapsulated due to photochemical reactions. Inverted architecture devices have improved lifetime as a result of the better stability of the extraction layer materials: PEDOT:PSS which is used in regular architecture devices has often been seen to be unstable in ambient conditions, with TiO_2 or ZnO performing better [156,283]. Calcium used in regular architecture, is also unstable under ambient conditions while the inverted alternative MoO_3 is less susceptible to the environment and protects the active layer from contaminants [284], Suggestions to limit such degradation processes include the use of increase molecular weight polymers and crosslinking density [285], together with selection of molecules that are more photo-stable e.g. IDT derivatives [283], or removing impurities to lessen recombination sites and impurity ingress [286].

5.3 "Burn-in" process

Many OPV devices have historically suffered from an initial drop in efficiency during the first phase of the device operation, which were thought to be intrinsic and unavoidable. This so-called "burn-in" loss accounts for an efficiency drop of around 10-20 % (or sometimes more) in the early stage of the device lifetime. Light degradation is a common cause of "burn-in", in which photochemical reactions (e.g. breaking C-H bonds [287] or UV-induced crosslinking [288]) cause trap-assisted recombination resulting in losses [289]. Other factors which affect device stability are also reported causes of "burn-in" loss, for example, performance losses due to residual solvent [253], impurities within the film [290,291], and thermal degradation [292].

However, promising new results show that "burn-in"-free polymer solar cells can be achieved. Researchers have shown that crystalline materials have reduced trap-assisted recombination, reduced V_{OC} loss and reduced burn in losses [293]. Gaspirini and coworkers compared "burn-in" loss in fullerene and non-fullerene acceptors, finding that while PCBM suffered about 30 % burn-in loss, the IDT-derived acceptor had no such loss due to its high crystallinity which inhibited defect-induced loss pathways [230]. There is also evidence that acceptors incorporating alkyl side chains can be modified to resist photo-oxidation through oxy-alkyl bonds, which could reduce recombination and "burn-in" loss [294].

5.4 Thickness dependence & Printable Devices

Thicker films, i.e. having active layers greater than 200 nm are desirable for ease of processing and improving light absorption. However, increasing film thickness also increases the chances of recombination if charge mobility is not sufficiently high [254]. Since the thickness dependence correlates with charge mobility, which in turn is improved by crystallization, new generations of non-fullerene acceptors with optimized properties are poised to overcome the thickness issue. Indeed, there are increasing reports of devices with high crystallinity, high charge mobility and thickness independence [64,99,169,188,295]. In recent examples, Li et al. achieved over 11 % in PM6:IDIC OPV devices having a thickness between 100 and 200 nm [296] and Zhang et al. achieved 9.1 % in devices incorporating a 300 nm thick film of PffBT4T-2OD:EH-IDTBR [297].

If high performance can be achieved using thicker films, different processing routes become available for film deposition. There are increasing reports of high performance devices being realized using scalable casting techniques such as slot-die [298–300], blade [301,302] or roll [303–307] coating, and ability to cast on non-traditional substrates such as plastics [308] opens a pathway to flexible solar cell devices [309–311]. The onset of high performance large-area printable devices bodes well for the commercial future of OPVs.

6. Conclusions

Throughout this review, we have outlined how advances in molecular structure and processing techniques have provided researchers with better understanding and tighter control of the morphological conditions required to yield highly efficient polymer:non-fullerene solar cells. Key advancements include better understanding of phase separation, domain size and spacing and crystallization, and optimization of their characteristics allows reduced recombination rates and increased charge mobility. Better control of these morphological properties has been achieved through processing techniques like the use of solvent additives and thermal/solvent annealing to suppress or promote traits such as aggregation in solution, blend miscibility and crystallization. These techniques have led to increased mobility and reduced recombination, which have meant that systems can be designed without the driving force previously needed to overcome intermediate/trap states that have led to recombination. These new molecules, designed with little or no offset, have reduced V_{OC} loss and increased device performance. Molecular design is also a powerful tool used to control such characteristics, with control of back bone structure, side chain length and composition being used to favorably orient the molecules and adjust conjugation lengths and stacking distances, as well as affect steric conditions and miscibility. With a better understanding of the tools and techniques available to understand and optimize both donor and acceptor properties, the field of non-fullerene OPVs is likely to continue to grow and see further increases in device efficiency. Attention now turns to factors such as long-term device stability, green processing, and up-scaling, all of which show promising signs for the potential commercial success of non-fullerene solar cell devices.

Acknowledgments

References

[1]   Scharber M C, Mühlbacher D, Koppe M, Denk P, Waldauf C, Heeger A J and Brabec C J 2006 Design rules for donors in bulk-heterojunction solar cells—towards 10 % energy-conversion efficiency Adv. Mater. **18** 789–94

[2]   Zhao J, Li Y, Yang G, Jiang K, Lin H, Ade H, Ma W and Yan H 2016 Efficient organic solar cells processed from hydrocarbon solvents Nat. Energy **1** 15027

[3]   He Y, Chen H, Hou J and Li Y 2010 Indene-C60 bisadduct: a new acceptor for high-performance polymer solar cells J. Am. Chem. Soc. **132** 1377–82

[4]   Lenes M, Wetzelaer G J A H, Kooistra F B, Veenstra S C, Hummelen J C and Blom P W M 2008 Fullerene bisadducts for enhanced open-circuit voltages and efficiencies in polymer solar cells Adv. Mater. **20** 2116–9

[5]   Bloking J T et al 2014 Comparing the device physics and morphology of polymer solar cells employing fullerenes and non-fullerene acceptors Adv. Energy Mater. **4** 1301426

[6]   Schilinsky P, Waldauf C and Brabec C J 2002 Recombination and loss analysis in polythiophene based bulk heterojunction photodetectors Appl. Phys. Lett. **81** 3885–7

[7]   Wang T, Pearson A J, Lidzey D G and Jones R A L 2011 Evolution of structure, optoelectronic properties, and device performance of polythiophene:fullerene solar cells during thermal annealing Adv. Funct. Mater. **21** 1383–90

[8]   Wang T et al 2012 Correlating structure with function in thermally annealed PCDTBT:PC70BM photovoltaic blends Adv. Funct. Mater. **22** 1399–408

[9]   Zhan X et al 2007 A high-mobility electron-transport polymer with broad absorption and its use in field-effect transistors and all-polymer solar cells J. Am. Chem. Soc. **129** 7246–7

[10]   Zhao W, Li S, Yao H, Zhang S, Zhang Y, Yang B and Hou J 2017 Molecular optimization enables over 13% efficiency in organic solar cells J. Am. Chem. Soc. **139** 7148–51

[11]   Fei Z et al 2018 An alkylated indacenodithieno[3,2-b]thiophene-based nonfullerene acceptor with high crystallinity exhibiting single junction solar cell efficiencies greater than 13% with low voltage losses Adv. Mater. **30** 1705209

[12]   Xu X, Yu T, Bi Z, Ma W, Li Y and Peng Q 2017 Realizing over 13% efficiency in green-solvent-processed nonfullerene organic solar cells enabled by 1,3,4-thiadiazole-based wide-bandgap copolymers Adv. Mater. 1703973

[13]   Li W, Chen M, Cai J, Zhang H, Gurney R S, Liu D, Xiao Z, Ding L and Wang T 2019 Molecular order control of non-fullerene acceptors for high-efficiency polymer solar cells Joule 10.1016/j.joule.2018.11.023

[14]   Zhang S, Qin Y, Zhu J and Hou J 2018 Over 14% efficiency in polymer solar cells enabled by a chlorinated polymer donor Adv. Mater. **30** 1800868

[15]   Li S, Ye L, Zhao W, Yan H, Yang B, Liu D, Li W, Ade H and Hou J 2018 A wide band gap polymer with a deep highest occupied molecular orbital level enables 14.2% efficiency in polymer solar cells J. Am. Chem. Soc. **140** 7159–67

[16]   Xiao Z, Jia X and Ding L 2017 Ternary organic solar cells offer 14% power conversion efficiency Sci. Bull. **62** 1562–4

[17]   Li H, Xiao Z, Ding L and Wang J 2018 Thermostable single-junction organic solar cells with a power conversion efficiency of 14.62% Sci. Bull. **63** 340–2

[18]   Meng L et al 2018 Organic and solution-processed tandem solar cells with 17.3% efficiency Science **361** 1094–8

[19]   Vandewal K et al 2008 The relation between open-circuit voltage and the onset of photocurrent generation by charge-transfer absorption in polymer: fullerene bulk heterojunction solar cells Adv. Funct. Mater. **18** 2064–70

[20]   Shockley W and Queisser H J 1961 Detailed balance limit of efficiency of p-n junction solar cells J.

Appl. Phys. **32** 510–9

[21]   Scharber M C and Sariciftci N S 2013 Efficiency of bulk-heterojunction organic solar cells Prog. Polym. Sci. **38** 1929–40

[22]   Scharber M C 2016 On the efficiency limit of conjugated polymer:fullerene-based bulk heterojunction solar cells Adv. Mater. **28** 1994–2001

[23]   Li W, Hendriks K H, Furlan A, Wienk M M and Janssen R A J 2015 High quantum efficiencies in polymer solar cells at energy losses below 0.6 eV J. Am. Chem. Soc. **137** 2231–4

[24]   Bansal N et al 2013 Influence of crystallinity and energetics on charge separation in polymer-inorganic nanocomposite films for solar cells Sci. Rep. **3** 1531

[25]   Bakulin A A, Akshay Rao, Vlad G. Pavelyev, Paul H.M. van Loosdrecht, Maxim S. Pshenichnikov, Dorota Niedzialek, Jérôme Cornil, David Beljonne and Friend R H 2012 The role of driving energy and delocalized states for charge separation in organic semiconductors Science **335** 1340–4

[26]   Deibe C, Strobe T and Dyakonov V 2010 Role of the charge transfer state in organic donor-acceptor solar cells Adv. Mater. **22** 4097–111

[27]   Menke S M, Ran N A, Bazan G C and Friend R H 2018 Understanding energy loss in organic solar cells: toward a new efficiency regime Joule **2** 25–35

[28]   Wang Y, Qian D, Cui Y, Zhang H, Hou J, Vandewal K, Kirchartz T and Gao F 2018 Optical gaps of organic solar cells as a reference for comparing voltage losses Adv. Energy Mater. **8** 1801352

[29]   Li S, Liu W, Li C-Z, Shi M and Chen H 2017 Efficient organic solar cells with non-fullerene acceptors Small 1**3** 1701120

[30]   Chen Z, Cai P, Chen J, Liu X, Zhang L, Lan L, Peng J, Ma Y and Cao Y 2014 Low band-gap conjugated polymers with strong interchain aggregation and very high hole mobility towards highly efficient thick-film polymer solar cells Adv. Mater. **26** 2586–91

[31]   Vohra V, Kawashima K, Kakara T, Koganezawa T, Osaka I, Takimiya K and Murata H 2015 Efficient inverted polymer solar cells employing favourable molecular orientation Nat. Photon. **9** 403–8

[32]   Baran D et al 2016 Reduced voltage losses yield 10% efficient fullerene free organic solar cells with >1 V open circuit voltages Energy Environ. Sci. **9** 3783–93

[33]   Kim H Do, Yanagawa N, Shimazaki A, Endo M, Wakamiya A, Ohkita H, Benten H and Ito S 2017 Origin of open-circuit voltage loss in polymer solar cells and perovskite solar cells ACS Appl. Mater. Interfaces **9** 19988–97

[34]   Hoke E T et al 2013 Recombination in polymer:fullerene solar cells with open-circuit voltages approaching and exceeding 1.0 V Adv. Energy Mater. **3** 220–30

[35]   Nuzzo D Di, Wetzelaer G J A H, Bouwer R K M, Gevaerts V S, Meskers S C J, Hummelen J C, Blom P W M and Janssen R A J 2013 Simultaneous open-circuit voltage enhancement and short-circuit current loss in polymer:fullerene solar cells correlated by reduced quantum efficiency for photoinduced electron transfer Adv. Energy Mater. **3** 85–94

[36]   Göhler C, Wagenpfahl A and Deibel C 2018 Nongeminate recombination in organic solar cells Adv. Electron. Mater. **4** 1700505

[37]   Gasparini N, Wadsworth A, Moser M, Baran D, McCulloch I and Brabec C J 2018 The physics of small molecule acceptors for efficient and stable bulk heterojunction solar cells Adv. Energy Mater. **8** 1703298

[38]   Gélinas S, Rao A, Kumar A, Smith S L, Chin A W, Clark J, Poll T S Van Der, Bazan G C and Friend R H 2014 Ultrafast long-range charge photovoltaic diodes Science **343** 512–6

[39] Chen K, Barker A J, Reish M E, Gordon K C and Hodgkiss J M 2013 Broadband ultrafast photoluminescence spectroscopy resolves charge photogeneration via delocalized hot excitons in polymer:fullerene photovoltaic blends J. Am. Chem. Soc. **135** 18502–12

[40] Yao H, Qian D, Zhang H, Qin Y, Xu B, Cui Y, Yu R, Gao F and Hou J 2018 Critical role of molecular electrostatic potential on charge generation in organic solar cells Chinese J. Chem. **36** 491–4

[41] Leong W L, Cowan S R and Heeger A J 2011 Differential resistance analysis of charge carrier losses in organic bulk heterojunction solar cells: observing the transition from bimolecular to trap-assisted recombination and quantifying the order of recombination Adv. Energy Mater. **1** 517–22

[42] Burke T M, Sweetnam S, Vandewal K and McGehee M D 2015 Beyond Langevin recombination: how equilibrium between free carriers and charge transfer states determines the open-circuit voltage of organic solar cells Adv. Energy Mater. **5** 1500123

[43] Nelson J 2011 Polymer:fullerene bulk heterojunction solar cells Mater. Today **14** 462–70

[44] Koster L J A, Mihailetchi V D and Blom P W M 2006 Bimolecular recombination in polymer/fullerene bulk heterojunction solar cells Appl. Phys. Lett. **88** 052104

[45] Lakhwani G, Rao A and Friend R H 2014 Bimolecular recombination in organic photovoltaics Annu. Rev. Phys. Chem. **65** 557–81

[46] Yan H, Manion J G, Yuan M, García de Arquer F P, McKeown G R, Beaupré S, Leclerc M, Sargent E H and Seferos D S 2016 Increasing polymer solar cell fill factor by trap-filling with F4-TCNQ at parts per thousand concentration Adv. Mater. **28** 6491–6

[47] Wetzelaer G J A H, Van Der Kaap N J, Koster J A and Blom P W M 2013 Quantifying bimolecular recombination in organic solar cells in steady state Adv. Energy Mater. **3** 1130–4

[48] Juška G, Arlauskas K, Stuchlik J and Österbacka R 2006 Non-Langevin bimolecular recombination in low-mobility materials J. Non. Cryst. Solids **352** 1167–71

[49] Credgington D and Durrant J R 2012 Insights from transient optoelectronic analyses on the open-circuit voltage of organic solar cells J. Phys. Chem. Lett. **3** 1465–78

[50] Deibel C, Wagenpfahl A and Dyakonov V 2009 Origin of reduced polaron recombination in organic semiconductor devices Phys. Rev. B **80** 075203

[51] Schell M, Kapral R and Cukier R I 1981 Recombination kinetics: Langevin dynamics with a space dependent friction coefficient J. Chem. Phys. **75** 5879

[52] Groves C and Greenham N C 2008 Bimolecular recombination in polymer electronic devices Phys. Rev. B **78** 155205

[53] Armin A, Durrant J R and Shoaee S 2017 Interplay between triplet-, singlet-charge transfer states and free charge carriers defining bimolecular recombination rate constant of organic solar cells J. Phys. Chem. C **121** 13969–76

[54] Liu Y, Zojer K, Lassen B, Kjelstrup-hansen J, Rubahn H and Madsen M 2015 Role of the charge-transfer state in reduced Langevin recombination in organic solar cells : a theoretical study J. Phys. Chem. C **119** 26588−26597

[55] Shuttle C G, O'regan B, Ballantyne A M, Nelson J, Bradley D D C, De Mello J and Durrant J R 2008 Experimental determination of the rate law for charge carrier decay in a polythiophene:fullerene solar cell Appl. Phys. Lett. **92** 093311

[56] Zheng Z et al 2017 Efficient charge transfer and fine-tuned energy level alignment in a THF-processed fullerene-free organic solar cell with 11.3% efficiency Adv. Mater. **29** 1604241

[57] Pivrikas A, Juška G, Mozer A J, Scharber M, Arlauskas K, Sariciftci N S, Stubb H and Österbacka R

2005 Bimolecular recombination coefficient as a sensitive testing parameter for low-mobility solar-cell materials Phys. Rev. Lett. **94** 176806

[58]   Wright B, Nakajima Y, Clarke T M, Okuda K, Paananen H, Mozer A J and Mori S 2017 Quantifying recombination losses during charge extraction in bulk heterojunction solar cells using a modified charge extraction technique Adv. Energy Mater. **7** 1602026

[59]   Adriaenssens G J and Arkhipov V I 1997 Non-Langevin recombination in disordered materials with random potential distributions Solid State Commun. **103** 541–3

[60]   Zhou Y et al 2014 High performance all-polymer solar cell via polymer side-chain engineering Adv. Mater. **26** 3767–72

[61]   Vandewal K et al 2014 Efficient charge generation by relaxed charge-transfer states at organic interfaces Nat. Mater. **13** 63–8

[62]   Xie S, Xia Y, Zheng Z, Zhang X, Yuan J, Zhou H and Zhang Y 2018 Effects of nonradiative losses at charge transfer states and energetic disorder on the open-circuit voltage in nonfullerene organic solar cells Adv. Funct. Mater. **28** 1705659

[63]   Ran N A et al 2018 Charge generation and recombination in an organic solar cell with low energetic offsets Adv. Energy Mater. **8** 1701073

[64]   Liu J et al 2016 Fast charge separation in a non-fullerene organic solar cell with a small driving force Nat. Energy **1** 16089

[65]   Wan J, Xu X, Zhang G, Li Y, Feng K and Peng Q 2017 Highly efficient halogen-free solvent processed small-molecule organic solar cells enabled by material design and device engineering Energy Environ. Sci. **10** 1739–45

[66]   Yan C, Barlow S, Wang Z, Yan H, Jen A K Y, Marder S R and Zhan X 2018 Non-fullerene acceptors for organic solar cells Nat. Rev. Mater. **3** 18003

[67]   Sonar P, Singh S P, Li Y, Soh M S and Dodabalapur A 2010 A low-bandgap diketopyrrolopyrrole-benzothiadiazole-based copolymer for high-mobility ambipolar organic thin-film transistors Adv. Mater. **22** 5409–13

[68]   Nielsen C B, Holliday S, Chen H-Y, Cryer S J and McCulloch I 2015 Non-fullerene electron acceptors for use in organic solar cells Acc. Chem. Res. **48** 2803–12

[69]   Kawashima K, Tamai Y, Ohkita H, Osaka I and Takimiya K 2015 High-efficiency polymer solar cells with small photon energy loss Nat. Commun. **6** 10085

[70]   Li Y et al 2016 Non-fullerene acceptor with low energy loss and high external quantum efficiency: towards high performance polymer solar cells J. Mater. Chem. A **4** 5890–7

[71]   Qian D et al 2018 Design rules for minimizing voltage losses in high-efficiency organic solar cells Nat. Mater. **17** 703–9

[72]   Liu J et al 2018 Carboxylate substitution position influencing polymer properties and enabling non-fullerene organic solar cells with high open circuit voltage and low voltage loss J. Mater. Chem. A **6** 16874–81

[73]   Chen S et al 2018 Efficient nonfullerene organic solar cells with small driving forces for both hole and electron transfer Adv. Mater. **30** 1804215

[74]   Zhang X, Zuo X, Xie S, Yuan J, Zhou H and Zhang Y 2017 Understanding charge transport and recombination losses in high performance polymer solar cells with non-fullerene acceptors J. Mater. Chem. A **5** 17230–9

[75]   Lin Y, Wang J, Zhang Z, Bai H, Li Y, Zhu D and Zhan X 2015 An electron acceptor challenging fullerenes for efficient polymer solar cells Adv. Mater. **27** 1170–4

[76]   Zhao W, Qian D, Zhang S, Li S, Inganäs O, Gao F and Hou J 2016 Fullerene-free polymer solar cells with over 11% efficiency and excellent thermal stability Adv. Mater. **28** 4734–9

[77]   Hou J, Inganäs O, Friend R H and Gao F 2018 Organic solar cells based on non-fullerene acceptors Nat. Mater. **17** 119–28

[78]   Li S, Ye L, Zhao W, Zhang S, Mukherjee S, Ade H and Hou J 2016 Energy-level modulation of small-molecule electron acceptors to achieve over 12% efficiency in polymer solar cells Adv. Mater. **28** 9423–9

[79]   Zhang J, Jiang K, Yang G, Ma T, Liu J, Li Z, Lai J Y L, Ma W and Yan H 2017 Tuning energy levels without negatively affecting morphology: a promising approach to achieving optimal energetic match and efficient nonfullerene polymer solar cells Adv. Energy Mater. **7** 1602119

[80]   Shi J et al 2018 Designing high performance all-small-molecule solar cells with non-fullerene acceptors: comprehensive studies on photoexcitation dynamics and charge separation kinetics Energy Environ. Sci. **11** 211–20

[81]   Li W et al 2018 Correlating three-dimensional morphology with function in PBDB-T:IT-M non-fullerene organic solar cells Sol. RRL **2** 1800114

[82]   Li W, Cai J, Cai F, Yan Y, Yi H, Gurney R S, Liu D, Iraqi A and Wang T 2018 Achieving over 11% power conversion efficiency in PffBT4T-2OD-based ternary polymer solar cells with enhanced open-circuit-voltage and suppressed charge recombination Nano Energy **44** 155–63

[83]   Ma W, Tumbleston J R, Wang M, Gann E, Huang F and Ade H 2013 Domain purity, miscibility, and molecular orientation at donor/acceptor interfaces in high performance organic solar cells: Paths to further improvement Adv. Energy Mater. **3** 864–72

[84]   Sun K, Xiao Z, Hanssen E, Klein M F G, Dam H H, Pfaff M, Gerthsen D, Wong W W H and Jones D J 2014 The role of solvent vapor annealing in highly efficient air-processed small molecule solar cells J. Mater. Chem. A **2** 9048–54

[85]   Osaka M, Mori D, Benten H, Ogawa H, Ohkita H and Ito S 2017 Charge transport in intermixed regions of all-polymer solar cells studied by conductive atomic force microscopy ACS Appl. Mater. Interfaces **9** 15615–22

[86]   Tamai Y, Ohkita H, Benten H and Ito S 2015 Exciton diffusion in conjugated polymers: from fundamental understanding to improvement in photovoltaic conversion efficiency J. Phys. Chem. Lett. **6** 3417–28

[87]   Lin J D A et al 2014 Systematic study of exciton diffusion length in organic semiconductors by six experimental methods Mater. Horiz. **1** 280–5

[88]   Zhao F et al 2017 Single-junction binary-blend nonfullerene polymer solar cells with 12.1% efficiency Adv. Mater. **29** 1700144

[89]   Cha H, Wheeler S, Holliday S, Dimitrov S D, Wadsworth A, Lee H H, Baran D, McCulloch I and Durrant J R 2017 Influence of blend morphology and energetics on charge separation and recombination dynamics in organic solar cells incorporating a nonfullerene acceptor Adv. Funct. Mater. **28** 1704389

[90]   Hwang Y J, Li H, Courtright B A E, Subramaniyan S and Jenekhe S A 2016 Nonfullerene polymer solar cells with 8.5% efficiency enabled by a new highly twisted electron acceptor dimer Adv. Mater. **28** 124–31

[91]   Hoppe H and Sariciftci N S 2006 Morphology of polymer/fullerene bulk heterojunction solar cells J. Mater. Chem. **16** 45–61

[92]   Mukherjee S, Proctor C M, Tumbleston J R, Bazan G C, Nguyen T Q and Ade H 2015 Importance of domain purity and molecular packing in efficient solution-processed small-molecule solar cells Adv.

Mater. **27** 1105–11

[93]   Yan Y, Liu X and Wang T 2017 Conjugated-polymer blends for organic photovoltaics: Rational control of vertical stratification for high performance Adv. Mater. **29** 1601674

[94]   Liu Y et al 2014 Aggregation and morphology control enables multiple cases of high-efficiency polymer solar cells Nat. Commun. **5** 5293

[95]   Collins B A, Li Z, Tumbleston J R, Gann E, McNeill C R and Ade H 2013 Absolute measurement of domain composition and nanoscale size distribution explains performance in PTB7:PC70BM solar cells Adv. Energy Mater. **3** 65–74

[96]   Stuart A C, Tumbleston J R, Zhou H, Li W, Liu S, Ade H and You W 2013 Fluorine substituents reduce charge recombination and drive structure and morphology development in polymer solar cells J. Am. Chem. Soc. **135** 1806–15

[97]   Dimitrov S D and Durrant J R 2014 Materials design considerations for charge generation in organic solar cells Chem. Mater. **26** 616–30

[98]   Mukherjee S, Jiao X and Ade H 2016 Charge creation and recombination in multi-length scale polymer:fullerene BHJ solar cell morphologies Adv. Energy Mater. **6** 1600699

[99]   Liu X, Ye L, Zhao W, Zhang S, Li S, Su G M, Wang C, Ade H and Hou J 2017 Morphology control enables thickness-insensitive efficient nonfullerene polymer solar cells Mater. Chem. Front. **1** 2057–64

[100]   Wang G et al 2018 Photoactive blend morphology engineering through systematically tuning aggregation in all-polymer solar cells Adv. Energy Mater. **8** 1702173

[101]   Ye L et al 2017 Precise manipulation of multilength scale morphology and its influence on eco-friendly printed all-polymer solar cells Adv. Funct. Mater. **27** 1702016

[102]   Lan S, Yang H, Zhang G, Wu X, Chen Q, Chen L, Chen H and Guo T 2017 Importance of solvent removal rate on the morphology and device performance of organic photovoltaics with solvent annealing ACS Appl. Mater. Interfaces **9** 20679–85

[103]   Hu H, Jiang K, Chow P C Y, Ye L, Zhang G, Li Z, Carpenter J H, Ade H and Yan H 2018 Influence of donor polymer on the molecular ordering of small molecular acceptors in nonfullerene polymer solar cells Adv. Energy Mater. **8** 1701674

[104]   Chen W et al 2011 Hierarchical nanomorphologies promote exciton dissociation in polymer/fullerene bulk heterojunction solar cells Nano Lett. **11** 3707–13

[105]   Yao H, Yu R, Shin T J, Zhang H, Zhang S, Jang B, Uddin M A, Woo H Y and Hou J 2016 A wide bandgap polymer with strong π–π interaction for efficient fullerene-free polymer solar cells Adv. Energy Mater. **6** 1600742

[106]   Schaffer C J, Schlipf J, Dwi Indari E, Su B, Bernstorff S and Müller-Buschbaum P 2015 Effect of blend composition and additives on the morphology of PCPDTBT:PC70BM thin films for organic photovoltaics ACS Appl. Mater. Interfaces **7** 21347–55

[107]   Richter L J, Delongchamp D M, Bokel F A, Engmann S, Chou K W, Amassian A, Schaible E and Hexemer A 2014 In situ morphology studies of the mechanism for solution additive effects on the formation of bulk heterojunction films Adv. Energy Mater. **5** 1400975

[108]   DeLongchamp D M, Kline R J and Herzing A 2012 Nanoscale structure measurements for polymer-fullerene photovoltaics Energy Environ. Sci. **5** 5980

[109]   Guilbert A A Y, Zbiri M, Jenart M V C, Nielsen C B and Nelson J 2016 New insights into the molecular dynamics of P3HT:PCBM bulk heterojunction: a time-of-flight quasi-elastic neutron scattering study J. Phys. Chem. Lett. **7** 2252–7

[110] Chen D, Nakahara A, Wei D, Nordlund D and Russell T P 2011 P3HT/PCBM bulk heterojunction organic photovoltaics: correlating efficiency and morphology Nano Lett. **11** 561–7

[111] Bulle-Lieuwma C W T, Van Gennip W J H, Van Duren J K J, Jonkheijm P, Janssen R A J and Niemantsverdriet J W 2003 Characterization of polymer solar cells by TOF-SIMS depth profiling Appl. Surf. Sci. **203**–**204** 547–50

[112] Van Duren J K J, Yang X, Loos J, Bulle-Lieuwma C W T, Sieval A B, Hummelen J C and Janssen R A J 2004 Relating the morphology of poly(p-phenylene vinylene)/ methanofullerene blends to solar-cell performance Adv. Funct. Mater. **14** 425–34

[113] Liu F, Gu Y, Shen X, Ferdous S, Wang H W and Russell T P 2013 Characterization of the morphology of solution-processed bulk heterojunction organic photovoltaics Prog. Polym. Sci. **38** 1990–2052

[114] Subbiah J, Amb C M, Reynolds J R and So F 2012 Effect of vertical morphology on the performance of silole-containing low-bandgap inverted polymer solar cells Sol. Energy Mater. Sol. Cells **97** 97–101

[115] Xu Z, Chen L M, Yang G, Huang C H, Hou J, Wu Y, Li G, Hsu C S and Yang Y 2009 Vertical phase separation in poly(3-hexylthiophene): fullerene derivative blends and its advantage for inverted structure solar cells Adv. Funct. Mater. **19** 1227–34

[116] Huang L et al 2018 Vertical stratification engineering for organic bulk-heterojunction devices ACS Nano **12** 4440–52

[117] Yan Y et al 2018 Correlating nanoscale morphology with device performance in conventional and inverted PffBT4T-2OD:PC70BM polymer solar cells ACS Appl. Energy Mater. **1** 3505–12

[118] Yi X et al 2018 Impact of nonfullerene molecular architecture on charge generation, transport, and morphology in PTB7-Th-based organic solar cells Adv. Funct. Mater. **28** 1802702

[119] Li W et al 2018 Contrasting effects of energy transfer in determining efficiency improvements in ternary polymer solar cells Adv. Funct. Mater. **28** 1704212

[120] Wang T et al 2013 Fabricating high performance, donor-acceptor copolymer solar cells by spray-coating in air Adv. Energy Mater. **3** 505–12

[121] Ma Z, Geng H, Wang D and Shuai Z 2016 Influence of alkyl side-chain length on the carrier mobility in organic semiconductors: herringbone vs. pi–pi stacking J. Mater. Chem. C **4** 4546–55

[122] Li Z et al 2016 High performance all-polymer solar cells by synergistic effects of fine-tuned crystallinity and solvent annealing J. Am. Chem. Soc. **138** 10935–44

[123] Stoltzfus D M, Clulow A J, Jin H, Burn P L and Gentle I R 2016 Impact of dimerization on phase separation and crystallinity in bulk heterojunction films containing non-fullerene acceptors Macromolecules **49** 4404–15

[124] Wang T, Pearson A J and Lidzey D G 2013 Correlating molecular morphology with optoelectronic function in solar cells based on low band-gap copolymer:fullerene blends J. Mater. Chem. C **1** 7266

[125] Zhan C and Yao J 2016 More than conformational "twisting" or "coplanarity": molecular strategies for designing high-efficiency nonfullerene organic solar cells Chem. Mater. **28** 1948–64

[126] Li Z, Jiang K, Yang G, Lai J Y L, Ma T, Zhao J, Ma W and Yan H 2016 Donor polymer design enables efficient non-fullerene organic solar cells Nat. Commun. **7** 13094

[127] Chen M H, Hou J, Hong Z, Yang G, Sista S, Chen L M and Yang Y 2009 Efficient polymer solar cells with thin active layers based on alternating polyfluorene copolymer/fullerene bulk heterojunctions Adv. Mater. **21** 4238–42

[128] Qin Y et al 2016 Highly efficient fullerene-free polymer solar cells fabricated with polythiophene

derivative Adv. Mater. **28** 9416–22

[129] Son H J, Wang W, Xu T, Liang Y, Wu Y, Li G and Yu L 2011 Synthesis of fluorinated polythienothiophene-co-benzodithiophenes and effect of fluorination on the photovoltaic properties J. Am. Chem. Soc. **133** 1885–94

[130] Hsiao Y T, Li C H, Chang S L, Heo S, Tajima K, Cheng Y J and Hsu C S 2017 Haptacyclic carbazole-based ladder-type nonfullerene acceptor with side-chain optimization for efficient organic photovoltaics ACS Appl. Mater. Interfaces **9** 42035–42

[131] Uddin M A et al 2015 Interplay of intramolecular noncovalent coulomb interactions for semicrystalline photovoltaic polymers Chem. Mater. **27** 5997–6007

[132] Yiu A T, Beaujuge P M, Lee O P, Woo C H, Toney M F and Fréchet J M J 2012 Side-chain tunability of furan-containing low-band-gap polymers provides control of structural order in efficient solar cells J. Am. Chem. Soc. **134** 2180–5

[133] Tumbleston J R, Collins B A, Yang L, Stuart A C, Gann E, Ma W, You W and Ade H 2014 The influence of molecular orientation on organic bulk heterojunction solar cells Nat. Photonics **8** 385–91

[134] Ran N A et al 2017 Impact of interfacial molecular orientation on radiative recombination and charge generation efficiency Nat. Commun. **8** 79

[135] Sreearunothai P, Morteani A C, Avilov I, Cornil J, Beljonne D, Friend R H, Phillips R T, Silva C and Herz L M 2006 Influence of copolymer interface orientation on the optical emission of polymeric semiconductor heterojunctions Phys. Rev. Lett. **96** 117403

[136] Lin Y and Zhan X 2014 Non-fullerene acceptors for organic photovoltaics: An emerging horizon Mater. Horizons **1** 470–88

[137] Rajaram S, Shivanna R, Kandappa S K and Narayan K S 2012 Nonplanar perylene diimides as potential alternatives to fullerenes in organic solar cells J. Phys. Chem. Lett. **3** 2405–8

[138] Ye L, Jiao X, Zhao W, Zhang S, Yao H, Li S, Ade H and Hou J 2016 Manipulation of domain purity and orientational ordering in high performance all-polymer solar cells Chem. Mater. **28** 6178–85

[139] Gregg B A 2011 Entropy of charge separation in organic photovoltaic cells: the benefit of higher dimensionality J. Phys. Chem. Lett. **2** 3013–5

[140] Clarke T M and Durrant J R 2010 Charge photogeneration in organic solar cells Chem. Rev. **110** 6736–67

[141] Ye L, Jiao X, Zhou M, Zhang S, Yao H, Zhao W, Xia A, Ade H and Hou J 2015 Manipulating aggregation and molecular orientation in all-polymer photovoltaic cells Adv. Mater. **27** 6046–54

[142] Zhou D, Qin Y, Zhong R, Xu H, Tong Y, Hu B and Xie Y 2018 Diblock conjugated polyelectrolyte electron transport layer modulating the morphology of the active layer for efficient nonfullerene organic solar cells J. Mater. Sci. Mater. Electron. **29** 18458–64

[143] Upama M B, Elumalai N K, Mahmud M A, Xu C, Wang D, Wright M and Uddin A 2018 Enhanced electron transport enables over 12% efficiency by interface engineering of non-fullerene organic solar cells Sol. Energy Mater. Sol. Cells **187** 273–82

[144] Liu C, Zhang D, Li Z, Zhang X, Guo W, Zhang L, Shen L, Ruan S and Long Y 2017 Boosted electron transport and enlarged built-in potential by eliminating the interface barrier in organic solar cells ACS Appl. Mater. Interfaces **9** 8830–7

[145] Liu J, Chen L, Gao B, Cao X, Han Y, Xie Z and Wang L 2013 Constructing the nanointerpenetrating structure of PCDTBT:PC70BM bulk heterojunction solar cells induced by aggregation of PC₇₀BM via mixed-solvent vapor annealing J. Mater. Chem. A **1** 6216–25

[146] van Bavel S S, Sourty E, de With G and Loos J 2009 Three-dimensional nanoscale organization of

bulk heterojunction polymer solar cells Nano Lett. **9** 507–13

[147] Huang J, Carpenter J H, Li C Z, Yu J S, Ade H and Jen A K Y 2016 Highly efficient organic solar cells with improved vertical donor-acceptor compositional gradient via an inverted off-center spinning method Adv. Mater. **28** 967–74

[148] Guerrero A, Dörling B, Ripolles-Sanchis T, Aghamohammadi M, Barrena E, Campoy-Quiles M and Garcia-Belmonte G 2013 Interplay between fullerene surface coverage and contact selectivity of cathode interfaces in organic solar cells ACS Nano **7** 4637–46

[149] Hansson R et al 2015 Vertical and lateral morphology effects on solar cell performance for a thiophene–quinoxaline copolymer:PC70BM blend J. Mater. Chem. A **3** 6970–9

[150] Moon B J, Lee G-Y, Im M J, Song S and Park T 2014 In situ modulation of the vertical distribution in a blend of P3HT and PC60BM via the addition of a composition gradient inducer Nanoscale **6** 2440–6

[151] Vaynzof Y, Brenner T J K, Kabra D, Sirringhaus H and Friend R H 2012 Compositional and morphological studies of polythiophene/polyflorene blends in inverted architecture hybrid solar cells Adv. Funct. Mater. **22** 2418–24

[152] Wang Y et al 2017 The effect of donor and nonfullerene acceptor inhomogeneous distribution within the photoactive layer on the performance of polymer solar cells with different device structures Polymers **9** 571

[153] Lu Z, Jiang B, Zhang X, Tang A, Chen L, Zhan C and Yao J 2014 Perylene-diimide based non-fullerene solar cells with 4.34% efficiency through engineering surface donor/acceptor compositions Chem. Mater. **26** 2907–14

[154] McNeill C R 2012 Morphology of all-polymer solar cells Energy Environ. Sci. **5** 5653–67

[155] Rujisamphan N, Murray R E, Deng F, Ni C and Shah S I 2014 Study of nanoscale morphology of polythiophene fibrils and fullerene derivative ACS Appl. Mater. Interfaces **6** 11965−11972

[156] Wang Y, Wu B, Wu Z, Lan Z, Li Y, Zhang M and Zhu F 2017 Origin of efficient inverted nonfullerene organic solar cells: enhancement of charge extraction and suppression of bimolecular recombination enabled by augmented internal electric field J. Phys. Chem. Lett. **8** 5264–71

[157] Schroeder B C et al 2012 Synthesis of novel thieno [3, 2-b] thienobis (silolothiophene) based low bandgap polymers for organic photovoltaics Chem. Commun. **48** 7699–701

[158] Zhou H, Yang L, Stuart A C, Price S C, Liu S and You W 2011 Development of fluorinated benzothiadiazole as a structural unit for a polymer solar cell of 7% efficiency Angew. Chem.-Int. Ed. **123** 3051–4

[159] Hartnett P E et al 2014 Slip-stacked perylenediimides as an alternative strategy for high efficiency nonfullerene acceptors in organic photovoltaics J. Am. Chem. Soc. **136** 16345–56

[160] Chen W and Zhang Q 2017 Recent progress in non-fullerene small molecule acceptors in organic solar cells (OSCs) J. Mater. Chem. C **5** 1275–302

[161] Eftaiha A F, Sun J-P, Hill I G and Welch G C 2014 Recent advances of non-fullerene, small molecular acceptors for solution processed bulk heterojunction solar cells J. Mater. Chem. A **2** 1201–13

[162] Lin Y and Zhan X 2014 Non-fullerene acceptors for organic photovoltaics: an emerging horizon Mater. Horizons **1** 470–88

[163] Zhou Y, Ding L, Shi K, Dai Y-Z, Ai N, Wang J and Pei J 2012 A non-fullerene small molecule as efficient electron acceptor in organic bulk heterojunction solar cells Adv. Mater. **24** 957–61

[164] Ye L, Jiang W, Zhao W, Zhang S, Qian D, Wang Z and Hou J 2014 Selecting a donor polymer for

realizing favorable morphology in efficient non-fullerene acceptor-based solar cells Small **10** 4658–63

[165]   Ludwigs S 2014 P3HT Revisited – From Molecular Scale to Solar Cell Devices vol 265 (Springer)

[166]   Holliday S et al 2016 High-efficiency and air-stable P3HT-based polymer solar cells with a new non-fullerene acceptor Nat. Commun. **7** 11585

[167]   Tan C H, Gorman J, Wadsworth A, Holliday S, Subramaniyan S, Jenekhe S A, Baran D, McCulloch I and Durrant J R 2018 Barbiturate end-capped non-fullerene acceptors for organic solar cells: tuning acceptor energetics to suppress geminate recombination losses Chem. Commun. **54** 2966–9

[168]   Zang Y, Li C-Z, Chueh C C, Williams S T, Jiang W, Wang Z-H, Yu J S and Jen A K Y 2014 Integrated molecular, interfacial, and device engineering towards high-performance non-fullerene based organic solar cells Adv. Mater. **26** 5708–14

[169]   Zhang G et al 2017 High-performance ternary organic solar cell enabled by a thick active layer containing a liquid crystalline small molecule donor J. Am. Chem. Soc. **139** 2387–95

[170]   Wan Q, Guo X, Wang Z, Li W, Guo B, Ma W, Zhang M and Li Y 2016 10.8% efficiency polymer solar vells based on PTB7-Th and PC$_{71}$BM via binary solvent additives treatment Adv. Funct. Mater. **26** 6635–40

[171]   Jiang Z-Q, Wang T-T, Wu F-P, Lin J-D and Liao L-S 2018 Recent advances in electron acceptors with ladder- type backbone for organic solar cells J. Mater. Chem. A **6** 17256–87

[172]   Zhang J, Tan H S, Guo X, Facchetti A and Yan H 2018 Material insights and challenges for non-fullerene organic solar cells based on small molecular acceptors Nat. Energy **3** 720–31

[173]   Wang Y et al 2018 (Semi)ladder-type bithiophene imide-based all-acceptor semiconductors: synthesis, structure-property correlations, and unipolar n-type transistor performance J. Am. Chem. Soc. **140** 6095–108

[174]   Wang Y et al 2017 Effects of bithiophene imide fusion on the device performance of organic thin-film transistors and all-polymer solar cells Angew. Chem. - Int. Ed. **56** 15304–8

[175]   Wang Y, Guo H, Ling S, Arrechea-Marcos I, Wang Y, López Navarrete J T, Ortiz R P and Guo X 2017 Ladder-type heteroarenes: up to 15 rings with five imide groups Angew. Chem. - Int. Ed. **56** 9924–9

[176]   Gao L, Zhang Z G, Bin H, Xue L, Yang Y, Wang C, Liu F, Russell T P and Li Y 2016 High-efficiency nonfullerene polymer solar cells with medium bandgap polymer donor and narrow bandgap organic semiconductor acceptor Adv. Mater. **28** 8288–95

[177]   Bin H, Zhang Z G, Gao L, Chen S, Zhong L, Xue L, Yang C and Li Y 2016 Non-fullerene polymer solar cells based on alkylthio and fluorine substituted 2D-conjugated polymers reach 9.5% efficiency J. Am. Chem. Soc. **138** 4657–64

[178]   Bin H et al 2016 11.4% Efficiency non-fullerene polymer solar cells with trialkylsilyl substituted 2D-conjugated polymer as donor Nat. Commun. **7** 13651

[179]   Badgujar S, Song C E, Oh S, Shin W S, Moon S-J, Lee J-C, Jung I H and Lee S K 2016 Highly efficient and thermally stable fullerene-free organic solar cells based on a small molecule donor and acceptor J. Mater. Chem. A **4** 16335–40

[180]   Cha H et al 2017 An efficient, "burn in" free organic solar cell employing a nonfullerene electron acceptor Adv. Mater. **29** 1701156

[181]   Liu F, Zhou Z, Zhang C, Zhang J, Hu Q, Vergote T, Liu F, Russell T P and Zhu X 2017 Efficient semitransparent solar cells with high NIR responsiveness enabled by a small-bandgap electron acceptor Adv. Mater. **29** 1606574

[182]   Täuber D, Tian Y, Xia Y, Inganäs O and Scheblykin I G 2017 Nanoscale chain alignment and morphology in all-polymer blends visualized using 2D polarization fluorescence imaging: correlation to power conversion efficiencies in solar cells J. Phys. Chem. C **121** 21848–56

[183]   Zhang H, Li S, Xu B, Yao H, Yang B and Hou J 2016 Fullerene-free polymer solar cell based on a polythiophene derivative with an unprecedented energy loss of less than 0.5 eV J. Mater. Chem. A **4** 18043–9

[184]   Gao H H, Sun Y, Wan X, Kan B, Ke X, Zhang H, Li C and Chen Y 2017 Design and synthesis of low band gap non-fullerene acceptors for organic solar cells with impressively high Jsc over 21 mA cm^2 Sci. China Mater. **60** 819–28

[185]   Lin Y et al 2016 High-performance electron acceptor with thienyl side chains for organic photovoltaics J. Am. Chem. Soc. **138** 4955–61

[186]   Yang Y, Zhang Z G, Bin H, Chen S, Gao L, Xue L, Yang C and Li Y 2016 Side-chain isomerization on an n-type organic semiconductor ITIC acceptor makes 11.77% high efficiency polymer solar cells J. Am. Chem. Soc. **138** 15011–8

[187]   Cheng Y J, Wu J S, Shih P I, Chang C Y, Jwo P C, Kao W S and Hsu C S 2011 Carbazole-based ladder-type heptacylic arene with aliphatic side chains leading to enhanced efficiency of organic photovoltaics Chem. Mater. **23** 2361–9

[188]   Gasparini N et al 2017 Polymer:nonfullerene bulk heterojunction solar cells with exceptionally low recombination rates Adv. Energy Mater. **7** 1701561

[189]   Kim W, Kim J K, Kim E, Ahn T K, Wang D H and Park J H 2015 Conflicted effects of a solvent additive on PTB7:$PC_{71}BM$ bulk heterojunction solar cells J. Phys. Chem. C **119** 5954–61

[190]   Liao S H, Jhuo H J, Cheng Y S and Chen S A 2013 Fullerene derivative-doped zinc oxide nanofilm as the cathode of inverted polymer solar cells with low-bandgap polymer (PTB7-Th) for high performance Adv. Mater. **25** 4766–71

[191]   Xiao B, Zhao Y, Tang A, Wang H, Yang J and Zhou E 2017 PTB7-Th based organic solar cell with a high Voc of 1.05 V by modulating the LUMO energy level of benzotriazole-containing non-fullerene acceptor Sci. Bull. **62** 1275–82

[192]   Sun J et al 2018 High performance non-fullerene polymer solar cells based on PTB7-Th as the electron donor with 10.42% efficiency J. Mater. Chem. A **6** 2549

[193]   Zhao J et al 2015 High-efficiency non-fullerene organic solar cells enabled by a difluorobenzothiadiazole-based donor polymer combined with a properly matched small molecule acceptor Energy Environ. Sci. **8** 520–5

[194]   Lin Y, Zhang Z-G, Bai H, Wang J, Yao Y, Li Y, Zhu D and Zhan X 2015 High-performance fullerene-free polymer solar cells with 6.31% efficiency Energy Environ. Sci. **8** 610–6

[195]   Song X, Gasparini N, Ye L, Yao H, Hou J, Ade H and Baran D 2018 Controlling blend morphology for ultrahigh current density in nonfullerene acceptor-based organic solar cells ACS Energy Lett. **3** 669–76

[196]   Xiao Z et al 2017 26 mA cm^{-2} Jsc from organic solar cells with a low-bandgap nonfullerene acceptor Sci. Bull. **62** 1494–6

[197]   Warnan J, El Labban A, Cabanetos C, Hoke E T, Shukla P K, Risko C, Brédas J-L, McGehee M D and Beaujuge P M 2014 Ring substituents mediate the morphology of PBDTTPD-PCBM bulk-heterojunction solar cells Chem. Mater. **26** 2299–306

[198]   Qian D et al 2012 Design, application, and morphology study of a new photovoltaic polymer with strong aggregation in solution state Macromolecules **45** 9611–7

[199] Ye L, Zhang S Q, Huo L J, Zhang M J and Hou J H 2014 Molecular design toward highly efficient photovoltaic polymers based on two-dimensional conjugated benzodithiophene Acc. Chem. Res. **47** 1595–603

[200] Zhao W, Ye L, Zhang S, Sun M and Hou J 2015 A universal halogen-free solvent system for highly efficient polymer solar cells J. Mater. Chem. A **3** 12723–9

[201] Zhang H, Wang X, Yang L, Zhang S, Zhang Y, He C, Ma W and Hou J 2017 Improved domain size and purity enables efficient all-small-molecule ternary solar cells Adv. Mater. **29** 1703777

[202] Zhang M, Zhang F, An Q, Sun Q, Wang J, Li L, Wang W and Zhang J 2015 High efficient ternary polymer solar cells based on absorption complementary materials as electron donor Sol. Energy Mater. Sol. Cells **141** 154–61

[203] Kumari T, Lee S M, Kang S-H, Chen S and Yang C 2017 Ternary solar cells with a mixed face-on and edge-on orientation enable an unprecedented efficiency of 12.1% Energy Environ. Sci. **10** 258–65

[204] Wang Z, Zhang Y, Zhang J, Wei Z and Ma W 2016 Optimized "alloy-parallel" morphology of ternary organic solar cells Adv. Energy Mater. **6** 1502456

[205] Zhao F et al 2017 Combining energy transfer and optimized morphology for highly efficient ternary polymer solar cells Adv. Energy Mater. **7** 1602552

[206] Lu L, Kelly M A, You W and Yu L 2015 Status and prospects for ternary organic photovoltaics Nat. Photonics **9** 491–500

[207] Yu R, Yao H and Hou J 2018 Recent progress in ternary organic solar cells based on nonfullerene acceptors Adv. Energy Mater. **8** 1702814

[208] Ameri T, Khoram P, Min J and Brabec C J 2013 Organic ternary solar cells: a review Adv. Mater. **25** 4245–66

[209] Gasparini N, Lucera L, Salvador M, Prosa M, Spyropoulos G D, Kubis P, Egelhaaf H-J, Brabec C J and Ameri T 2017 High-performance ternary organic solar cells with thick active layer exceeding 11% efficiency Energy Environ. Sci. **10** 885–92

[210] Jiang W et al 2018 Ternary nonfullerene polymer solar cells with 12.16% efficiency by introducing one acceptor with cascading energy level and complementary absorption Adv. Mater. **30** 1703005

[211] Zhao W, Li S, Zhang S, Liu X and Hou J 2017 Ternary polymer solar cells based on two acceptors and one donor for achieving 12.2% efficiency Adv. Mater. **29** 1604059

[212] Xu W and Gao F 2018 The progress and prospects of non-fullerene acceptors in ternary blend organic solar cells Mater. Horizons **5** 206–21

[213] Baran D et al 2016 Reducing the efficiency–stability–cost gap of organic photovoltaics with highly efficient and stable small molecule acceptor ternary solar cells Nat. Mater. **16** 363–9

[214] Ma X, Mi Y, Zhang F, An Q, Zhang M, Hu Z, Liu X, Zhang J and Tang W 2018 Efficient ternary polymer solar cells with two well-compatible donors and one ultranarrow bandgap nonfullerene acceptor Adv. Energy Mater. **8** 1702854

[215] Xu X, Bi Z, Ma W, Wang Z, Choy W C H, Wu W, Zhang G, Li Y and Peng Q 2017 Highly efficient ternary-blend polymer solar cells enabled by a nonfullerene acceptor and two polymer donors with a broad composition tolerance Adv. Mater. **29** 1704271

[216] Huang Y, Cheng H and Han C C 2010 Temperature induced structure evolution of regioregular poly(3-hexylthiophene) in dilute solution and its influence on thin film morphology Macromolecules **43** 10031–7

[217] Wang T et al 2010 The development of nanoscale morphology in polymer:fullerene photovoltaic blends during solvent casting Soft Matter **6** 4128–34

[218]   Friedel B, Brenner T J K, McNeill C R, Steiner U and Greenham N C 2011 Influence of solution heating on the properties of PEDOT:PSS colloidal solutions and impact on the device performance of polymer solar cells Org. Electron. **12** 1736–45

[219]   Bartelt J A, Douglas J D, Mateker W R, Labban A El, Tassone C J, Toney M F, Fréchet J M J, Beaujuge P M and McGehee M D 2014 Controlling solution-phase polymer aggregation with molecular weight and solvent additives to optimize polymer-fullerene bulk heterojunction solar cells Adv. Energy Mater. **4** 1301733

[220]   Zheng Y Q et al 2017 Unraveling the solution-state supramolecular structures of donor–acceptor polymers and their influence on solid-state morphology and charge-transport properties Adv. Mater. **29** 1701072

[221]   Kline R J, McGehee M D, Kadnikova E N, Liu J, Fréchet J M J and Toney M F 2005 Dependence of regioregular poly(3-hexylthiophene) film morphology and field-effect mobility on molecular weight Macromolecules **38** 3312–9

[222]   Yu F and Kuppa V K 2015 Solution aging effects on the performance and morphology of P3HT:PCBM bulk heterojunction solar cells Nano Life **05** 1550005

[223]   Han P, Balderrama V S, Mihi A, Formentin P, Ferre-Borrull J, Pallarés J and Marsal L F 2015 Improving the efficiency of PTB1:PCBM bulk heterojunction solar cells by polymer blend solution aging IEEE J. Photovoltaics **5** 889–96

[224]   Liu Y et al 2015 A tetraphenylethylene core-based 3D structure small molecular acceptor enabling efficient non-fullerene organic solar cells Adv. Mater. **27** 1015–20

[225]   Cheng P, Yan C, Li Y, Ma W and Zhan X 2015 Diluting concentrated solution: a general, simple and effective approach to enhance efficiency of polymer solar cells Energy Environ. Sci. **8** 2357–64

[226]   Bertho S et al 2007 Influence of thermal ageing on the stability of polymer bulk heterojunction solar cells Sol. Energy Mater. Sol. Cells **91** 385–9

[227]   Li W, Yang L, Tumbleston J R, Yan L, Ade H and You W 2014 Controlling molecular weight of a high efficiency donor-acceptor conjugated polymer and understanding its significant impact on photovoltaic properties Adv. Mater. **26** 4456–62

[228]   Eastham N D et al 2017 Small molecule acceptor and polymer donor crystallinity and aggregation effects on microstructure templating: understanding photovoltaic response in fullerene-free solar cells Chem. Mater. **29** 4432–44

[229]   Ma W et al 2015 Influence of processing parameters and molecular weight on the morphology and properties of high-performance PffBT4T-2OD:PC70BM organic solar cells Adv. Energy Mater. **5** 1501400

[230]   Huang W, Gann E, Cheng Y B and McNeill C R 2015 In-depth understanding of the morphology-performance relationship in polymer solar cells ACS Appl. Mater. Interfaces **7** 14026–34

[231]   O'Hara K A, Ostrowski D P, Koldemir U, Takacs C J, Shaheen S E, Sellinger A and Chabinyc M L 2017 Role of crystallization in the morphology of polymer:non-fullerene acceptor bulk heterojunctions ACS Appl. Mater. Interfaces **9** 19021–9

[232]   Deibel C, Baumann A and Dyakonov V 2008 Polaron recombination in pristine and annealed bulk heterojunction solar cells Appl. Phys. Lett. **93** 386

[233]   Riobóo R J, Philipp M, Ramos M A and Krüger J K 2009 Concentration and temperature dependence of the refractive index of ethanol-water mixtures: influence of intermolecular interactions. Eur. Phys. J. E Soft Matter **30** 19–26

[234]   Yu X, Yang H, Wu S, Wang L, Geng Y and Han Y 2015 Crystallization-dominated and microphase separation/crystallization-coexisted structure of all-conjugated phenylene-thiophene diblock

copolymers J. Polym. Sci. Part B Polym. Phys. **53** 1718–26

[235] Sun J P, Hendsbee A D, Dobson A J, Welch G C and Hill I G 2016 Perylene diimide based all small-molecule organic solar cells: Impact of branched-alkyl side chains on solubility, photophysics, self-assembly, and photovoltaic parameters Org. Electron. physics, Mater. Appl. **35** 151–7

[236] Zhang Z, Li M, Liu Y, Zhang J, Feng S, Xu X, Song J and Bo Z 2017 Simultaneous enhancement of the molecular planarity and the solubility of non-fullerene acceptors: effect of aliphatic side-chain substitution on the photovoltaic performance J. Mater. Chem. A **5** 7776–83

[237] Liang N, Jiang W, Hou J and Wang Z 2017 New developments in non-fullerene small molecule acceptors for polymer solar cells Mater. Chem. Front. **1** 1291–303

[238] Qiu N et al 2017 A new nonfullerene electron acceptor with a ladder type backbone for high-performance organic solar cells Adv. Mater. **29** 1604964

[239] Liang Y, Xu Z, Xia J, Tsai S T, Wu Y, Li G, Ray C and Yu L 2010 For the bright future-bulk heterojunction polymer solar cells with power conversion efficiency of 7.4% Adv. Mater. **22** 135–8

[240] Love J A, Chou S H, Huang Y, Bazan G C and Nguyen T Q 2016 Effects of solvent additive on "s-shaped" curves in solution-processed small molecule solar cells Beilstein J. Org. Chem. **12** 2543–55

[241] Liu F, Zhao W, Tumbleston J R, Wang C, Gu Y, Wang D, Briseno A L, Ade H and Russell T P 2014 Understanding the morphology of PTB7:PCBM blends in organic photovoltaics Adv. Energy Mater. **4** 1301377

[242] Van Franeker J J, Turbiez M, Li W, Wienk M M and Janssen R A J 2015 A real-time study of the benefits of co-solvents in polymer solar cell processing Nat. Commun. **6** 6229

[243] Richter L J, Delongchamp D M and Amassian A 2017 Morphology development in solution-processed functional organic blend films: an in situ viewpoint Chem. Rev. **117** 6332–66

[244] Song X, Gasparini N and Baran D 2018 The influence of solvent additive on polymer solar cells employing fullerene and non-fullerene acceptors Adv. Electron. Mater. **4** 1700358

[245] Jiang X, Xu Y, Wang X, Wu Y, Feng G, Li C, Ma W and Li W 2017 Non-fullerene organic solar cells based on diketopyrrolopyrrole polymers as electron donors and ITIC as an electron acceptor Phys. Chem. Chem. Phys. **19** 8069–75

[246] Ye L, Zhao W, Li S, Mukherjee S, Carpenter J H, Awartani O, Jiao X, Hou J and Ade H 2017 Efficiency nonfullerene organic solar cells: critical factors that affect complex multi-length scale morphology and device performance Adv. Energy Mater. **7** 1602000

[247] Li H, Hwang Y-J, Courtright B A E, Eberle F N, Subramaniyan S and Jenekhe S A 2015 Fine-tuning the 3d structure of nonfullerene electron acceptors toward high-performance polymer solar cells Adv. Mater. **27** 3266–72

[248] Schubert M et al 2014 Correlated donor/acceptor crystal orientation controls photocurrent generation in all-polymer solar cells Adv. Funct. Mater. **24** 4068–81

[249] Aïch B R, Lu J, Beaupré S, Leclerc M and Tao Y 2012 Control of the active layer nanomorphology by using co-additives towards high-performance bulk heterojunction solar cells Org. Electron. physics, Mater. Appl. **13** 1736–41

[250] Zhao J, Zhao S, Xu Z, Qiao B, Huang D, Zhao L, Li Y, Zhu Y and Wang P 2016 Revealing the effect of additives with different solubility on the morphology and the donor crystalline structures of organic solar cells ACS Appl. Mater. Interfaces **8** 18231–7

[251] Kim Y J, Ahn S, Wang D H and Park C E 2015 A mechanistic understanding of a binary additive system to synergistically boost efficiency in all-polymer solar cells Sci. Rep. **5** 18024

[252] Tremolet De Villers B J, O'Hara K A, Ostrowski D P, Biddle P H, Shaheen S E, Chabinyc M L,

Olson D C and Kopidakis N 2016 Removal of residual diiodooctane improves photostability of high-performance organic solar cell polymers Chem. Mater. **28** 876–84

[253] Holliday S and Luscombe C K 2018 Low boiling point solvent additives for improved photooxidative stability in organic photovoltaics Adv. Electron. Mater. **4** 1700416

[254] Zhang L, Lin B, Ke Z, Chen J, Li W, Zhang M and Ma W 2017 A universal approach to improve electron mobility without significant enlarging phase separation in IDT-based non-fullerene acceptor organic solar cells Nano Energy **41** 609–17

[255] Li W et al 2019 Retarding the crystallization of a non-fullerene electron-acceptor for high performance polymer solar cells Adv. Funct. Mater. **29** 1807662

[256] Ni W, Li M, Kan B, Liu F, Wan X, Zhang Q, Zhang H, Russell T P and Chen Y 2016 Fullerene-free small molecule organic solar cells with a high open circuit voltage of 1.15 V Chem. Commun. **52** 465–8

[257] Kwon O K, Park J-H, Kim D W, Park S K and Park S Y 2015 An all-small-molecule organic solar cell with high efficiency nonfullerene acceptor Adv. Mater. **27** 1951–6

[258] Pan D H K and Prest W M 1985 Surfaces of polymer blends: X-ray photoelectron spectroscopy studies of polystyrene/poly(vinyl methyl ether) blends J. Appl. Phys. **58** 2861–70

[259] Bergqvist J et al 2014 Sub-glass transition annealing enhances polymer solar cell performance J. Mater. Chem. A **2** 6146–52

[260] Jamieson F C, Domingo E B, McCarthy-Ward T, Heeney M, Stingelin N and Durrant J R 2012 Fullerene crystallisation as a key driver of charge separation in polymer/fullerene bulk heterojunction solar cells Chem. Sci. **3** 485–92

[261] Li S, Liu W, Shi M, Mai J, Lau T-K, Wan J, Lu X, Li C-Z and Chen H 2016 A spirobifluorene and diketopyrrolopyrrole moieties based non-fullerene acceptor for efficient and thermally stable polymer solar cells with high open-circuit voltage Energy Environ. Sci. **9** 604–10

[262] Kwon O K, Uddin M A, Park J H, Park S K, Nguyen T L, Woo H Y and Park S Y 2016 A high efficiency nonfullerene organic solar cell with optimized crystalline organizations Adv. Mater. **28** 910–6

[263] Xia Y et al 2016 Inverted all-polymer solar cells based on a quinoxaline–thiophene/naphthalene-diimide polymer blend improved by annealing J. Mater. Chem. A **4** 3835–43

[264] Vogelsang J, Brazard J, Adachi T, Bolinger J C and Barbara P F 2011 Watching the annealing process one polymer chain at a time Angew. Chem. - Int. Ed. **50** 2257–61

[265] Min J, Jiao X, Ata I, Osvet A, Ameri T, Bäuerle P, Ade H and Brabec C J 2016 Time-dependent morphology evolution of solution-processed small molecule solar cells during solvent vapor annealing Adv. Energy Mater. **6** 1502579

[266] Babics M, Liang R Z, Wang K, Cruciani F, Kan Z, Wohlfahrt M, Tang M C, Laquai F and Beaujuge P M 2018 Solvent vapor annealing-mediated crystallization directs charge generation, recombination and extraction in BHJ solar cells Chem. Mater. **30** 789–98

[267] Zheng Y, Li S, Zheng D and Yu J 2014 Effects of different polar solvents for solvent vapor annealing treatment on the performance of polymer solar cells Org. Electron. **15** 2647–53

[268] Jung B, Kim K, Eom Y and Kim W 2015 High-pressure solvent vapor annealing with a benign solvent to rapidly enhance the performance of organic photovoltaics ACS Appl. Mater. Interfaces **7** 13342–9

[269] Xin R, Feng J, Zeng C, Jiang W, Zhang L, Meng D, Ren Z, Wang Z and Yan S 2017 Nonfullerene-acceptor all-small-molecule organic solar cells based on highly twisted perylene bisimide with an

efficiency of over 6% ACS Appl. Mater. Interfaces **9** 2739–46

[270]   Zhang X, Zhan C and Yao J 2015 Non-fullerene organic solar cells with 6.1% efficiency through fine-tuning parameters of the film-forming process Chem. Mater. **27** 166–73

[271]   Miller S, Fanchini G, Lin Y Y, Li C, Chen C W, Su W F and Chhowalla M 2008 Investigation of nanoscale morphological changes in organic photovoltaics during solvent vapor annealing J. Mater. Chem. **18** 306–12

[272]   Wessendorf C D et al 2014 Efficiency improvement of solution-processed dithienopyrrole-based A-D-A oligothiophene bulk-heterojunction solar cells by solvent vapor annealing Adv. Energy Mater. **4** 1400266

[273]   Cui Y, Yao H, Gao B, Qin Y, Zhang S, Yang B, He C, Xu B and Hou J 2017 Fine-tuned photoactive and interconnection layers for achieving over 13% efficiency in a fullerene-free tandem organic solar cell J. Am. Chem. Soc. **139** 7302–9

[274]   Zhang S, Ye L, Zhang H and Hou J 2016 Green-solvent-processable organic solar cells Mater. Today **19** 533–43

[275]   McDowell C and Bazan G C 2017 Organic solar cells processed from green solvents Curr. Opin. Green Sustain. Chem. **5** 49–54

[276]   Wadsworth A et al 2017 Highly efficient and reproducible nonfullerene solar cells from hydrocarbon solvents ACS Energy Lett. **2** 1494–500

[277]   Byers J C, Heiser T, Skorobogatiy M and Semenikhin O A 2016 Effect of aging and PCBM content on bulk heterojunction organic solar cells studied by intensity modulated photocurrent spectroscopy ACS Appl. Mater. Interfaces **8** 28789–99

[278]   Klumbies H, Karl M, Hermenau M, Rösch R, Seeland M, Hoppe H, Müller-Meskamp L and Leo K 2014 Water ingress into and climate dependent lifetime of organic photovoltaic cells investigated by calcium corrosion tests Sol. Energy Mater. Sol. Cells **120** 685–90

[279]   Zhang Y, Yi H, Iraqi A, Kingsley J, Buckley A, Wang T and Lidzey D G 2017 Comparative indoor and outdoor stability measurements of polymer based solar cells Sci. Rep. **7** 1305

[280]   Angmo D and Krebs F C 2015 Over 2 years of outdoor operational and storage stability of ITO-free, fully roll-to-roll fabricated polymer solar cell modules Energy Technol. **3** 774–83

[281]   Roesch R, Eberhardt K R, Engmann S, Gobsch G and Hoppe H 2013 Polymer solar cells with enhanced lifetime by improved electrode stability and sealing Sol. Energy Mater. Sol. Cells **117** 59–66

[282]   Song B, Burlingame Q C, Lee K and Forrest S R 2015 Reliability of mixed-heterojunction organic photovoltaics grown via organic vapor phase deposition Adv. Energy Mater. **5** 1401952

[283]   Cheng P and Zhan X 2016 Stability of organic solar cells: challenges and strategies Chem. Soc. Rev. **45** 2544–82

[284]   Hao X, Wang S, Sakurai T, Masuda S and Akimoto K 2015 Improvement of stability for small molecule organic solar cells by suppressing the trap mediated recombination ACS Appl. Mater. Interfaces **7** 18379

[285]   Cheacharoen R et al 2017 Assessing the stability of high performance solution processed small molecule solar cells Sol. Energy Mater. Sol. Cells **161** 368–76

[286]   Mateker W R et al 2013 Improving the long-term stability of PBDTTPD polymer solar cells through material purification aimed at removing organic impurities Energy Environ. Sci. **6** 2529–37

[287]   Street R A and Davies D M 2013 Kinetics of light induced defect creation in organic solar cells Appl. Phys. Lett. **102** 4043305

[288] Tournebize A, Bussière P O, Rivaton A, Gardette J L, Medlej H, Hiorns R C, Dagron-Lartigau C, Krebs F C and Norrman K 2013 New insights into the mechanisms of photodegradation/stabilization of P3HT:PCBM active layers using poly(3-hexyl- d13-thiophene) Chem. Mater. **25** 4522–8

[289] Shah S and Biswas R 2015 Atomic pathways underlying light-induced changes in organic solar cell materials J. Phys. Chem. C **119** 20265–71

[290] Meier C B, Sprick R S, Monti A, Guiglion P, Lee J S M, Zwijnenburg M A and Cooper A I 2017 Structure-property relationships for covalent triazine-based frameworks: the effect of spacer length on photocatalytic hydrogen evolution from water Polym. **126** 283–90

[291] Peters C H et al 2012 The mechanism of burn-in loss in a high efficiency polymer solar cell Adv. Mater. **24** 663–8

[292] Sachs-Quintana I T, Heumüller T, Mateker W R, Orozco D E, Cheacharoen R, Sweetnam S, Brabec C J and McGehee M D 2014 Electron barrier formation at the organic-back contact interface is the first step in thermal degradation of polymer solar cells Adv. Funct. Mater. **24** 3978–85

[293] Heumueller T, Mateker W R, Sachs-Quintana I T, Vandewal K, Bartelt J A, Burke T M, Ameri T, Brabec C J and McGehee M D 2014 Reducing burn-in voltage loss in polymer solar cells by increasing the polymer crystallinity Energy Environ. Sci. **7** 2974–80

[294] Silva H S, Tournebize A, Bégué D, Peisert H, Chassé T, Gardette J-L, Therias S, Rivaton A and Hiorns R C 2014 A universal route to improving conjugated macromolecule photostability RSC Adv. **4** 54919–23

[295] Fan Q, Su W, Meng X, Guo X, Li G, Ma W, Zhang M and Li Y 2017 High-performance non-fullerene polymer solar cells based on fluorine substituted wide bandgap copolymers without extra treatments Sol. RRL **1** 1700020

[296] Fan Q et al 2018 High-performance as-cast nonfullerene polymer solar cells with thicker active layer and large area exceeding 11% power conversion efficiency Adv. Mater. **30** 1704546

[297] Zhang G, Xia R, Chen Z, Xiao J, Zhao X, Liu S, Yip H L and Cao Y 2018 Overcoming space-charge effect for efficient thick-film non-fullerene organic solar cells Adv. Energy Mater. **8** 1801609

[298] Pröller S, Liu F, Zhu C, Wang C, Russell T P, Hexemer A, Müller-Buschbaum P and Herzig E M 2016 Following the morphology formation in situ in printed active layers for organic solar cells Adv. Energy Mater. **6** 1501580

[299] Pérez-Gutiérrez E, Lozano J, Gaspar-Tánori J, Maldonado J-L, Gómeza B, López L, Amores-Tapia L-F, Barbosa-García O and Percino M-J 2017 Organic solar cells all made by blade and slot–die coating techniques Sol. Energy **146** 79–84

[300] Liu F, Ferdous S, Schaible E, Hexemer A, Church M, Ding X, Wang C and Russell T P 2015 Fast printing and in situ morphology observation of organic photovoltaics using slot-die coating Adv. Mater. **27** 886–91

[301] Ye L, Xiong Y, Zhang Q, Li S, Wang C, Jiang Z, Hou J, You W and Ade H 2018 Surpassing 10% efficiency benchmark for nonfullerene organic solar cells by scalable coating in air from single nonhalogenated solvent Adv. Mater. **30** 1705485

[302] Ro H W et al 2016 Morphology changes upon scaling a high-efficiency, solution-processed solar cell Energy Environ. Sci. **9** 2835–46

[303] Liu K, Larsen-Olsen T T, Lin Y, Beliatis M, Bundgaard E, Jørgensen M, Krebs F C and Zhan X 2016 Roll-coating fabrication of flexible organic solar cells: comparison of fullerene and fullerene-free systems J. Mater. Chem. A **4** 1044–51

[304] Liu W et al 2015 Roll-coating fabrication of ITO-free flexible solar cells based on a non-fullerene small molecule acceptor RSC Adv. **5** 36001–6

[305]   dos Reis Benatto G A, Roth B, Corazza M, Søndergaard R R, Gevorgyan S A, Jørgensen M and Krebs F C 2016 Roll-to-roll printed silver nanowires for increased stability of flexible ITO-free organic solar cell modules Nanoscale **8** 318–26

[306]   Gu X et al 2017 Roll-to-roll printed large-area all-polymer solar cells with 5% efficiency based on a low crystallinity conjugated polymer blend Adv. Energy Mater. **7** 1602742

[307]   Rossander L H, Zawacka N K, Dam H F, Krebs F C and Andreasen J W 2014 In situ monitoring of structure formation in the active layer of polymer solar cells during roll-to-roll coating AIP Adv. **4** 087105

[308]   Yan H, Chen Z, Zheng Y, Newman C, Quinn J R, Dötz F, Kastler M and Facchetti A 2009 A high-mobility electron-transporting polymer for printed transistors Nature **457** 679–86

[309]   Wang Y, Jia B, Qin F, Wu Y, Meng W, Dai S, Zhou Y and Zhan X 2016 Semitransparent, non-fullerene and flexible all-plastic solar cells Polym. **107** 108–12

[310]   Kim T et al 2015 Flexible, highly efficient all-polymer solar cells Nat. Commun. **6** 8547

[311]   Qian Y, Zhang X, Xie L, Qi D, Chandran B K, Chen X and Huang W 2016 Stretchable organic semiconductor devices Adv. Mater. **28** 9243–65